AMERICAN UNIVERSITY OF BEIRUT

NON-INVASIVE, CONTINUOUS, VASCULATURE-ANATOMY-INSPIRED RF-BASED SENSOR FOR GLYCEMIC MEASUREMENTS

by
JESSICA JOSEPH HANNA

A dissertation
submitted in partial fulfillment of the requirements
for the degree of Doctor of Philosophy
to the Program of Biomedical Engineering
of the Maroun Semaan Faculty of Engineering and Architecture and the Faculty
of Medicine
at the American University of Beirut

Beirut, Lebanon
May 2021

AMERICAN UNIVERSITY OF BEIRUT

NON-INVASIVE, CONTINUOUS,

VASCULATURE-ANATOMY-INSPIRED

RF-BASED SENSOR FOR GLYCEMIC

MEASUREMENTS

by
JESSICA JOSEPH HANNA

Approved by:

_____

Prof. Zaher Dawy, Associate Provost   Chair of Committee
Electrical and Computer Engineering

_____

Prof. Joseph Costantine, Associate Professor   Advisor
Electrical and Computer Engineering

Rouwaida Kanj Digitally signed by Rouwaida Kanj
DN: cn=Rouwaida Kanj, o=MSFEA AUB,
ou=ECE, email=rk105@aub.edu.lb, c=US
Date: 2021.04.26 17:19:16 +03'00'

_____

Prof. Rouwaida Kanj, Associate Professor   Advisor
Electrical and Computer Engineering

Prof. Assaad Eid, Associate Professor
Anatomy, Cell Biology and Physiological Sciences   Advisor

Prof. Nadine Darwiche, Professor   Member of Committee
Biochemistry and Molecular Genetics

Prof. Youssef Tawk, Assistant Professor   Member of Committee
Electrical and Computer Engineering

Prof. Nadey Hakim, President's Envoy   Member of Committee
Imperial College

Prof. Sami Azar, Professor   Member of Committee
Internal Medicine

Prof. Emmanouil Tentzeris, Professor   Member of Committee
School of Electrical and Computer Engineering at Georgia Tech

Prof. Ali Ramadan, Assistant Professor   Member of Committee
Electrical and Computer Engineering at Fahad Bin Sultan University

Date of thesis/dissertation defense: April 16, 2021

AMERICAN UNIVERSITY OF BEIRUT

THESIS, DISSERTATION, PROJECT RELEASE FORM

Student Name: _____
Hanna   Jessica   Joseph

◯ Master's Thesis   ◯ Master's Project   ⊗ Doctoral Dissertation

☐ I authorize the American University of Beirut to: (a) reproduce hard or electronic copies of my thesis, dissertation, or project; (b) include such copies in the archives and digital repositories of the University; and (c) make freely available such copies to third parties for research or educational purposes.

☒ I authorize the American University of Beirut, to: (a) reproduce hard or electronic copies of it; (b) include such copies in the archives and digital repositories of the University; and (c) make freely available such copies to third parties for research or educational purposes after: **One** ___ year from the date of submission of my thesis, dissertation or project.
  Two ___ years from the date of submission of my thesis, dissertation or project.
  Three ✗ years from the date of submission of my thesis, dissertation or project.

Jessica Hanna 27 - 4 - 2021
Signature   Date

This form is signed when submitting the thesis, dissertation, or project to the University Libraries

Acknowledgements

When I look back towards my journey as a PhD student, during which we faced a revolution, a global pandemic followed by a huge blast that devastated large parts of Beirut, I feel very lucky to be surrounded by some amazing people without whom this work would not have been possible. I feel very lucky to be part of this prestigious institute and be able to work with intelligent and wonderful people. I am thankful to the entire AUB community for providing such an awesome research experience. This dissertation was the result of many experiences I have encountered at AUB from dozens of remarkable individuals who I wish to acknowledge.

First and foremost, I thank my advisors Professor Joseph Costantine, Professor Rouwaida Kanj, and Professor Assaad Eid for supporting me, not only by providing research assistantship over the past five years, but also academically and emotionally through the rough road we encountered to finish this dissertation. I have learned so much from each one of them, both personally and professionally and for that, I am sincerely grateful. I would like to thank them for challenging me to think further, work harder and dream bigger. It has been a privilege to work with each one of them.

I am also thankful to Dr. Youssef Tawk and Dr. Ali Ramadan for their encouraging comments during our weekly meetings. I got many interesting ideas from the discussions we had and also got to expand my thinking about this project.

To my committee members, I am grateful for providing so much knowledge and insight. To my dissertation chair, Professor Zaher Dawy, I extend my sincerest gratitude to you for believing in me. You have showed me, by example, what a good scientist (and person) should be.

I would also like to thank Dean Shihadeh for believing in this project and for his constant and continuous support during these 5 years.

This work would not have been completed without my family members. I'm forever grateful for mom and dad who supported my dreams and every decision I took throughout my career. I'm also thankful for my brother, for standing by my side through the toughest years of my PhD and for reassuring me that everything will work out in the long run. He has kept me going when I felt like giving up, in ways that you may not even be aware of. He was always there no matter how

busy life was. My gratitude for him is infinite and endless.

I would like to also thank my cousin Sandy for always being there for me. I would not have survived the past 5 years without her continuous support. She supported me from the beginning and encouraged me to keep going. And of course I would like to thank her for being the most creative/talented graphic designer and for creating amazing videos and photos for this project.

Lastly, I would like to thank my friends and my lab mates who have laughed with me, joined me in much needed talks, lunch breaks, and study meetings. We had such an amazing time at AUB. I am grateful for the opportunity to share this journey with all of them. I truly wouldn't have done this without any one of them.

An Abstract of the Dissertation of

Jessica Joseph Hanna   for   Doctor of philosophy

Major: Biomedical Engineering

Title: NON-INVASIVE, CONTINUOUS, VASCULATURE-ANATOMY
-INSPIRED RF-BASED SENSOR FOR GLYCEMIC MEASUREMENTS

Diabetes is a chronic disease that affects more than 8.5% of the worldwide population. The glucometer, which is invasive, is the standard tool for monitoring glucose levels. This approach is painful and uncomfortable. Furthermore, it is not befitting to provide continuous glucose monitoring, often leading to missing some serious hyperglycemic and hypoglycemic events that could occur between finger-prick measurements. To overcome this problem, minimally invasive technologies have been developed. However, the frequent use of such techniques causes discomfort and pain in addition to high socio-economic burdens. Therefore, painless, needle-free, and continuous glucose monitoring sensors are needed to enhance the quality of life of millions of diabetic patients around the world. Today, holistic non-invasive approaches are not commercially available. Different approaches have been introduced in research such as: reverse iontophoresis, bio-impedance spectroscopy, infrared and ocular spectroscopy and ultrasound. Such technologies suffer from several difficulties. For instance, interstitial fluid glucose levels measurements carry a serious time-delay compared to the plasma glucose levels. Additionally, the stability, safety and portability of the underlying technologies constitute their main challenges. Nowadays, researchers are focusing on electromagnetism as a leading technology to achieve noninvasive and continuous glucose monitoring.

Here, we propose a non-invasive continuous wearable glycemic monitoring electromagnetic based multi-sensor system with enhanced sensitivity. The system wirelessly senses hypo- to hyper-glycemic variations with very high accuracy. It leverages novel vasculature-anatomy-inspired electromagnetic front-end components. These components are designed to target simultaneously multiple body locations. Multiple environmental and physiological sensors are also integrated

in the proposed system to calibrate out the perturbing factors. The system is validated on serum, animal tissues and in a clinical setting. Serum-based and ex-vivo experiments demonstrate high precision across the diabetic glucose range (10mg/dl - 600mg/dl). Human trials exhibit clinical accuracy of 98% in fifty five subjects who underwent around hundred Oral Glucose Tolerance Tests. The proposed sensors are embedded in a glove and a sock; results are validated on the sensors both standalone and collectively. The system captures the clinical glycemic variations without any time-lag, reporting up to 96% correlation between the system's physical parameters and blood glucose levels. To our knowledge this is one of the rare studies to assess the sensitivity of the proposed sensors over a wide glycemic range (10mg/dl to 600 mg/dl), in different experimental setups and to calibrate out the multiple environmental and physiological factors.

Contents

List of Figures

List of Tables

Chapter 1

Introduction

Diabetes is a chronic disease that affects more than 8.5% of the worldwide population [1]. The glucometer, which is invasive, is the standard tool for monitoring glucose levels. This approach is painful and uncomfortable. Furthermore, it is not befitting to provide continuous glucose monitoring (CGM), often leading to missing some serious hyperglycemic and hypoglycemic events that could occur between finger-prick measurements. To overcome this problem, minimally invasive technologies have been developed. However, the frequent use of such techniques causes discomfort and pain in addition to high socio-economic burdens [2]. Therefore, the development of an affordable non-invasive CGM device will be life-changing for diabetic patients worldwide. This chapter provides an overview of diabetes and its complications. In this context, the importance of self-monitoring of blood glucose (SMBG) and the available SMBG methods are highlighted. After that, the different proposed noninvasive glucose monitoring technologies are briefly reviewed and the importance of the electromagnetic (EM) technique is highlighted. Finally, the thesis objective and focus are discussed.

1.1   Diabetes and its complications

Diabetes is considered a chronic metabolic disease that affects millions of people around the world. It occurs when the pancreas is unable to produce insulin (Type I) or when the body is unable to use the produced insulin efficiently (Type II). The elevated blood glucose levels caused by the lack of effective insulin can induce damage to the body and can cause failure of several organs and tissues over the long term. Diabetes is the leading cause of blindness and non-traumatic leg and foot amputations. It is responsible for serious damage to the heart, kidney, and nerves. Hence, diabetic patients are urged to maintain tight glycemic control by monitoring their blood glucose levels on a regular basis, in order to prevent such complications [3].

1.2 Importance of self-monitoring of blood glucose

Self-monitoring of blood glucose levels is highly recommended for diabetic patients in order to help them control glucose levels, manage its progression, and delay its complications. Regular tracking of glucose levels allows healthcare professionals to plan personalized diabetes treatment regimens for patients based on their individual glycemic profile. SMBG allows patients and their parents to take proper decisions when it comes to their diet and physical activities. Additionally, it enhances the patient's recognition and control of serious hypoglycemic events. Several clinical studies assessing patients' compliance to monitor glycaemia shows that the frequency of monitoring is subjective. Most of medical professionals agree that diabetic patients treated with insulin should track their glucose variations at least four times a day [4].

1.3 Available methods for SMBG

An invasive technique using the glucometer is the most accurate method for self-glucose monitoring. This technique requires extracting a drop of blood from the finger-tip using a lancet. The blood is then placed on a test strip that uses glucose oxidase mechanism to determine glycemic levels. As mentioned before, the SMBG should be repeated at least 4 times per day for diabetic patients treated with insulin [4], this renders this technique painful especially for kids. It also increases the chances of infections and damages the finger tissues over the long term. Most importantly, one of the main problems with this tool is its inability to provide CGM, and hence missing some serious hyperglycemic and hypoglycemic events that could occur between the finger-prick measurements [5].

To overcome this problem, minimally invasive technologies have been developed [6, 7]. These devices mainly solve the continuity problem of the invasive techniques, by continuously providing information about the glucose levels. The available real-time minimally invasive CGM systems monitor the glucose levels in the interstitial fluid (IF) and based on the acquired values, the blood glucose levels are estimated. These devices are usually composed of three elements: 1) a small electrochemical sensor which is subcutaneously inserted under the skin (upper arm or abdominal region), 2) a transmitter that sends data wirelessly to 3) a receiver that displays the estimated glucose levels in function of time. Partially implantable solutions are also available for CGM [8]. They rely on measuring glucose in subcutaneous IF, using enzymatic sensors, which will be replaced after a certain period of time (90 days for the Food and Drug Administration (FDA)-approved Eversense device [9]).

Importance of continuous monitoring of glucose levels. CGM devices provide information about the changes in glucose levels, at regular intervals, 24 hours

a day. They interpret the acquired data and translate them into dynamic plots providing information about the rate and the direction of glucose change during the day, month and year[10]. In addition to the advantages of SMBG in terms of allowing patients to control their meals, physical activities and treatment, CGM presents additional benefits; some studies show that the tight glycemic control provided by the CGM systems will reduce the levels of glycated haemoglobin (HbA1c). For instance, according to [11] the HbA1c is reduced by 0.15% for every additional day of CGM device usage. Moreover, CGM will also reduce the number of hypoglycemic episodes for both adults and children. A study shows that the regular SMBG technique can miss 71% of hypoglycemic incidents when blood glucose level is monitored 4 times per day. This percentage is reduced to 58% missed episodes when the frequency of monitoring the glucose levels increases to 7 times per day [12].

However, all currently minimally invasive CGM devices, approved by U.S. FDA, are short-term, where the disposable needle-type inserted in the skin, which is an amperometric enzyme electrode, lasts only up to 14 days. Another problem with such devices is the time delay between the plasma glucose levels and the glucose levels in the IF [6] making them in need of daily calibration through finger pricking technique. Although the newer versions don't need calibration anymore, they still have high socio-economic burdens [2]. The implantable sensors available in the market are short-term devices as well, where the sensor needs to be changed every 90 days and it can be used only by people of 18 years of age and older [9].

1.3.1 Noninvasive glucose monitoring approaches

On the other hand, alternative noninvasive glucose monitoring solutions are introduced using various techniques including reverse iontophoresis [13, 14], bio-impedance spectroscopy [15, 16], infrared and ocular spectroscopy [17] and ultrasound [18, 19]. These technologies present several technical difficulties. For instance, the results obtained by reverse iontophoresis, which measures the glucose levels in the IF are altered by sweating, in addition to the fact that it causes skin irritation. Another problem with such technology is the time delay between the plasma glucose levels and the IF glucose levels. Bio-impedance spectroscopy uses alternating currents to measure the underlying tissue's impedance which in turn are related to the glucose variations. However, it's highly affected by the water content[20]. On the other hand, the ocular spectroscopy, which measures the glucose levels in tears, suffers from a serious time lag and poor correlation between the measured glucose levels and the reference blood glucose levels[20]. Ultrasound is also suggested as a tool to export the IF to skin level and measure the glucose levels using electrochemical sensing, however, stability, safety, and portability are still its main challenges [5, 21, 20, 22].

Today, researchers are focusing on electromagnetism as one of the top technologies for achieving noninvasive and continuous glucose monitoring [23, 24]. EM-based

technologies present several advantages. They enable the development of compact and miniaturized systems and can provide CGM, while handling safety provisions. Many studies, presented in Chapter 2, found that dielectric spectroscopy, which is based on EM, allows continuous, noninvasive glucose monitoring through skin and underlying tissues with good sensitivity. However, most of the proposed systems rely slowly on EM sensors. Yet, in daily-life situations, the dielectric spectroscopy could be affected by a variety of environmental and physiological factors. Hence any noninvasive glucose monitoring system based on EM technology must also take into consideration the different perturbing factors.

Table 1.1 presents a list of recent common techniques available in the literature along with the results obtained during clinical trials (if available). Note that these techniques were tested in different experimental setups and on a different number of participants. In addition, they relied on different performance metrics making it hard to compare between them. In terms of mean absolute relative difference (MARD) and Clark error grid (CEG), we can clearly see that our proposed system stands well compared with other technologies and provides lower error and better prediction accuracy.

1.4   Thesis Focus and Rationale

All the available CGM devices, in the market today, are short-term solutions, either based on minimally invasive needles that should be replaced every 10-14 days or partially implantable devices that last around 90 days and target patients of 18 years of age and older. The main goal of this work is to develop a wearable painless continuous monitoring EM-based system, which can sense glucose variations with high accuracy. All age groups including diabetic and non-diabetic people (such as athletics) could use the proposed system. Such system could be connected eventually to the cloud and allows the patient to send the collected data to healthcare professionals to adjust the treatment. To satisfy these design objectives, the system needs; an EM-based sensor to monitor the glucose with high accuracy. Environmental and physiological sensors to calibrate out the potential perturbing factors. A signal processing system to process the output of the EM-sensor and a regression model to convert these readings into absolute glucose levels.

Herein, we introduce a noninvasive wearable approach that relies on flexible EM sensors that can be aligned with body curvatures and adjust to small movements, while focusing on the effective tailoring of EM waves to directly monitor the glucose levels from blood as shown in Figure 1.1(US Patent No. 93 PCT/US2018/054627 [25], US Patent No. 6161-044.PROV [26], US Patent No. PCT/US19/39238 [27]). We demonstrate that the selection of the appropriate operational frequencies while taking into consideration the targeted on-body location is of utmost importance for our application. We also present a strategy that

allows the EM technology to be integrated in a multi-sensing wearable format. The system is composed of flexible EM-Vessels-like sensors targeting multiple on-body locations along with several environmental and physiological sensors. We prove that monitoring the glucose variations simultaneously from different body locations using a multi-sensor approach improves the accuracy of the system by calibrating out the different perturbing factors.

1.5   Thesis Outline

This dissertation is organized into eight chapters. Chapter 1 gives the motivations of this research with an introduction about diabetes, its complications and the prevention techniques and introduces the main objectives of this work. Chapter 2 presents a literature review on EM-based sensors developed specifically for non-invasive glucose monitoring, starting with an introduction about glucose-dependent dielectric properties of the blood and the importance of the frequency choice. In Chapter 3 we discuss the EM-sensors design concept, the sensing location and the frequency of choice. This chapter presents the fabrication and simulation results of the hand and leg antennas. In Chapter 4 we discuss the regression modeling techniques utilized to find dependence between the recorded responses of the proposed sensors and the glucose levels. Chapter 5 and Chapter 6 concentrate on the glove and the socks sensor's performance in different experimental setups, respectively, showing the capability of proposed designs to monitor the glucose variations using serum solutions in in-vitro experiments, followed by ex-vivo experiments on rat tissues. Finally, the sensitivity of the proposed sensors, tested in real-time in-vivo settings on healthy and diabetic volunteers is presented. Chapter 7 discusses the importance of adding environmental and physiological sensors to the EM-based sensing system to overcome the technical difficulties introduced by some environmental factors. In this context, the proposed antennas along with other sensors are joined into a multi-sensing system and tested in different experimental setups. Finally, Chapter 8 presents the conclusions of this work and potential avenues for future research.
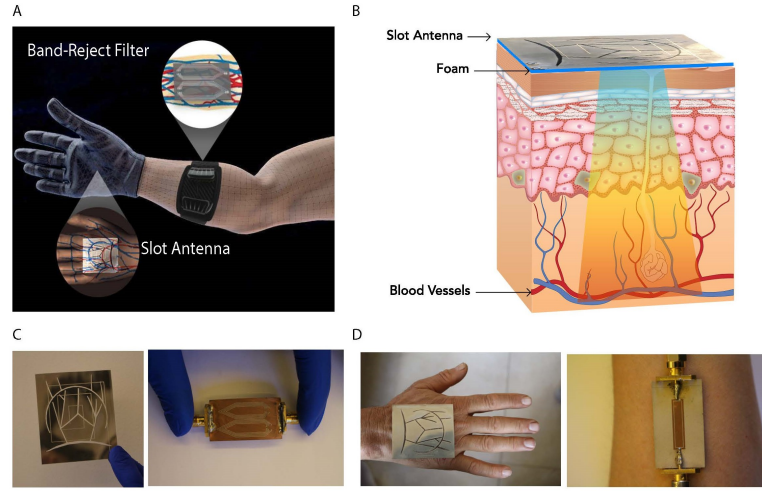
Figure 1.1: Mimicking vasculature anatomy EM sensors.(A) The antenna slots (US Patent No. PCT/US19/39238) and the filter (US Provisional Patent No.62/811,760) are inspired by the anatomy of the veins and arteries of the hand and the arm (US Patent No. PCT/US2018/054627), respectively. (B) The proposed sensors operate at the ultra-high frequency and microwave bands ensuring enough EM waves penetration depth to reach the targeted veins and arteries along with a wide characterization range, (Image modified from YokoDesign/shutterstock). (C) Left: the top sensing layer of the flexible slot antenna prototype. Right: to sensing layer of the band-reject filter prototype. (D) Left: Schematic of the flexible slot antenna targeting the hand's vessels. Right: the Bottom layer of the proposed band-reject filter mounted on the arm. Photo Credit: Jessica Hanna, American University of Beirut.

Method	Device	Technology	Measurement Site	Continuous Monitoring	Accuracy		Reference
					Clarke Error Grid	MARD	
Noninvasive	Cnoga Glucometer	NIR spectroscopy	Finger	No	Zone A: 91.1%, Zone B:7.8%	18.10%	[28]
	OrSense NBM-200G	NIR Occlusion spectroscopy	Finger	Yes (professional use only)	Zone A: 69.7%, Zone B:25.7%	17.2%	[29]
	XizmiTM	NIR Spectroscopy	Arm wrist	Yes	Zone A: 93%, Zone B:7%	7.23%	[30]
	GlucoTrack	Ultrasound, EM and thermal	Ear lobe	No	Zone A: 62.4%, Zone B:37.6%	19.7%	[31]
	Split Ring Resonator	EM	Abdomen	Yes	Zone A+B: 98.13%	22.7%	[32]
	GlucoWise	EM	Hand	No	NA	NA	[33]
	SugarBEAT	Reverse iontophoresis	Upper arm	Yes	NA	13.39% - 12.44%	[34]
Minimally Invasive	Eversense	Fluorescence	Upper arm	Yes	Zone A+B: 99%	9.4%	[35]
Our proposed system Noninvasive	Ediamond	EM	Multi locations	Yes	Zone A+B:100%	5% -6%	

Table 1.1: Benchmark list of recent common techniques available in the literature. The corresponding results obtained during clinical trials are presented if available.

Chapter 2

Electromagnetic based noninvasive glucose monitoring technology

In this chapter we explain how technologies based on electromagnetism are used for noninvasive glucose monitoring. We present a literature review on recent EM-based components, including waveguides, antennas, filters and resonators, designed specifically for glucose monitoring. Finally, we discuss the need for a new approach.

2.1   General description

Today, researchers are focusing on electromagnetism as one of the top technologies for achieving noninvasive and continuous glucose monitoring [23, 24]. Using EM sensors to monitor glucose variation is based on two important factors: (i) the dielectric properties of the medium under test (MUT), which control the behavior of the EM waves in that medium and (ii) the glucose level, which alters the dielectric properties of the blood. Therefore, when EM waves, out of an EM sensor are transmitted to the body, the reflected and the transmitted waves are impacted by the underlying tissues and carry valuable information of their properties [36]. More precisely, the changes in the S-parameters, in terms of magnitude and phase shifts, are associated with the glucose fluctuations in the MUT. By monitoring these variations, the blood glucose levels are determined. EM-based technologies present several advantages. They enable the development of compact and miniaturized systems and can provide CGM, while handling safety provisions.

2.2 Glucose dependent dielectric properties of the blood

During the last decade, many researchers studied the interaction of the EM waves with the human tissues. Knowing that the dielectric properties of the MUT influence the waves in that medium, lots of work has been done to characterize the effects of different diseases on the dielectric properties of the biological tissues. In this context, using the EM-based techniques to non-invasively monitor the blood glucose levels has gained a lot of attention recently [37]. The effect of glucose variation on the dielectric properties of water and blood has been intensively studied. **Karacolak et al.** [38] studied the dielectric properties (permittivity and conductivity) of blood containing glucose concentrations ranging between 0 mg/dl to 16000 mg/dl over a frequency span from 0.5 GHz to 20 GHz using in-vitro human blood samples. The results show that both the relative permittivity and conductivity vary linearly with the change of glucose concentrations as shown in Figure 2.1. More precisely, the relative permittivity decreases as the frequency increases whereas the conductivity increases with the frequency. On the other hand, the permittivity decreases when the glucose levels increase and the conductivity varies insignificantly at low frequencies in response to glucose variation. The conductivity variation becomes clearer at higher frequencies where it varies inversely proportional to the glucose variation. However, for both parameters, small changes in the blood permittivity/conductivity is governed by large variations in glucose levels, equivalent to 16000 mg/dl, requiring a very sensitive EM-based sensor to capture these changes [38].

2.3 Frequency of choice and penetration depth

One of the main characteristics of any EM-based sensor is the operational frequency. In fact, the behavior of the dielectric properties of the MUT is checked in function of frequency. Such analysis is important in order to determine with certainty the appropriate frequency of operation of the proposed sensor. Figure 2.1 shows the effect of glucose concentration on (a) the dielectric constant and (b) conductivity for frequencies ranging from 500 MHz to 20 GHz [38]. **Karacolak et al.** [38] noted, in their study, that the variation of the dielectric constant due to glucose levels is somehow greater than the variation of conductivity, and these changes increase as a function of frequency. Hence, higher frequencies induce greater changes in terms of dielectric properties. Different frequencies have been adopted in the literature to capture the glucose variation and the obtained results are highly dependent on the MUT and the targeted location.

However, there is another important factor to consider when it comes to the frequency choice, which is the depth of penetration (DOP). Any wave transmitted into a lossy material will be attenuated after a certain depth. The DOP is the

are caused by the slight hand motion and the antennas displacements during the experiments. For good measurements, a change of 0.8 dB in the $|S21|$ response is detected for a total of 24 mmol/dl (432 mg/dl) variation in the glucose levels with a delay of 3 min between the glucose spike and the $|S21|$ spike as shown in Figure 2.6 (B). Additional measurements are done on a pigs's ear under IVGTT [45], Figure 2.6 (C). Different antenna's positions and distances are studied. A change of 0.6 dB in the transmission coefficients $|S21|$ at 60.25 GHz is achieved for a total glucose variation of around 40 mmol/l (720 mg/dl) with a delay of 13 min between the S21 spike and the glucose spike as shown in Figure 2.6 (D).
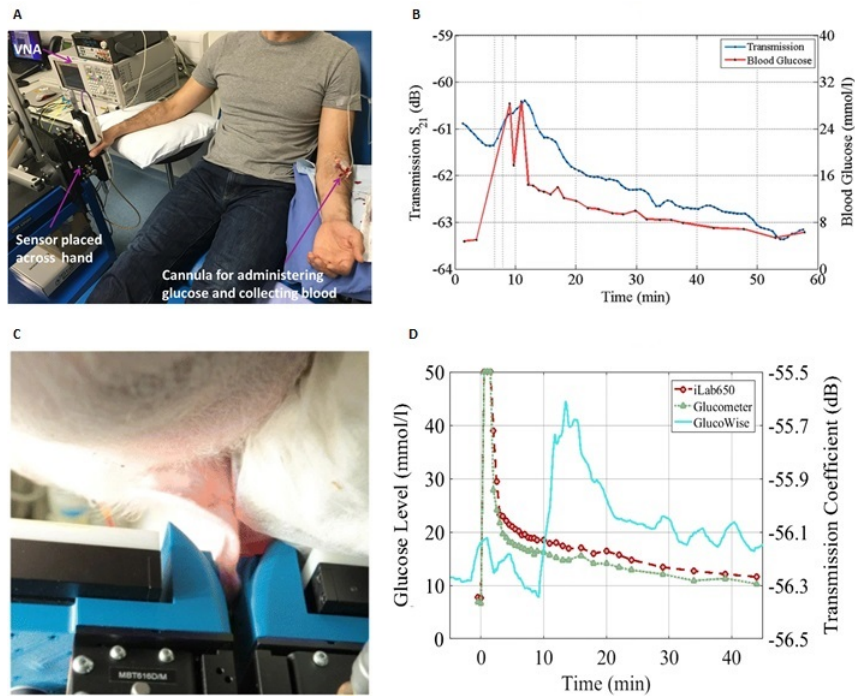
Figure 2.6: Microstrip patch antennas operating at millimeter-wave band for glucose monitoring. (A), The performance of the proposed system is testes in real-time in-vivo settings on human subjects. The antennas are placed across the area between the thumb and the index finger. (B), the antenna's transmission response S21 is compared with the actual glucose level variation across time. (C), the antennas are also tested on anesthetic pigs, where the antennas are placed across the pig's ear. (D), The glucose levels obtained by a traditional glucometer are compared with the transmission coefficient obtained by the antennas over time. Extracted from [43, 45].

2.4.3 Filters for glucose monitoring

A band-pass filter, operating at 1.9 GHz, is designed by **R. Baghbani et al.** [46] for noninvasive monitoring of glucose levels through the thumb finger. The filter is composed of a triangular patch with slots, as shown in Figure 2.7. The slots concentrate the electrical current across the finger. The reflection and transmission coefficients are monitored during a clinical trial on a healthy human subject. Linear variation of the $\mid S11 \mid$ and $\mid S21 \mid$ coefficients with respect to the glucose variation is achieved. However, such a design can be highly affected by the pressure applied by the human subject which may result in a bigger variation in the $\mid S11 \mid$ and $\mid S21 \mid$ parameters than that induced by the glucose variation.
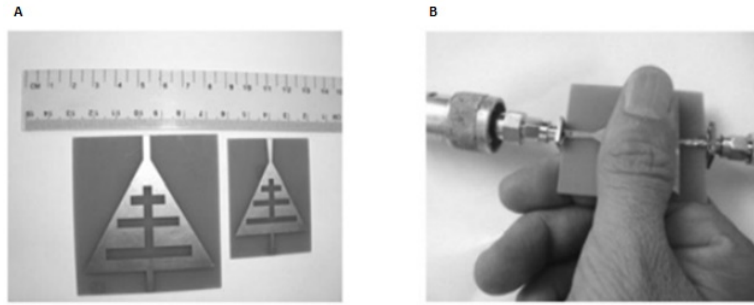
Figure 2.7: Band pass filter for glucose monitoring. (A), The fabricated band pass filter for blood glucose monitoring. (B), the proposed filter is tested on human subject where the finger of the subject is placed on the slots. Extracted from [46].

2.4.4 Resonators for glucose monitoring

Two-ports, on body patch resonator operating between 2.4 and 2.48 GHz is proposed by **T. Yilmaz et al.** [47] for glucose levels monitoring, shown in Figure 2.8. The resonator is tested on tissue mimicking phantom composed of 4 types of layers: wet skin, fat, blood and muscle, shown in Figure 2.8 (B). The input impedance of the resonator, Re(Zin) and Im(Zin), is monitored for four different blood layers containing different glucose levels ranging between 0 and 12 mmol/dl (equivalent to 2160 mg/dl). A total change of only -0.24 Ω and +0.38 Ω is achieved in the real and imaginary part of the input impedance, respectively, over the whole range of glucose variations.

Two split ring resonators, shown in Figure 2.9, operating around 1.4 GHz are proposed by **H. Choi et al.** [32, 48]. One of these resonators is used for glucose sensing and the other one is used as reference to calibrate out the temperature effect. First, in-vitro measurements using a Franz cell are conducted. The effect of different endogenous interference agents is studied. The authors are able to
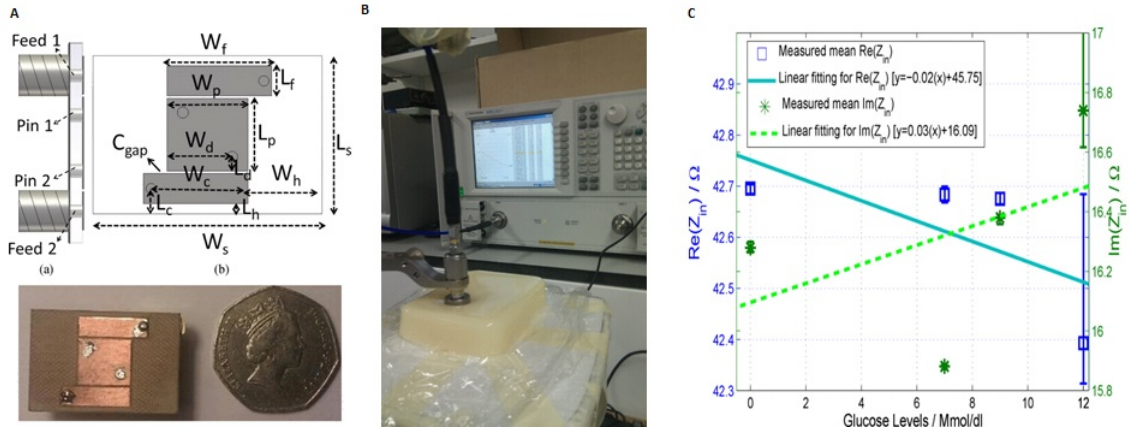
Figure 2.8: On body matched resonator for glucose monitoring. (A), the designed and fabricated prototype of the proposed resonator. (B), the resonator is tested on tissue mimicking phantom with 4 different levels of glucose. (C), the input impedance Re and Im are monitoring. Extracted from [47].

prove that their system is three times more sensitive toward the glucose variations in comparison to other sugars (maltose, fructose, and galactose). Additionally, their sensing system does not capture the variation of ascorbic acids and uric acids levels. These results highlight the selectivity of the proposed system toward the glucose variations and its ability to differentiate between the different blood constituents. As a final step, the authors conducted a human trial on 24 diabetic and non-diabetic patients. They converted the resonator response into glucose levels without discussing the utilized regression techniques neither the resonator's parameter/features used. Out of 214 collected point, 210 points are considered clinically acceptable as they happened to be in zone A and B of the Clarke error grid as shown in Figure 2.9 (C).

Another resonator operational at 4.8 GHz is designed to monitor the glucose levels at the finger level [49, 50]. The proposed resonator resemble to an interdigital capacitor, as shown in Figure 2.10. This configuration increases the concentration of the electrical fields and therefore improves the sensitivity of the system toward the blood permittivity changes induced by the glucose variation. In-vitro experiments on water/glucose solutions are conducted. Glucose concentrations are varied from 0 to 2000 mg/dl, as shown in Figure 2.10 (B). A total linear frequency shift of 32 MHz equivalent to a deviation of 11 KHz/(mg/dl) is achieved. However when tested on a human subject no frequency shift is detected.

Three versions of a two-port, open-loop, microstrip resonator, operating at 2, 5.7 and 8 GHz in free space are proposed by **C. G. Juan et al.** [51] mounted with polytetrafluoroethylene solutions containers. Figure 2.11 shows the microstrip resonator operating at 5.7 GHz. Microliter volume of water/ glucose solutions containing two different glucose levels (0% and 10%) are used to test the perfor-

Figure 2.9: Two port resonator for glucose monitoring. (A), The proposed blood glucose sensing system composed of a pair of rings. (B), The system is tested on human subjects and the proposed system is placed on the abdominal region of the patients. (C), the Clarke error grid showing the majority of the predictions in zone A and B. Extracted from [48, 32].
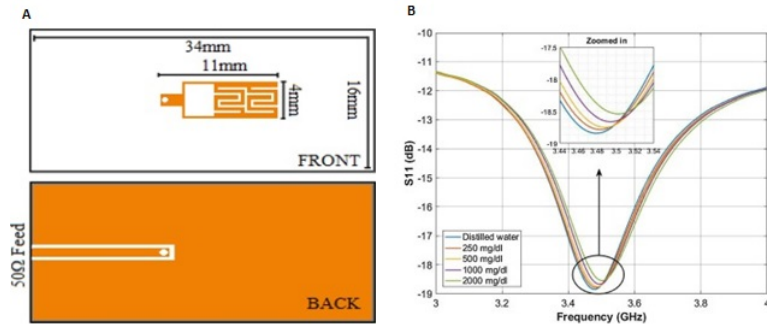
Figure 2.10: A resonator designed for glucose monitoring at the finger level. (A), the front and back layer of the designed resonator. (B), The resonator is tested on water with different glucose levels ranging from 0 to 2000 mg/dl. The $\mid S11 \mid$ response shows a sensitivity of 11 KHz/(mg/dl). Extracted from [49].

mance of these resonators. The authors monitored the glucose variations using the Q factor of the resonator as sensing parameter. The Q factor of the three resonators varied linearly with the glucose variation, however a total maximum change of only 7 units is achieved for a glucose change of 10% ($\sim 10000 mg/dl$).

2.5 The need for a new approach

It is clear from the previous section that various ranges of frequencies are investigated in the literature. Such investigation does not conclude with an ideal frequency as the optimal and most suitable one for non-invasive glucose monitoring EM systems. Frequencies in the low microwave range are utilized for deeper tissue penetration. Frequencies in the upper microwave and millimeter-
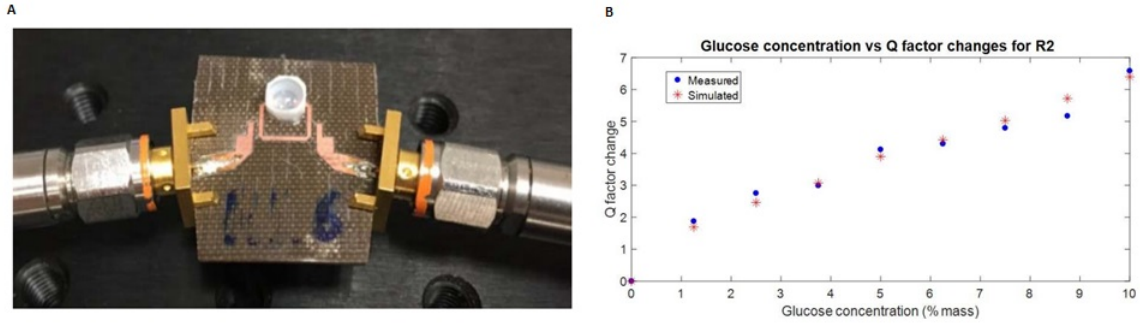
Figure 2.11: Two port, open-loop, microstrip resonators for glucose monitoring. (A), the fabricated resonator operating at 5.7 GHz mounted with a PTEE container. (B), The Q factor change is monitored for the different glucose levels showing a linear variation. Extracted from [51].

wave range can be used when deep penetration is not needed, especially when targeting thin tissues such as the earlobe, or the fingertip. The frequency of operation also affects the accuracy and precision of the system, considering that higher frequencies provide better sensitivity towards the glucose variations. Hence, the frequency of choice must be carefully selected during the development of a non-invasive glucose monitoring system.

Additionally, we can see that most researchers resort to 'standard' EM-sensors and very little optimization is done to adapt the proposed sensor to the anticipated body location. When developing a wearable continuous non-invasive EM-based sensor, the form of the final device must be taken into consideration from the beginning. Moreover, most of the proposed sensors are tested only on water/glucose solutions. When tested in real-time monitoring settings on human subjects many of the techniques in the literature fail to provide good sensitivity towards the glucose variations mainly due to environmental perturbations. Hence any noninvasive glucose monitoring system based on EM technology must also take into consideration the different perturbing factors.

17

Chapter 3

Wearable, on-body matched, Vasculature anatomy inspired EM-Based sensors

The sensor is the most important component of our system. To improve the sensitivity of the EM-based sensors many design aspects were considered. In this chapter we introduce a novel noninvasive wearable approach that relies on flexible EM-sensors, while focusing on the effective tailoring of EM waves to directly monitor the glucose level from blood (US Patent No. PCT/US2018/054627) [27]. The design details of the proposed EM-sensors that target two different on-body locations and rely on multi-operating frequencies is discussed. The frequency of choice and the targeted sensing location are discussed, followed by the human phantom models utilized during the design of the antennas. This chapter presents also the simulated and fabricated results for the designed antennas. Finally the safety considerations are presented.

3.1   Antenna design concept

The first step to develop the EM-based noninvasive glucose monitoring system is to design a sensing element (1) exhibiting high sensitivity towards glycemic fluctuations, (2) achieving high accuracy along the hypo to hyper-glycemic range and (3) maintaining good performance when loaded with a lossy medium (the human body).
To achieve high sensitivity towards the glucose variations, different aspects are considered. First, the proposed sensors are designed to operate in the upper ultra-high frequency (UHF) and lower microwave bands between 500 MHz and 4 GHz. The frequency choice is one of the main characteristics during the design of any EM-based sensor. We can find different studies in the literature indicating good correlation between the EM-sensor's parameters and the glucose levels in

18

the MHz and the GHz range. When we selected the operational frequency range of the proposed antennas, we took into considerations different factors. These factors include: the targeted location, DOP, sensitivity, and size of the device for wearability. To achieve a good functional trade-off between the penetration depth and the sensitivity towards the glucose variation, detected at the targeted locations (hand and arm), the proposed sensors are optimized to have multi-bands in the UHF, L- and lower S-bands ranging between 500 MHz and 4 GHz. This frequency range allows enough penetration for the waves to reach the targeted veins and arteries while maintaining good sensitivity as discussed in Chapter 2. Secondly, the proposed structures mimic the vasculature anatomy as shown in Figure 1.1 (A). We verify, during in-vitro experiments, in Chapter 5, that by concentrating the EM waves directly towards the blood network we attain a higher sensitivity towards the glucose variations. Additionally, the multiple slots result in a multi-band response which allows the monitoring of glucose levels across a wide range of frequencies. According to the study conducted by **Yilmaz et al.** [37], a multi-band approach can provide better sensitivity/selectivity towards the glucose variations when compared to single frequency sensors. On the other hand, when it comes to comparing narrow-band to wide-band sensors, narrow-band sensors were able to achieve a better sensitivity towards the small variation of the effective permittivity [37]. We demonstrate later that this, in turn, improves the accuracy of glucose levels estimation using multi-variate regression-modeling techniques.

Moreover, the proposed antennas are designed when loaded with a human model. The operation of an antenna does not depend only on the physical dimensions of its structure, but also on the permittivity of the medium under test. Since in our application the antenna radiates near the human body, which is considered a high loss medium, a new design approach is adopted. Such approach matches the antenna to the human body and is named here "on-body matching". Traditional antennas suffer from strong reflections of the incident waves when in contact with a lossy medium such as the human body, especially at the air-skin interface. Such mismatch allows only a small percentage of the incident waves to penetrate the body [52]. Hence, the incident signal is degraded due to the mismatching of these antennas caused by the lossy medium. By matching the antenna to the human body, the reflections at air-skin boundary are reduced and more energy is transmitted into the body allowing a more reliable analysis of the blood glucose variations [52]. As a result, the proposed antennas are designed to operate when loaded with a human model using ANSYS Electronics Desktop Simulator (AED) [53]. Matching the antennas to the human body has been proven to be as of utmost importance to our application.

3.2 Sensing Locations

One of the very important factors to take into account when proposing a wearable sensor for continuous glucose monitoring system, is the sensing location. Different locations could be considered. As a first prototype, we targeted the hand as a sensing area. A wearable glove will ensure comfort for the patients in different scenarios (work environment, during physical activities, at school and during sleep), especially for kids, and athletics. It will also ensure good contact between the sensor and the hand with great stability. The radiating slots are inspired by the shape of the arteries and veins in a human hand, shown in Figure 3.1, mainly the deep palmar arch, the superficial palmar arch, the palmar digital arteries and the dorsal metacarpal veins; the radial artery and the ulnar artery are two main arteries that supply blood to the hand. The radial artery wraps around the thumb and comes across the deep palm in an arch shape forming the deep palmar arch. The ulnar artery comes across the palm also in a shape of arch forming the superficial palmar arch. The deep palmar arch and the superficial palmar arch supply blood to the different fingers though small branches. These branches are referred to as common digital arteries. On the other hand, the blood is drained from the hand by the dorsal venous plexus and via the cephalic vein and the basilic vein.
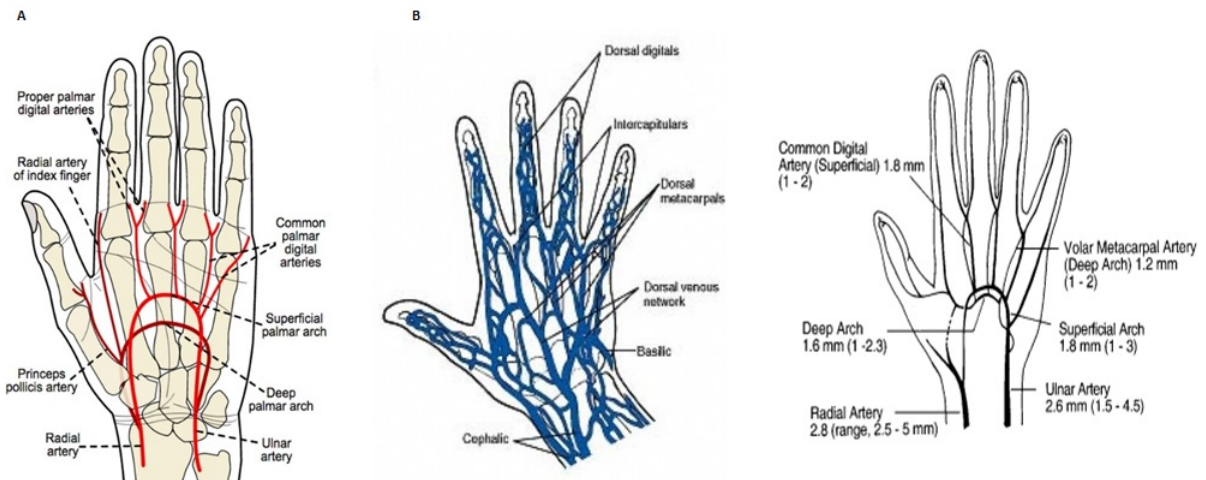
Figure 3.1: Hand vascular anatomy].(A), The antenna's slots are biologically inspired by the hand's blood vessels; the two semi-circle slots are inspired by the deep and superficial palmar arches, the small rectangular slots at the peripherals are inspired by the common palmar digital arteries and the middle small slots are targeting the dorsal venous network. (B), The average diameter of the different targeted blood vessels. Extracted from [54, 55].

After the hand, we targeted the lower leg as the second sensing area. The designed antennas are intended to be fitted inside a sock. The wearable sock will ensure

comfort for the patients, especially during sleep for kids. It will also ensure good contact between the sensor and the leg. The radiating slots are inspired by the shape of the arteries and veins in a human lower leg, shown in Figure 3.2, mainly the shape of the peroneal venae comites and posterior tibial venae comites. The sensor is used to transmit EM waves into human tissues in areas in close proximity to the main vanea comites veins.
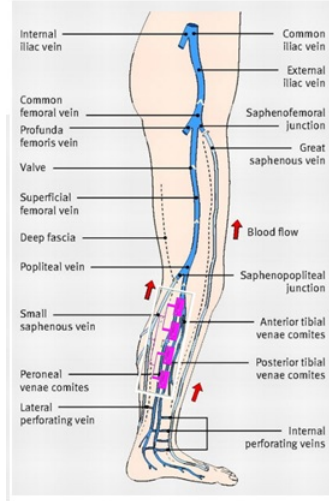
Figure 3.2: Leg vascular anatomy. The antenna's slots are biologically inspired by the leg's blood vessels; the two long slots are inspired by the mainly the shape of the peroneal venae comites and posterior tibial venae comites network.

Phantom used during the design of the antennas.
The on-body antenna is designed to operate in the presence of a human model parallel to the top sensing layer side of the antenna. The computational phantom VHP-Female v. 2.0 is used during the design of the proposed antenna. It is composed of 26 different tissue types and 184 individual tissue parts, in form of finite-element triangular surface meshes. The image dataset of each tissue part is obtained from the Visible Human Project®-Female dataset available at the National Library of Medicine [56]. The dielectric properties of the material are obtained from IT'IS Database [57]. To simplify the model and reduce the simulation time rectangular models were used. The material (in terms of dielectric properties) of this model are exported from the VHP-Female phantom as shown in Figure 3.3. The electrical properties of each layer, permittivity and conductivity are in function of frequency and they are exported from the IT'IS Database [57]. The human phantom is positioned in the radiative near-field region of the antenna. The radiative near field region of the antenna is calculated using the following equation:

$$0.62\sqrt{\frac{D^3}{\lambda}} < R < \frac{2D^2}{\lambda}$$

Where: D is the antenna's dimensions (length or diameter) and λ is the wavelength [58].
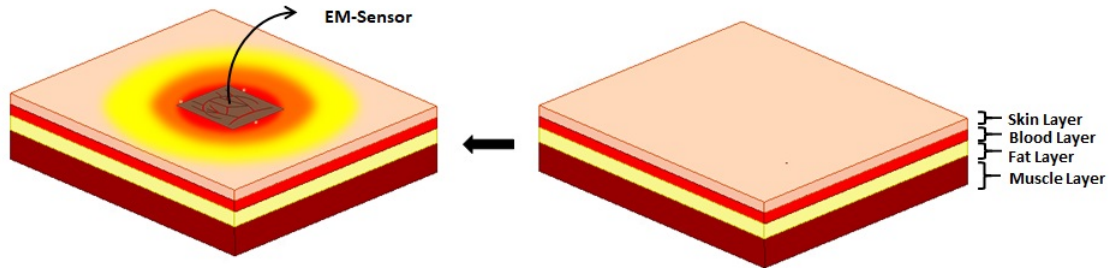
Figure 3.3: Human Phantoms. To simplify the model and to reduce the simulation time a rectangular hand model was used. The material (in terms of dielectric properties) of this model are exported from the VHP-Female phantom. The model composed of 4 layers: skin, blood, fat and muscle. The width of each layer are 1.5mm, 1mm, 1mm and 2mm respectively. The electrical properties of each layer, permittivity and conductivity are in function of frequency and they are exported from the IT'IS Database.

3.3 EM-Sensors design and operation

As a proof of concept, our first prototype is designed to mimic the blood network at two different locations: the hand and the leg. The designed antenna targeting the hand vessels is integrated as a part of a wearable glove, which monitors the blood glucose levels by sensing the hand's vasculature network. The antenna targeting the leg vessels is incorporated as part of a sock. Such diverse incorporation of the sensing components in multiple locations enables a higher accuracy and faster responsiveness in tracking blood glucose levels. Several prototypes catered for both sensing locations are developed. Conceptual prototypes are tested on semi-flexible substrates. A full flexible topology is then adopted to better fit the nature of the human body.

3.3.1 Glove sensors

Using the mentioned ideas, we designed two prototypes; a semi-flexible and a flexible antenna, shown in Figure 3.5 and Figure 3.7 respectively. Both antennas are designed and simulated by means of the ANSYS AED [53]. They are optimized and validated when loaded with human tissues. The proposed glove sensors are composed of three layers: the top sensing layer comprises the radiating slots, the middle layer includes the dielectric substrate, and the bottom layer contains the
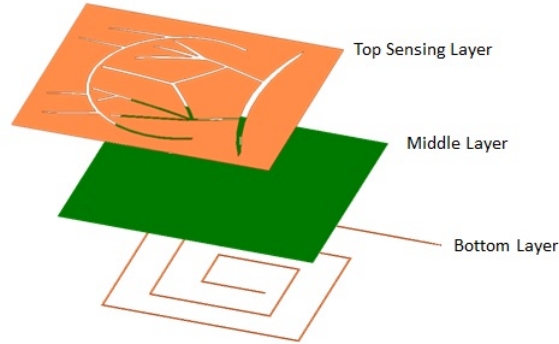
Figure 3.4: glove sensor layers. The top, middle and bottom layers of the glove sensor simulated using HFSS.

feeding line as shown in Figure 3.4.

The radiating slots are inspired by the anatomy of the arteries and veins in a human hand; mainly it emulates parts of the deep palmar arch, the superficial palmar arch, the palmar digital arteries and the dorsal metacarpal veins. The feeding structure consists of a spirally shaped feeding transmission line having 50Ω input impedance. The spirally shaped feeding line enhances the coupling between the feeding lines and the slots on the top layer of the antenna, allowing the various slots to be active and hence, enhancing the multi-band behavior of the antenna.

The antenna's slots are excited by relying on EM coupling through a spiral feed line. They are designed to operate in the UHF and lower microwave frequency band ranges. The dimensions of the substrate and the integrated slots that mimic the blood network of the hand are optimized to operate with great matching at the desired frequencies of operation, while being loaded by the human hand model. The width of the slots are optimized based on the average diameters of the different blood vessel, which range between 1.2 mm to 2.8 mm [55]. While the length of the slots are optimized to have multiple operational frequencies between 0.5 GHz and 3 GHz. The hand ranges between 167.9 mm to 187.9 mm in terms of length and between 75.2mm to 83.6mm in terms of breadth for women and men respectively [59]. After optimization, the final dimensions are set to 70x70 mm^2 for the semi-flexible antenna and 70x80 mm^2 for the flexible antenna. This size is optimized for integration in a wearable glove.

The antenna is designed to operate in the presence of a hand model parallel to the top layer side of the antenna with a 0.5 cm separation as shown in Figure 3.3. For the purpose of simulation, the hand model comprises 4 rectangular layers with different dielectric properties: skin, blood, fat and muscle. The width of each layer are 1.5mm, 1mm, 1mm and 2mm respectively. The dielectric properties of these tissues are extracted from the IT'IS Database [57] and set in the ANSYS AED [53] (Figure 3.3).

Fabrication

The glove sensors were fabricated on two types of substrates. Rogers RO3003 [60] substrate material of 0.5 mm thickness is used for the semi-flexible antenna. However, to adapt the antenna structure to the curvature of the hand, the flexible antenna is designed by relying on Polyethylene Terephthalate (PET) substrate material of 136 um thickness. The semi-flexible substrate was fabricated using computerized numerically controlled (CNC) milling machine. For the second type of substrate we used silver as conductive material and ink-jet printing for fabrication.

Semi-flexible antenna operation

The fabricated prototype of the semi-flexible antenna design is shown in Figure 3.5. To validate the performance of the fabricated semi-flexible sensor, its scattering parameters were measured.
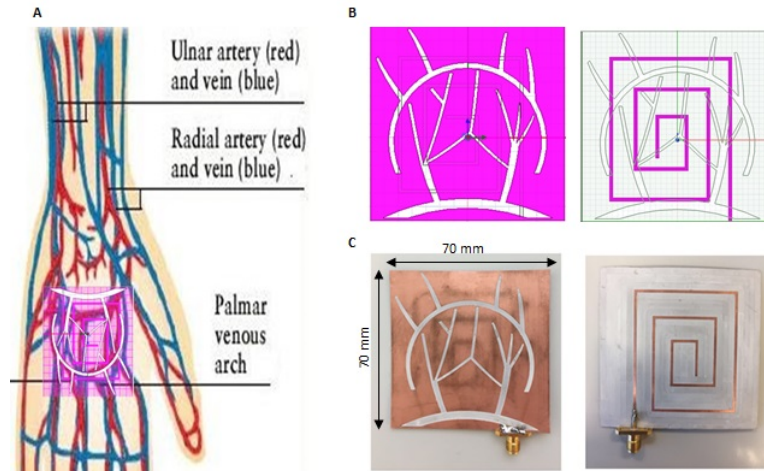
Figure 3.5: Semi-flexible antenna design. (A), the slots are inspired by the vasculature anatomy. (B), the top and bottom layers of the Semi-flexible simulated using HFSS. (C), the fabricated prototype on RO3003 substrate.

Figure 3.6 shows a comparison between simulated and measured reflection coefficients S11 in free space. The antenna's multi-band operation is verified as we can see in Figure 3.6 (A). As we mentioned previously, one of the main characteristics of the proposed antenna is the on-body matching. Figure 3.6,(B) presents the measured S11 in free space compared with the measured S11 when loaded with a human hand. This matching is well preserved, meeting our design objectives.
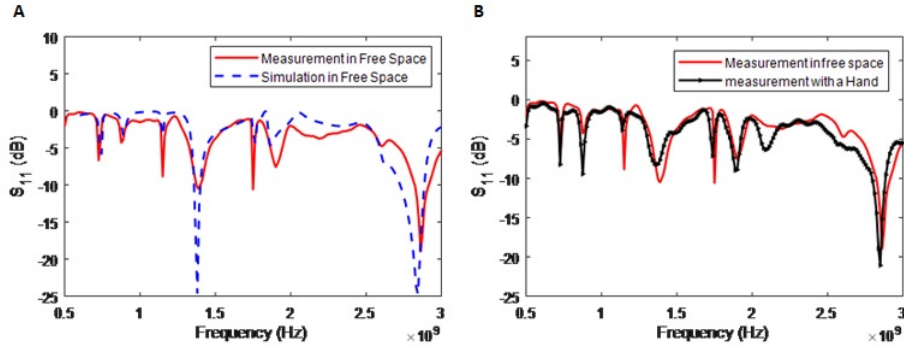
Figure 3.6: Semi-flexible antenna response.(A), the measurement versus simulation S11. The small deviation is due to fabrication errors. (B), the antenna's reflection coefficient, S11, measured in free space is almost preserved when the antenna is loaded with a human hand.

Flexible antenna operation

The flexible antenna is fabricated on a 136μ m thick PET substrate ($\epsilon r = 2.99$) using the Dimatix DMP-2850 inkjet printer with the DMC-11610 nozzles [61]. This printer works in a "drop on demand" manner where a voltage is supplied to a piezoelectric system, that in turns generates droplets on the substrate. The PET is first exposed to a UV ozone treatment for 2 minutes and 15 seconds, to promote better wetting conditions for the printed ink on the substrate. This treatment is often helpful when the substrate's surface is hydrophobic while the printed ink is hydrophilic. The substrate is then cleaned with Ethanol before being placed on the printer's platen heated up to 40°C. The cartridge is then filled with the JS-A102A silver nanoparticles-based ink from Novacentrix with 40% silver (Ag) content. Before placing the cartridge in the printer, the ink is sonicated for 2 minutes to avoid nozzles clogging during the printing. Three layers of JS-A102A are deposited on the substrate to ensure that all gaps are filled, and the printed surface is continuous. The substrate is then placed for 10 minutes on a 100°C heated plate to dry the solvent before completely sintering the ink in the oven at 160°C for 30 minutes.

The fabricated prototype of the flexible antenna is shown in Figure 3.7. A comparison between simulated and measured reflection coefficients S11 is presented in Figure 3.8 (A). The results show an excellent matching between the simulated and the measured measurements with multi-band behavior in the frequency range [0.5, 3 GHz]. The on-body matching is verified in Figure 3.8 (B) where the measured S11 in free space are compared with the measured S11 recorded when loaded with a human hand. The on-body matching characteristics of this antenna is also very clear when it is loaded with human hand. This matching is well preserved and even enhanced at certain frequencies, meeting our design objectives.

25
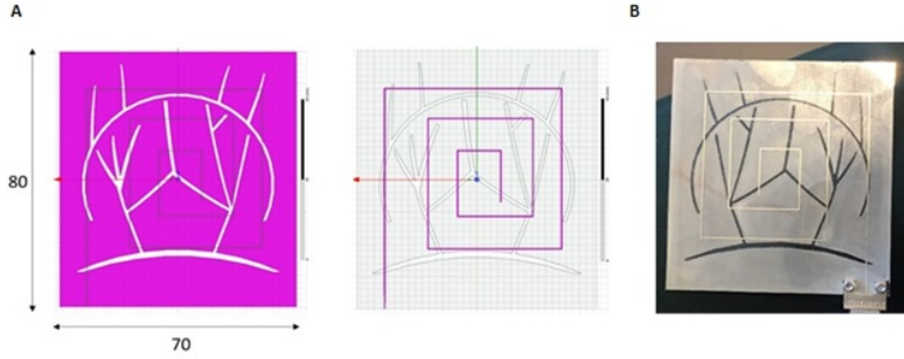
Figure 3.7: Flexible antenna design. (A), the top and bottom layers of the Semi-flexible simulated using HFSS. (B), the fabricated prototype on PET substrate.
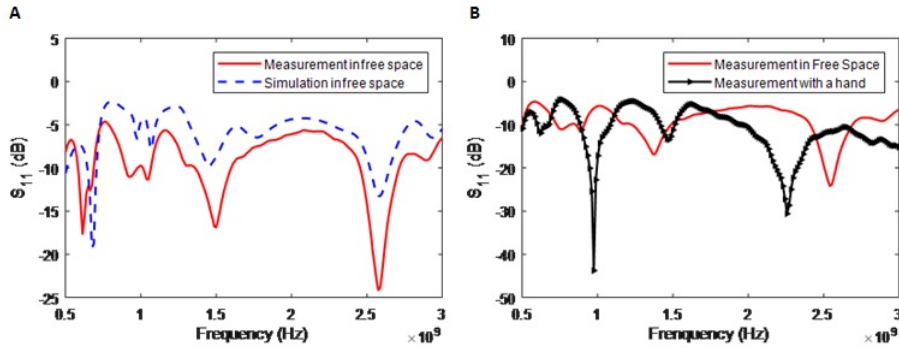
Figure 3.8: Flexible antenna response. (A), the measurement versus simulation S11. The small deviation is due to fabrication errors. (B), The antenna's reflection coefficient, S11, measured when loaded with human hand showing the on-body matched characteristic of the proposed antenna.

Bending analysis

It is important to note that the flexibility of the proposed system (Figure 3.9) and its wearability are intended to enhance the sensor's compatibility to expected body movements as well as adaptability to body surface. We evaluated the flexible antenna's performance in two different situations; first, we tested the antenna's performance over curvatures of different bending diameters. The flexible antenna maintained a stable performance for several configurations over planar or curved surfaces, as shown in Figure 3.9 (A), with minimal difference between the flat and bended S11 response of the antenna. For this experiment, we used cylindrically shaped foam surfaces with curvatures of 10 cm, 12 cm and 18 cm diameter respectively. Secondly, the flexible antenna is fixed inside a glove and separated from the skin surface by a flexible foam (with a thickness of 0.5 cm) allowing the antenna to move with the human body (Figure 3.9 (B)). Measurements with

fingers open and closed showed that the movements of the fingers do not affect the S11 parameters.
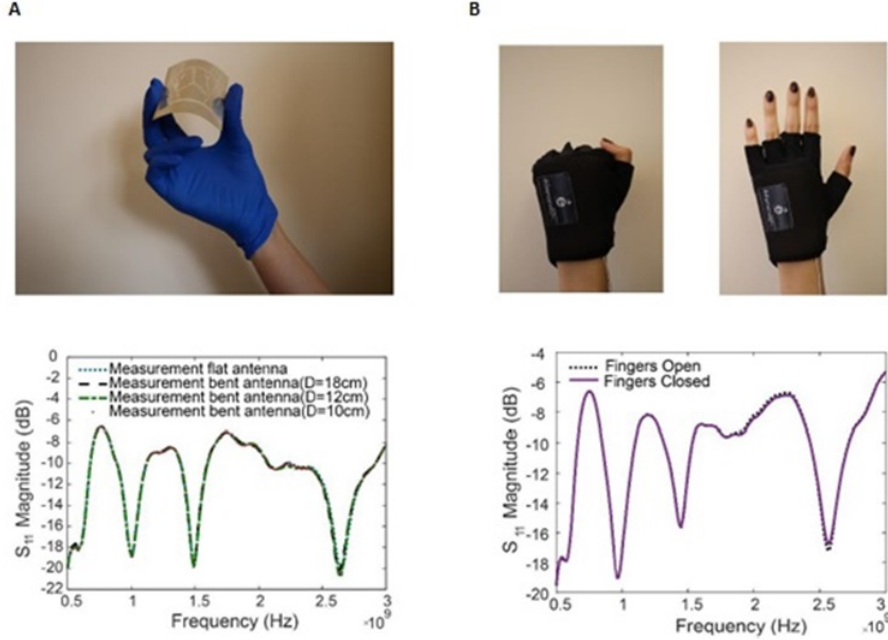
Figure 3.9: Bending analysis of the flexible antenna. (A), the effect of bending the antenna with different bending diameters on the S11 parameters. (B), The effect of opening and closing of the fingers on the flexible antenna's S11 parameters when integrated into a glove.

3.3.2 Sock sensors

To achieve high sensitivity towards the glucose variations, the same concept design, described previously, is considered for the sock sensors. The proposed EM sensors are designed to operate at multiple frequencies in the frequency band ranging between 0.5 and 4 GHz. We propose three different antennas targeting the lower leg's veins and arteries. These antennas are designed and simulated by means of the ANSYS AED [53]. Design #1 is a micro-strip patch antenna comprising slots following the leg's vessels as shown in Figure 3.11. Design #2, presented in Figure 3.12 is an antenna array composed of 4 identical elements. Design #3, shown in Figure 3.13, is an antenna quasi-array composed of 4 elements with non-identical slots, matching the targeted underlying vasculature anatomy.

The proposed antennas are composed of three layers: the top sensing layer comprises the radiating slots and the microstrip line feeding network used to power the antenna. Quarter-wave transformer (QWT) technique is utilized to provide

Chapter 4

Modeling regression to convert the antenna's response into glucose levels

In this chapter we present the means to convert the S-parameters into absolute glucose values. We first discuss the signal and data processing techniques. After that we present the different regression techniques utilized to convert the antenna's response, including the S11 magnitude and the S11 phase, into glucose levels, along with the feature selection techniques.

4.1 Data analysis

Our main objective is to model the correlation between the sensors' responses (S-parameter magnitude and phase) and the blood glucose levels. Since the glucose levels are continuous variables, regression-based modeling is required to create this mapping between: 1) $X \in \mathbb{R}d$: the d-dimensional input variables' vector (also referred to as the features' vector) which corresponds to the measured S-parameter obtained at the different frequencies over the operating frequency range and 2) $Y \in \mathbb{R}$ the outcome variable which corresponds to the reference glucose level. The data analysis and regression analysis parts are carried out using MATLAB R2017a software [63]. We relied on individual training of regression model to obtain the absolute levels and we compared the obtained values with the ones measured by a commercial, finger-prick glucometer.

4.1.1 Data collection

During the different experiments, the antenna's scattering parameters and the corresponding reference blood glucose levels (measured using a traditional invasive technique [64]) were collected using a portable VNA. The acquired data

from the antenna consisted of S11 magnitude and S11 phase corresponding to 201 different frequency points within the frequency sweep, ranging between 0.5 GHz and 4 GHz, resulting in different input variables for each reference blood glucose level.

4.1.2 Pre-processing of the data

For every reference glucose measurement, ten consecutive recordings of the antenna's response (S11 magnitude and phase) were acquired. The resultant set of replicated signals then undergoes signal averaging in order to eliminate the random noise introduced by the VNA. This technique averages out the uncorrelated noise, and helps improve the signal to noise ratio.

Around 402 features are measured for each reference glucose level. However, the S11 behavior trend in response to glucose level variation is very similar for frequencies that are nearby to each other. Therefore, to minimize redundancy between features, without loss of generality, 21 equally spaced frequencies were selected with a step of 0.125 GHz. The S11 magnitude and phase corresponding to these frequencies were then considered as input variables, resulting in 42 features in total. Once averaging is performed, the different features, which correspond to magnitude and phase values, are normalized between 0 and 1.

For the in-vivo experiments, the data sets corresponding to each OGTT experiment were processed separately. In the multi-sensing experiments (Chapter 7), where additional sensors are added to the system, the output of each sensor was normalized between 0 and 1 and used to create the regression model.

Finally, since the invasive reference glucose levels were taken every 15 minutes whereas the CGM using the proposed antennas were taken every 5 minutes, cubic spine interpolation [65, 66] was used for time synchronization between the two measurements.

4.1.3 Pseudo code explaining in details the data collection and processing steps

$- - --$

Outputs:

X: normalized feature vectors.

Y: reference glucose level dependent variable.

$- - --$

For each experiment,

Data collection Phase (Pre-processing):

- Every 5 minutes collect from the sensor the ith observation data points: $X_{S:pre}(i, :) = \{x_{S:pre}^j(i, :)\}$ with a total of 1206 features in $X_{S:pre}$, where i $\in$ [1, 23] represents the observation number, j $\in$ [1, 2] represents each of S11 magnitudes

35

and phase respectively, and each $x^j_{S:pre}$ comprises 201 features obtained over the frequency range [1-4] GHz,
- Every 15 minutes, perform a standard glucose monitoring, to collect the reference glucose level, collect: $y_{ref:meas}(m)$

Data Processing Phase:

- $Y = \{y_{ref(i)}\}$, where $y_{ref}(i)$ represents the reference glucose level obtained from $y_{ref:meas}(m)$ and/or using cubic splines for the ith observation point if $y_{ref:meas}(m)$ is missing at that time point to obtain a total of around 23 ref GL over the duration of the OGTT .
- $X_s = \{X^k_S\}$ is the set of ~ 42 feature vectors obtained by sampling $x^j_{S:pre}$ at steps of 0.125 GHz for all j. Therefore, $X^k_S(i)$ is the value of feature k for observation i, where $k \in [1, \ 42]$, and $i \in [1, \ 23]$.
- We normalize each feature vector, X^k_S, across all observations as follows.

$$X^k_{norm}(i) = \frac{X^k_S(i) - min(X^k_S)}{max(X^k_S) - min(X^k_S)}$$

- $X = \{X^k_{norm}\}$

4.2   Feature selection

To identify the features exhibiting the best sensitivity towards the glucose levels, and to reduce the dimensionality of the data, feature selection methods are applied. For this purpose, two different feature selection methods are considered: the filter and the wrapper methods.

1. Filters can be considered as pre-processing steps, and they are totally independent of the modelling step. Features are selected based on their statistical significance in terms of, for example, their correlation with the outcome variable. In this work, the significance of the features is calculated using the Pearson correlation coefficient (PCC). The PCC (61) between the input data X (S11 coefficient magnitude and phase) and the output Y (the reference glucose levels) is calculated using the following equation:

$$R = \frac{C_{xy}}{\sigma_x \sigma_y}$$

Where C_{xy} is the covariance between x and y and σ_x and σ_y are the standard deviation of x and y respectively. R ranges between -1 and 1, where the two extremes 1 and -1 present a perfect linear correlation between y and x (positive and negative respectively) and zero means there is no correlation between the two variables.

2. In wrapper techniques, the optimal feature subset is selected based on the regression model output. In this work we rely on the forward feature selection

(FFS) wrapper method where we start with zero features in the subset and for each iteration we add the feature providing the lowest model output mean percentage error. This method can provide a better selection of the features however it is usually computationally expensive.

4.3   Model evaluation

For the feature selection (and the kernel selection in the Gaussian Process models), 10-fold cross validation is utilized to minimize the feature subset selection bias; the data sets are divided randomly into 10 subsets with equal size. For each round, one out of the 10 subsets is used as a testing set and the remaining subsets are used as training sets. After 10 rounds, the mean percentage error is calculated (also called cross-validation error). This procedure is repeated for each feature set and the optimal feature set and kernel correspond to the combination providing the lowest cross-validation error.

Once the optimal feature subset is selected, the data sets are randomly divided into two sets: 2/3 as training sets used for model building and 1/3 as testing sets to assess the performance of the model. Because of the limited number of observations in the dataset, this process is repeated 10 times to cover as many glucose levels as possible. The glucose estimations, from the testing sets, obtained during the 10 repetitions are provided along with their mean value.

4.4   Regression techniques

In our application, we are faced with two main restrictions for purposes of the choice of the suitable regression techniques: 1) the small size of the dataset due to the limited number of reference glucose points, and 2) the high dimensionality of the dataset. To overcome these restrictions, and based on literature [67, 68, 69, 70, 71], the performance of several suitable regression techniques is evaluated: as such, Partial Least Square (PLS), Least Absolute Shrinkage and Selection Operator (LASSO), Gaussian Process (GP) and locally weighted PLS (LW-PLS) methods were considered, and their performance were compared using different performance metrics.

4.4.1   PLS

PLS is a regression methodology that handles the dimensionality reduction problem while maximizing correlation with the outcome. It creates new regressors by linearly combining the original features based on their univariate effect on the outcome variable. These regressors, called latent variables or principal components, are estimated by maximizing both their variance and their correlation with the outcome variable [68].

4.4.2 LASSO

LASSO, on the other hand, is a regression method that performs L1 regularization and feature selection. LASSO technique enforces sparsity and hence sets many feature coefficients to zero keeping only the features having the strongest effect on the estimation of glucose levels. In some cases, some variables set to zero may contain valuable glucose-related information [67].

4.4.3 LW-PLS

In LW-PLS, PLS is utilized for local modeling relying mainly on the similarity between the new query and the existing data points [69]. Whenever an estimation is needed for a new query xq, a local model is created from samples located in the neighborhood around the query using the following steps:
1. Calculate the similarity matrix $\Omega = (diag(\omega_1, \omega_2, \ldots, \omega_N))$
2. Multiply X and Y by the root square of the similarity.
3. Perform a PLS regression analysis using the weighted X and Y obtained from step 2.
4. Calculate yq.
The definition of the similarity between the query and the existing samples has a major influence on the LW-PLS performance. Here the similarity is based on the weighted Euclidean distance dn and it is given by the following equation:

$$\omega_n = exp\left(-\frac{d_n}{\sigma_d \varphi}\right)$$

where: $d_n = \sqrt{(x_n - x_q)^T \Theta (x_n - x_q)}$, $\Theta = diag(\Theta_1, \Theta_2, ..., \Theta_M)$, σ_d is the standard deviation of d_n, φ is a localization parameter, $\Theta \in \mathbb{R}^{M \times M}$ is a weighting matrix, and Θ_M is the weight for the m-th input variable. Here Θ_M is defined as the absolute value of the m-th input variable's regression coefficient of a global PLS model. φ is chosen to optimize the mean square error of the LW-PLS regression model [69].

4.4.4 GP

GP is a probabilistic modeling technique that provides both a prediction and an uncertainty on the prediction. It uses a "distribution across an infinite function space to determine functions that are concordant with the underlying training data set" [72]. It is a non-parametric kernel based probabilistic technique. The covariance function (or kernel function) comprises one of the most important characteristics of the GP. Generally, in supervised learning, it is most likely that the input data with comparable features' values (Xi), produces similar output (Y). In GP, the covariance function K(xi, xj) is responsible for comparing the input feature sets, xi and xj, and finding this similarity (where $i \neq j$,i=1..n and

xi and xj d by 1 vectors and d is the number of features, and n is the number of sample points). This covariance function can take different forms. The kernels we use are defined by two main hyperparameters: the standard deviation σf and the characteristic length scale σl. Using the exact GP regression method, the different model parameters are estimated. One approach for estimating the model parameters, which are the kernel hyperparameters and the noise variance, is by maximizing the likelihood P(y| X) as a function of kernel parameters and noise variance. To choose the best covariance function, five different kernels including exponential, squared exponential, matern 32, matern 52 and rational quadratic are tested [72]. These five covariance functions are used to create five GP regression models evaluated with different sets of features.

Derivation. The model parameters are estimated form the training set. For the test set, the predicted glucose levels are estimated as follow [72]: If we assume additive input, the covariance of the glucose levels (y) is expressed as followed:

$$cov(y) = K(X, X) + \mu I$$

With μ noise term.
For any point in the test set, the joint distribution of the reference glucose level (y) and estimated glucose level (y_*) is written as followed

$$\begin{bmatrix} y \\ y_* \end{bmatrix} \sim N \left(0, \begin{bmatrix} K(X, X) + \mu I & K(X, X^*) \\ K(X^*, X) & K(X^*, X^*) \end{bmatrix} \right)$$

This joint distribution is utilized to estimate the glucose levels for the GP regression using the training glucose levels:

$$p(y_* \mid X, y, x^*) \sim N(\overline{y}_*, cov(y_*))$$

Where the mean is calculated as followed:

$$\overline{y}_* \doteq \mathbb{E}[y_* \mid X, y, x^*] = K(X^*, X)[K(X, X) + \mu I]^{-1} y$$

And the covariance is calculated with

$$cov(y_*) = K(X^*, X^*) - K(X^*, X)[K(X, X + \mu I]^{-1} K(X, X^*)$$

The mean can be also calculated by minimizing the least squares problem, as described in [72]. Five GPR modules are built using the five kernels. And the kernel providing the lowest mean percentage error is selected for the estimation of the glucose levels.

Estimation of the glucose levels. The kernel and the feature subset providing the lowest cross-validation error, during the feature selection step, are

selected and used to construct the model for glucose estimation for each experiment separately. As we mentioned in the evaluation model section, the dataset is randomly divided into two sets: 2/3 to build the model and 1/3 to test its performance. Because of the limited number of observations in the datasets, this process is repeated 10 times.

While PLS, LASSO and LWPLS are considered linear regression techniques, GP is a nonlinear regression methodology. The GP is a probabilistic modeling technique that provides both the prediction and the uncertainty on the prediction. The advantage of this technique is that it relates one sample point to the other using a covariance function (kernel) [72]. The nonlinear kernels in turn capture the nonlinearities in the system. LASSO performs feature reduction implicitly. For PLS/ LWPLS deal with dimensionality reduction, 10-fold CV is utilized to select the critical number of principle components. Feature selection techniques are explicitly applied for GP models.

4.5 Performance metrics

To verify the accuracy of the estimated glucose levels and to compare the performance of the different regression techniques, a set of assessment criteria commonly used in the diabetes research community are computed. These assessment criteria include the mean percentage error also known as mean absolute relative difference and the standard error of prediction:

1. The mean absolute relative difference (MARD) [73], illustrates the relative percentage errors:

$$MARD = \frac{1}{N} \sum_{i=1}^{N} \frac{|y_i - \widehat{y_i}|}{y_i} \times 100$$

2. The standard error of prediction (SEP), measures the accuracy of prediction:

$$SEP = \sqrt{\frac{\sum_{i=1}^{N} (y_i - \widehat{y_i})^2)}{N}}$$

With: y_i the reference glucose levels of the N samples and $\widehat{y_i}$ the estimated glucose levels provided by the regression models.

While MARD and SEP compute the deviations of glucose estimates from the reference from a statistical perspective, it doesn't take into consideration the clinical impact of these deviations. Clark Error Grid (CEG) analysis, on the other hand, offers a means to measure the performance while taking into consideration the clinical relevance of the differences between the estimates and the reference glucose values. This performance criterion is specifically dedicated to evaluate the

point accuracy of the glucose sensors. It displays the estimated glucose levels versus the reference levels in a scatter plot divided into five zones: A to E, as shown in Figure 4.1. Zone A indicates that the estimated glucose levels within 20% of the reference values. Zone B comprises the estimated glucose levels that are outside the 20% but wouldn't induce any inappropriate treatment. Zones A and B are considered safe and are clinically acceptable. When the estimated glucose levels fall into zones C/D/E, the results are not safe and are considered clinically unacceptable. The estimates in these zones will lead to clinically unnecessary or even dangerous treatments [74].
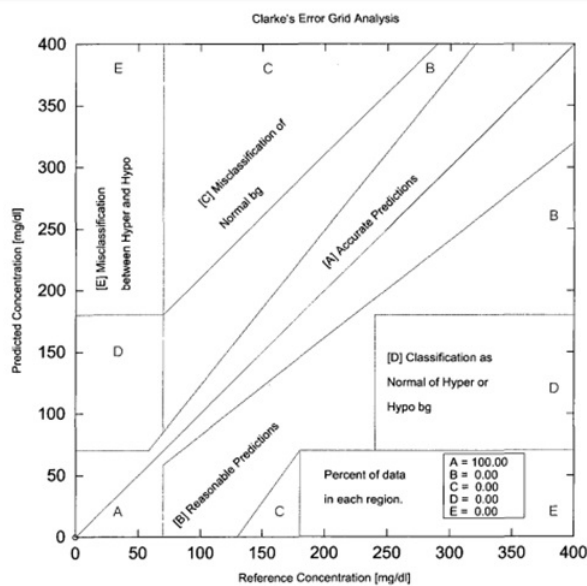
Figure 4.1: Clarke error grid. This grid is specifically dedicated for the evaluation of diabetes blood glucose monitoring systems by clinically classifying the errors between the estimated and the reference glucose levels into 5 different zone: A, B, C, D and E. While zones A and B identify the clinically acceptable estimations; zone A contains the points having 20% error with respect to the reference levels, region B identify the points that have significant quantitative error without misleading the clinical output hence the estimated levels are still labeled correctly as hypo-hyper and normal glycemic. Region C identify estimation that should be in the normal range but labeled incorrectly as hypo or hyperglycemic. Region D identify the estimation labeled normal but in reality should be considered as hypo- or hyperglycemic. Finally region E is the most dangerous region where the hypoglycemic points are estimated as hyperglycemic and vice versa. Extracted from [74].

4.6 Discussion

In this chapter we presented the data processing and regression techniques used to analyse the data collected from the proposed antennas. The raw data are first sampled and normalized. Feature selection techniques are then applied to identify the features (which correspond to frequencies) exhibiting the best sensitivity towards the glucose levels variation, and to reduce the dimensionality of the data. Finally, different regression techniques were considered to convert the scattering parameters into actual glucose values.

Chapter 5

Experimental measurements and results for the glove sensor design

In this chapter we discuss the performance of the proposed glove sensors in different set-up configurations and we focus on their sensing capabilities. We started with in-vitro experiments using fatal bovine serum (FBS)/glucose solutions, followed by ex-vivo experiments on rat tissues. Finally we validated the performance of the proposed system when tested on human volunteers.

5.1 In-vitro measurement

In this experiment, we study the sensitivity of the proposed antenna towards glucose variations using FBS/glucose solutions. The main objective of this experiment is to demonstrate the ability of the proposed sensors to detect very small glucose variations over the diabetic range.

5.1.1 Experimental setup

For the in-vitro sensitivity experiments, FBS/glucose solutions are used. Fetal bovine serum is a liquid fraction of clotted blood harvest from bovine fetuses. It contains a large number of nutritional factors and growth factors along with small molecules like amino acids, sugars, lipids, and hormones [75]. The initial glucose levels in FBS is usually less than 5 mg/dl. A container is designed using Styrofoam blue foam board to have the same dimensions of the antenna with a thickness of 0.5 cm. To avoid absorption of the FBS, the foam container is wrapped with a thin nylon film. The container is then filled with FBS solution equivalent to 6 mm of thickness. The antenna, connected to the portable VNA using flexible coaxial cables, is placed on a large foam board under the container and kept fixed throughout the entire experiment as shown in Figure 5.1.
Knowing that the normal blood glucose level at fasting is less than 100 mg/dl,

frequencies. Figure 5.3 (B) shows the S11 phase versus the reference glucose levels at two different frequencies. A very good correlation of $r > 0.96$ is achieved.
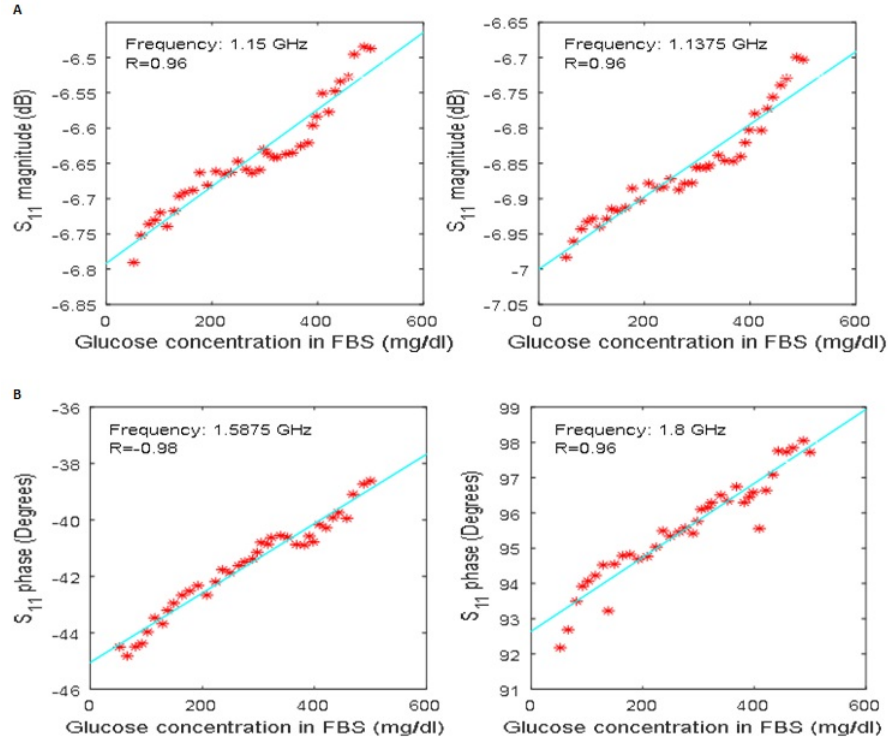
Figure 5.3: Flexible antenna's response to glucose variation during in-vitro experiment. The flexible antenna's response (S11) to glucose variation. Glucose concentration of the FBS solution was varied with very small steps from 50 mg/dl to 500 mg/dl. The normalized S11 versus the reference glucose levels obtained by the commercial invasive glucometer. The straight cyan line is the S11 fitted curve showing the trend of the antenna's response when the glucose levels increase. These S11-parameters correspond to different frequencies achieving high linear correlation between the S11 and the glucose reference levels. (A) shows the S11 magnitude for two frequencies. (B) shows the S11 phase vs the reference glucose levels collected at 1.5875 GHz and 1.8 GHz

Importance of the vasculature-inspired slots

The importance of concentrating the EM waves into the vessels' network is demonstrated in the following two experiments using the semi-flexible antenna and a vessel-like container: (1) the vessels of the container that are filled with FBS/glucose solution are aligned with and placed in parallel to the antenna's slots (Figure 5.4 (A)). (2) the container is rotated by 180°, as shown in Fig-

ure 5.4 (B), where the vessels are almost orthogonal to and hence not aligned with the antenna's slots (only small sections of the antenna's slots intersect with the vessels of the container). In both cases, the same experimental setup parameters are utilized and the corresponding curves showing the S11 responses versus the glucose levels are compared. The actual glucose levels are varied between 10 to 600 mg/dl as measured by the invasive method, representing a total change of 590 mg/dl. The total change in the S11 magnitude response corresponding for the highest correlated S parameter is improved from 0.29 dB for the misaligned rotated position to 1.55 dB for the aligned or parallel position (Figure 5.4 (C) Left). Moreover, the total change in S11's phase response is improved from 1.04° for the rotated position to 10° for the parallel position (Figure 5.4 (C) Right) and thus indicating an enhanced sensitivity. In fact, by aligning the vessel's network with the slots and concentrating the radiation on the vessels, the sensitivity of the antenna towards glucose variations is improved by more than 5 folds in terms of the corresponding S11 magnitude variation and 10 folds for the phase. To our knowledge, the research here represents the first direct demonstration of the importance of focusing the EM waves onto the vessels to increase the sensitivity of the proposed EM-based multi-band sensor toward glucose variations.

It is important to highlight that we were able to obtain high correlation (R>0.95) between the raw S-parameters and the glucose levels for both experiments. This high sensitivity is due to the concentration of the surface current around the slots and their extremities. This experiment was idealized to highlight the importance and the benefits of concentrating the EM waves on the vessels. In practical scenarios, the wearable nature of the design, limits the room for misalignment. Moreover, the concentration of the surface current not only on the slots but rather around them helps accommodate for any possible slight misalignment between the targeted vessels and the slots.

Response to common interferants.

To evaluate the effect of some common interferants, including fructose (FRU), oleic acid (OA) and acetaminophen (AC), on the proposed sensor's response, glucose (GLU) and these interferants were added to the FBS solution in concentrations much higher than their physiological ranges. We added successively 50 mg/dl of OC, AC, FRU and GLU to the same FBS solution. The S11 parameters showed minimal to no shift when the interferants were added. In contrast, a significant shift of S11 parameters is produced when the same amount of glucose is added to the solution, resulting in a correlation with the glucose levels of R > 0.9 (Figure 5.6).

The difference in response is due to the difference in terms of dielectric properties between these interferants. In a lossy medium, containing lossy materials such as these interferants, the effective complex permittivity is composed of $\epsilon'r$ which is the real permittivity that signifies the stored electric field energy, $\epsilon''r$ which is the
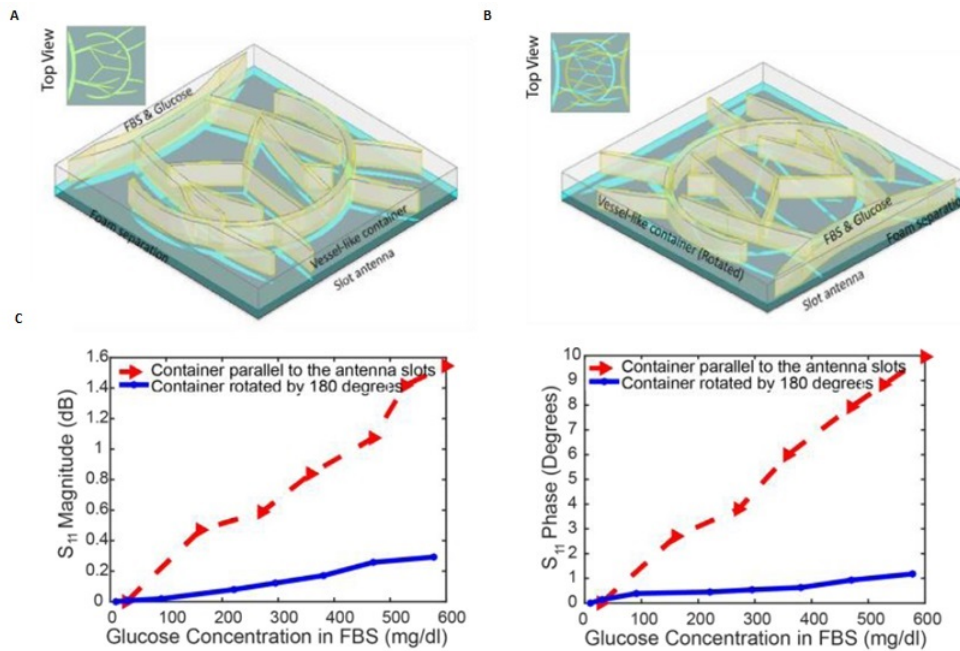
Figure 5.4: The importance of the blood vessels inspired slots. The FBS-glucose solution is filled inside a vessel-like container. (A), Left: The antenna is placed parallel to the vessel-like container, superposing the slots of the antenna upon that of the container (configuration 1). Right: the vessel-like container is left in the same position as in A left and the antenna is rotated with a 180° (configuration 2). (B), Comparison between the antenna's response (S11) versus the reference glucose levels obtained from the two configurations. The S11 magnitude and phase in both experiments corresponds the frequencies achieving the highest correlation between the S11 parameters and the reference glucose levels. S11 versus the reference glucose levels obtained using the configuration 2 (red) and using configuration 2 (blue). Left: S11 magnitude, showing a total change of 1.55 dB in configuration 1 and 0.29 dB in configuration 2 for glucose levels ranging from 10 to around 600 mg/dl. Right: S11 phase, showing a total change of 10 degrees in configuration 1 and 1.04 degrees in configuration 2.

imaginary permittivity that accounts for the losses in the medium and $tan\delta$ which is the loss tangent of the medium. Hence, the complex permittivity highly affects the EM waves properties in terms of magnitude and phase. We ran experiments in the lab where we subjected the different interferants to a dielectric sensor that is designed to identify the various material characteristics. Our results also show that from a dielectric perspective the glucose showed a clear distinction. Hence, its signature on the operating EM system is distinctive. Keeping in mind that even if some material had similar $\epsilon'r$, their loss tangent may vary significantly, which impacts our sensors' responses. We have also introduced these differences
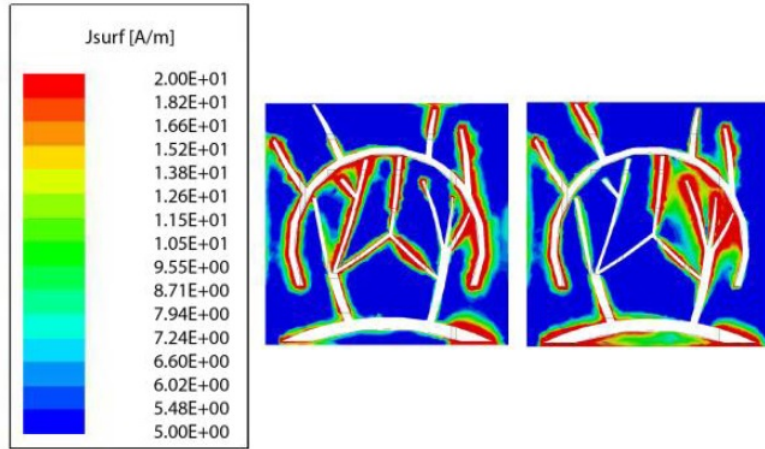
Figure 5.5: Surface current distribution. Antenna's current distribution at 0.8GHz (left) and 1.2 GHz (right).
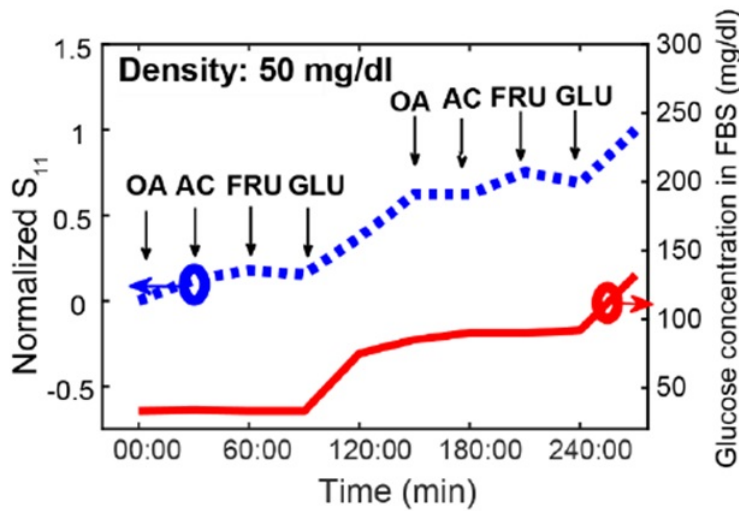
Figure 5.6: Selective response of the flexible glove sensor to glucose (GLU).

in our regression models where we are able to tailor our responses specifically to glucose variations.

Stability Analysis.

It is important to highlight that the antenna's S11 response remained stable over repeated experiments. We were able to identify multiple frequencies at which the physical parameters of the proposed sensor versus reference glucose levels remained stable in repeated experiments and demonstrated consistent behavior. Figure 5.7 shows the glucose measurement response from ~ 50 to $\sim 600 mg/dl$

with a step of 100 mg/dl repeated three times. The sensor's response remained stable in repeated experiments as shown in the Figure 5.7.
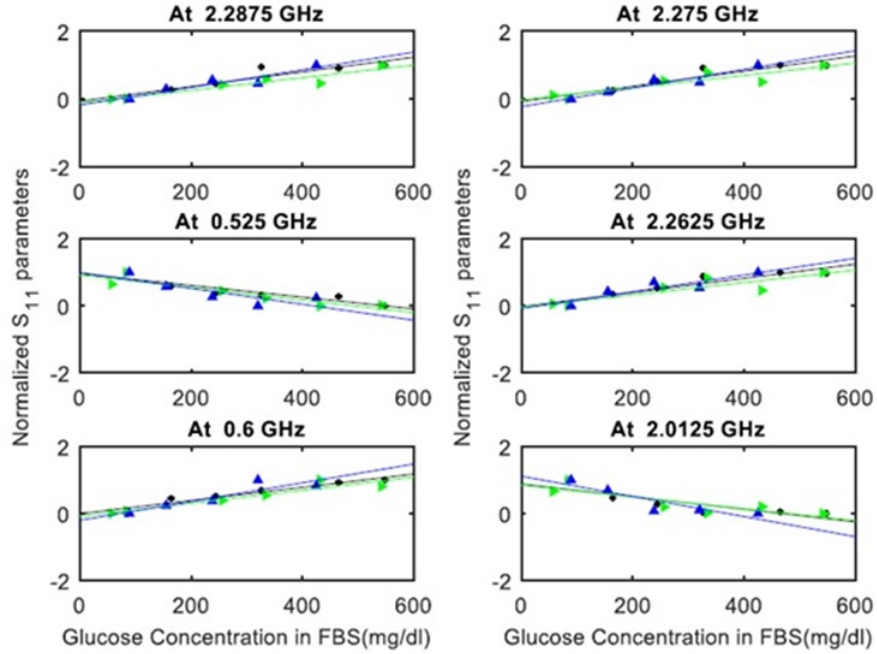
Figure 5.7: Stability test.The glucose measurement response was repeated three times.

5.1.3 Regression modeling results

For in-vitro sensitivity experiments, around 40 measurements are collected. The glucose levels ranged between 50 to 500 mg/dl. S11 magnitude and S11 phase are sampled at 21 different frequencies equally spaced. A total of 42 features are first processed to select the best features subset and the best kernel using both filter and wrapper feature selection techniques. After feature selection the dataset is divided into two subsets: Training (2/3) and testing (1/3). The first subset is used to identify the model's parameters and the second is used to test the models over "unseen" data. This process is repeated 10 times in order to cover most observations. The output of the model are the individual estimated glucose level points along with their mean values from the different replications.

Comparison between the different regression techniques

As discussed in Chapter 4, different regression techniques were considered. Figure 5.8 provides a comparison between PLS, LASSO and GP performances in terms of MARD and SEP for the semi-flexible and flexible glove sensors during

in-vitro experiments. GP models performed the best during our analysis. They provided the lowest mean percentage error as shown in Figure 5.8 (A). Additionally, they are able to provide very accurate estimations of the glucose levels ranging below 70 mg/dl with an SEP of 7.49 mg/dl for the semi- flexible glove sensor and SEP of 4.26 mg/dl for the flexible glove sensor. Similarly for the SEP averaged for blood glucose levels higher than 180 mg/dl, where GP provides lower mean relative error compared with PLS and LASSO. In what follows, we present the results obtained using the GP model.
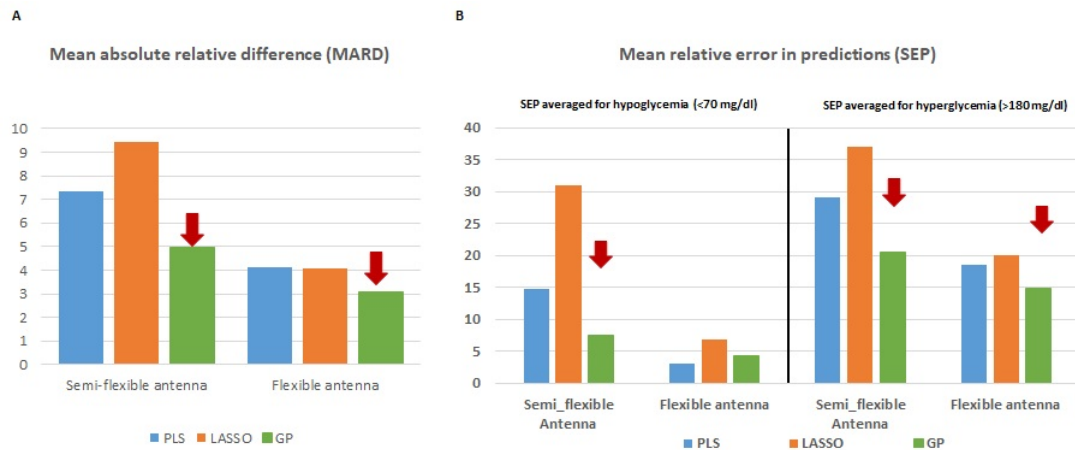
Figure 5.8: In-vitro experiments resulting different regression techniques.(A), A comparison between the mean absolute relative differences between the estimated and actual glucose levels obtained using PLS, LASSO and GP from the semi-flexible and flexible antennas. (B), the mean relative error in predictions (SEP) averaged for different glucose levels. The red arrows show the regression techniques providing the lowest prediction error.

Semi-flexible glove sensor glucose prediction results

Figure 5.9 (A) shows the mean percentage error in function of the number of features entered to the model for the different kernel functions using the two previously discussed feature selection techniques (wrapper and filter). It's clear that, for both techniques, the mean percentage error, or cross validation error, decreases when more features are added to the model until it reaches a minimum value and then it starts to increase again. For the in-vitro dataset, the wrapper technique resulted in a mean percentage error which dropped from 12 % to around 5 % for the best number of features and kernel function; on the other hand, for the filter technique the error dropped from 25 % to around 6%. By examining the datasets, we notice that the highest correlated features are usually very close in frequency, thereby increasing the redundancy of the features in the

filter technique; this explains the need for a larger number of features to allow for drop in error. The rational quadratic kernel provided the lowest mean percentage error using 11 features in the wrapper method while all the kernels provided very similar behavior in the filter method, with lowest percentage error achieved when using 20-25 features.

Figure 5.9 (B) presents estimated glucose levels Vs the reference glucose levels using GP regression models. In the left plot, the wrapper technique is used for the feature and the kernel selection. Using the rational quadratic as kernel function along with 11 features to build the model, a MARD of 4.96% is achieved. SEP-Hypo is 7.49 mg/dl, and SEP-Hyper is 20.48 mg/dl. As for the filter, Matern 32 is utilized as kernel function along with 23 features to build the model. MARD is 5.81%, SEP-Hypo is 8.77 mg/dl, and SEP-Hyper is 22.00 mg/dl.

Flexible glove sensor glucose prediction results

Figure 5.10 (A) shows the mean percentage error in function of the number of features entered to the model for the different kernel functions using the two previously discussed feature selection techniques (wrapper and filter). Using the flexible antenna, the mean percentage error obtained when using the wrapper method dropped from 10% for a single feature model to 2% for the best feature subset/kernel combination whereas for the filter technique the error dropped from 12% to 4%. Again, we notice that the highest correlated features are very close in frequency, which indicates increased redundancy in the feature subsets of the filter method. The Matern 52 kernel provided the lowest mean percentage error for 14 features in the wrapper method, while the Matern 32 kernel provided the lowest percentage error using 39 features in the filter method. Figure 5.10 (B) presents estimated glucose levels Vs the reference glucose levels using GP regression models. In the left plot, the wrapper technique is used for the feature and the kernel selection. Using Matern52 as kernel function along with 14 features to build the model, a MARD of 3.09% is achieved. SEP-Hypo is 4.26 mg/dl, and SEP-Hyper is 14.91 mg/dl. As for the filter, Matern 32 is utilized as kernel function along with 39 features to build the model. MARD is 4.23%, SEP-Hypo is 2.26 mg/dl, and SEP-Hyper is 17.55 mg/dl. We notice that in both experiments, the wrapper method provided lowest percentage error while using lowest number of features. Hence, for the following experiments, the wrapper method is adopted.

5.2 Ex-vivo experiments

Before testing the performance of the proposed antennas in an in-vivo configuration, ex-vivo experiments are conducted. The purpose of these experiments is to confirm the on-body matching of the proposed antennas and to test their abilities to detect the glucose variations through the different tissues.
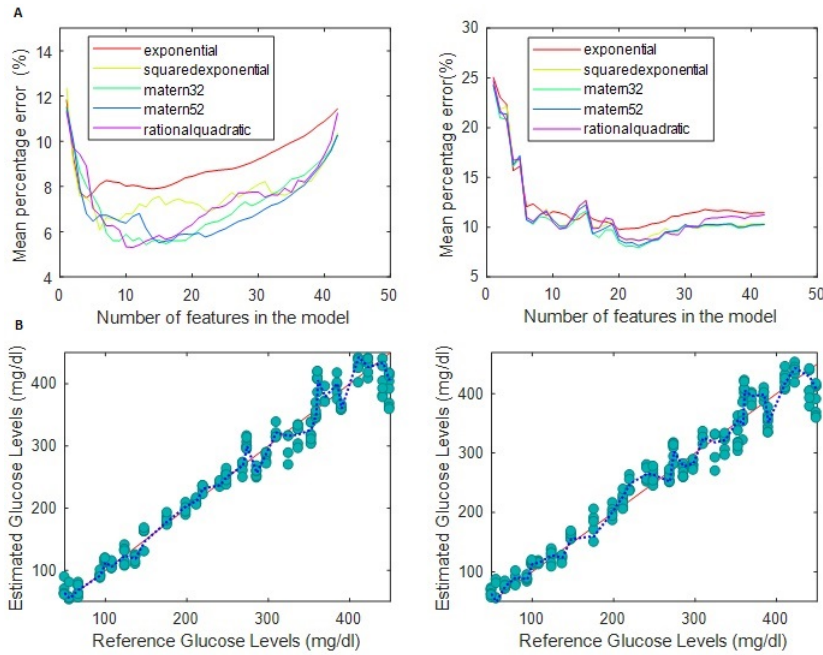
Figure 5.9: Feature selection and glucose levels estimation using semi-flexible antenna, tested during in-vitro experiment. (A), Features and kernel selections. The mean percentage error as a function of the number of features in the model using Left: the wrapper feature selection technique and Right: the filter. We can notice that the wrapper provide lower mean percentage error compared to the filter method. (B) Glucose levels estimation and model performance. The estimated glucose levels obtained by the proposed sensing system versus the reference glucose levels in the FBS solution (in red), using GP.The green filled circles represent the predicted glucose levels obtained during the 10 repetition of process and the blue dotted curve is the mean predicted value. Left: Using the wrapper for the feature and the kernel selection, rational quadratic is utilized as kernel function along with 11 features to build the model. The mean percentage error between the reference and the predicted glucose levels is 4.96%. SEP-hypo is 7.49 mg/dl, and SEP-Hyper is 20.48 mg/dl. Right: Using the filter for the feature and the kernel selection, Matern 32 is utilized as kernel function along with 23 features to build the model. The mean percentage error between the reference and the predicted glucose levels is 5.81%. SEP-hypo is 8.77 mg/dl, and SEP-Hyper is 22.00 mg/dl.

5.2.1 Experimental setup

Fresh abdominal unshaved rat skin, fat and muscle are dissected. They are cut into square pieces and then preserved in phosphate-buffered saline (PBS) on ice. The different layers with the PBS solution are placed inside a foam container above the antennas. A layer of FBS/glucose solution is then placed above the
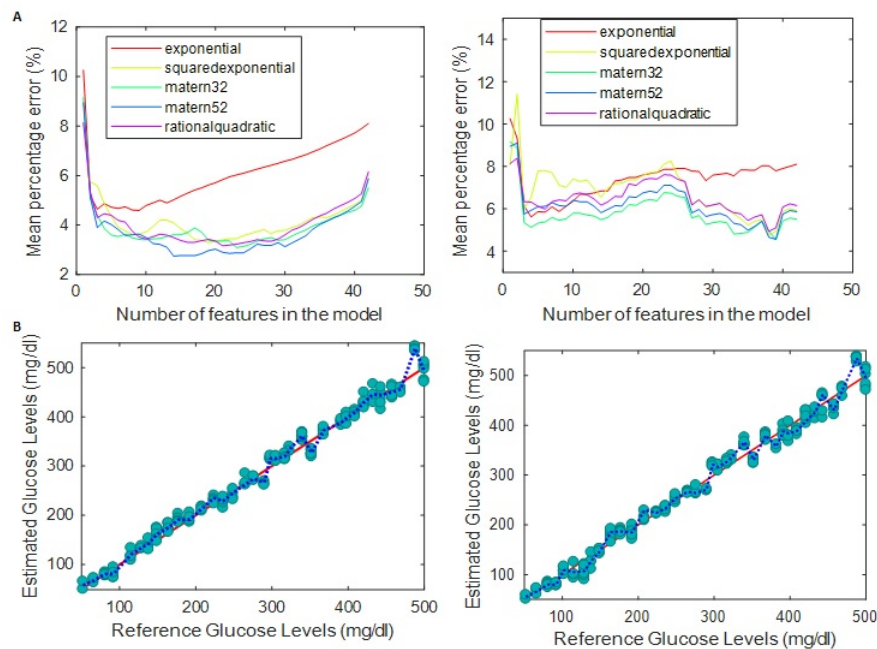
Figure 5.10: Feature selection and glucose levels estimation using the flexible glove sensor, tested during in-vitro experiment. (A), The mean percentage error as a function of the number of features in the model using Left: the wrapper feature selection technique and Right: the filter. (B), Glucose levels estimation and model performance. The predicted glucose levels obtained by the proposed sensing system versus the reference glucose levels in the FBS solution (in red), using GP. The data is randomly divided into two sets: 2/3 to build the model and 1/3 to test its performance. Because of the limited number of observation in the datasets, this process is repeated 10 times .The green filled circles represent the predicted glucose levels obtained during the 10 repetition of process and the blue dotted curve is the mean predicted value. Left: Using the wrapper for the feature and the kernel selection, Matern52 is utilized as kernel function along with 14 features to build the model. The mean percentage error between the reference and the predicted glucose levels is 3.09%. SEP-Hypo is 4.26 mg/dl, and SEP-Hyper is 14.91 mg/dl. Right: Using the filter for the feature and the kernel selection, Matern 32 is utilized as kernel function along with 39 features to build the model. The mean percentage error between the reference and the predicted glucose levels is 4.23%. SEP-Hypo is 2.26 mg/dl, and SEP-Hyper is 17.55mg/dl.

skin in a thin nylon container. Initial measurements using a VNA is taken at time zero. An amount of D-glucose, equivalent to 100 mg/dl, is added to the FBS solutions for each measurement. After the glucose addition, the FBS solution is well mixed and left for around 10 minutes to insure the homogeneity of the solution. A reference glucose level is then taken using the invasive glucometer

OGTTs.

5.3.1 Experimental setup

A total of 21 volunteers (11 females and 10 males 19-37 years of age) were recruited in this study. The International Review Board (IRB) approved the experiments and all volunteers signed a consent form. Subjects were considered eligible for the study if they were between 18 and 70 years of age and able to provide informed consent. There were no restrictions on either race, sex or ethnicity. Substance abuse, lactation, pregnancy, and being part of an interventional trial were the exclusive criteria. In the first phase of the study, only healthy subjects with HbA1c levels less than 6%, normal blood pressure and no sign of dyslipidemia were recruited. Each volunteer participated in multiple separate OGTT experiments. Ten minutes prior to sugar intake (75 grams of sugar), the developed sensors were placed on the corresponding sensing locations and fixed for the entire OGTT 2-hour time span. Finger prick glucose monitoring device (ROCHE glucometer [64]) was utilized for glucose fasting referencing. The timer was then started and the sugar intake was controlled to be within 10-15 minutes. Afterwards, finger-prick glucose monitoring was performed once every 15 minutes and VNA savings were taken every five minutes. We relied on interpolation to populate the remaining reference glucose points over 5 minute-intervals. During the experiment, volunteers were kept indoor and asked to sit on a chair to limit as much as possible their movements.

5.3.2 Scattering parameters Versus glucose levels

Semi-flexible glove sensor's response to glucose variation

Figure 5.13 (B) shows the S11 phase variation with time at 0.7995 GHz during one OGTT. We notice that the S11 phase (blue curve) follows the trend of blood glucose profile (red curve), achieving a very good correlation of 0.944. The difference in terms of S11 phase in function of frequency for three different glucose levels is presented in Figure 5.13 (B). This difference illustrates the good tracking of the glucose profile, at different frequencies. Figure 5.14 shows semi-flexible glove sensor response during representative 8 samples chosen from the 63 OGTTs experiments representing some of the best correlations obtained between the features (S11 magnitude and phase) and the reference blood glucose levels. We were able to have high correlated features for the majority of the 63 OGTTs experiments(Figure 5.14 (B)).

Flexible glove sensor's response to glucose variations

Figure 5.15 shows the S11 phase variation with time at 1.36 GHz during one OGTT. We notice that the S11 phase (blue curve) also follows the trend blood
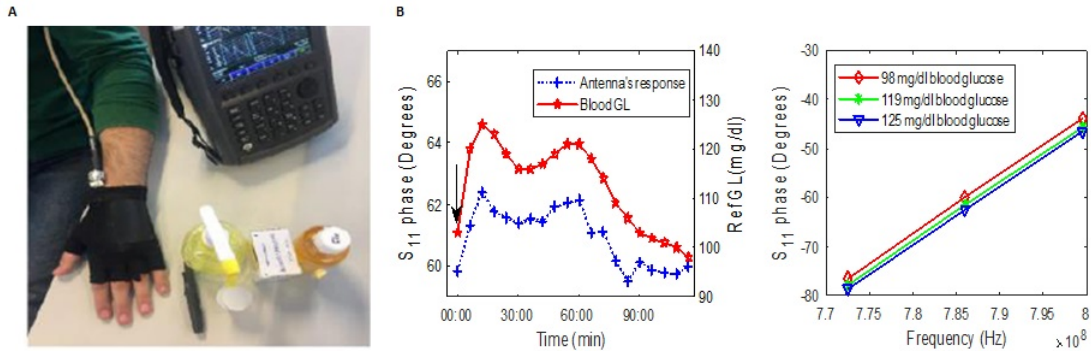
Figure 5.13: Semi-flexible glove sensor's response during one OGTT. (A), The experimental setup; the two antenna prototypes are placed on the volunteer's hands and readings are taken simultaneously from both antennas. (B), Antenna's response during one OGTT. Left: the blue curve shows the S11 phase response of the semi-flexible antenna collected at 0.7995 GHz versus time during an OGTT. This curve follows well the blood glucose profile curve shown in red, achieving a high correlation of 0.944 between the two measurements. The arrow indicates the onset of the glucose intake. Right: The antenna's S11 phase response around 0.7995 GHz, corresponding to three different blood glucose concentrations. This plot illustrates the good tracking of the glucose profile.

glucose profile (red curve), achieving a very good correlation of -0.94. Figure 5.16 shows the flexible glove sensor's response during representative 8 samples chosen from the 63 OGTTs experiments representing some of the best correlations obtained between the features (S11 magnitude and phase) and the reference blood glucose levels. We were able to have high correlated features for the majority of the 63 OGTTs experiments (Figure 5.16 (B)).

5.3.3 Regression modeling results

Semi-flexible glove sensor glucose prediction results

Figure 5.17 shows the results obtained from the data collected during the 3 OGTTs completed by volunteer #2 using the semi-flexible glove sensor. Using the wrapper feature selection technique, 12 features are selected along with the Matern 32 as kernel for the GP, which provides the lowest mean percentage error as shown in Figure 5.17(A). The dataset obtained from volunteer #2 is composed of 69 observations. After normalization and feature selection, this data set is divided into two independent subsets: 2/3 training set and 1/3 testing set. The training set is used to build the GP using the 12 predefined features and the Matern 32 as a kernel. And the testing set is used to test the performance of the model. Since the number of observations is small, this process is repeated 10 times by randomly dividing the dataset into training and testing sets.
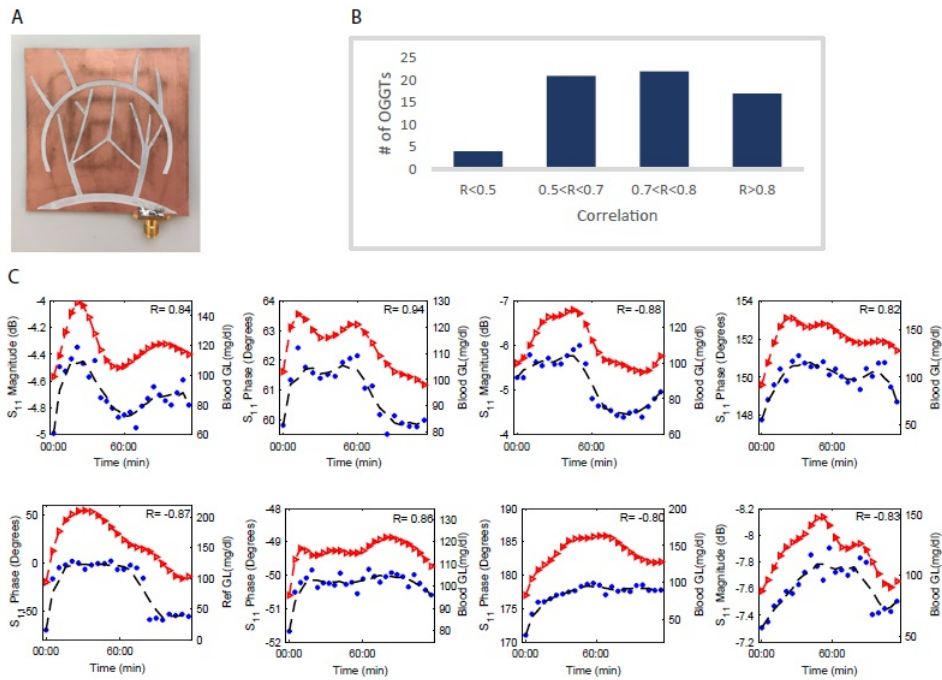
Figure 5.14: Human trials on healthy volunteers using the semi-flexible antenna.(A), The fabricated semi-flexible antenna prototype. (B), Best correlations obtained between the features (S11 magnitude and phase) and the reference blood glucose levels. We were able to have high correlated features for the majority of the 63 OGTTs experiments. (C), Antenna's response during representative 8 samples chosen from the 63 OGTTs experiments. The blue curve shows the S11 response versus time during an OGTT. This curve follows well the blood glucose profile curve shown in red, achieving high correlations and indicating good tracking of the glucose profile. We notice also that there is no significant time lag between the antenna's response and the blood glucose peaks where the predicted blood glucose levels, obtained using the proposed system, match well the reference blood glucose levels, and follow successfully the upward and downward trends of the reference blood glucose levels.

We achieved a MARD ranging between 0.02% and 21.2% with a mean percentage error of 3.35%. As shown in Figure 5.17 (B), the estimated glucose levels provided by the proposed system match well the reference blood glucose levels, and follow successfully the upward and downward trends of the reference blood glucose levels. More results are shown in Figure 5.18, showing the results for different volunteers obtained using the semi-flexible antenna.
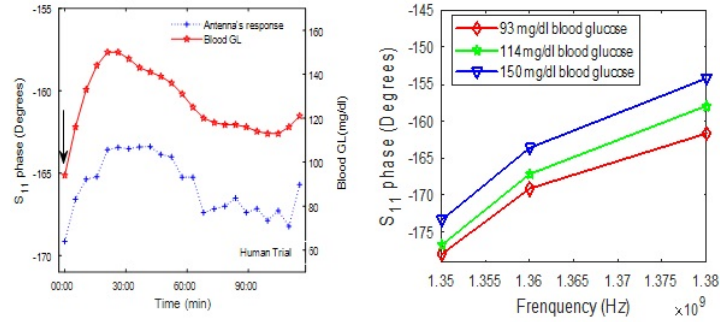
Figure 5.15: Flexible glove sensor's response during one OGTT. Left: the blue curve shows the S11 phase response of the flexible antenna collected at 1.36 GHz versus time during an OGTT. This curve follows well the blood glucose profile curve shown in red, achieving a high correlation of -0.94 between the two measurements. The arrow indicates the onset of the glucose intake. Right: The antenna's S11 phase response around 1.36 GHz, corresponding to three different blood glucose concentrations. This plot illustrates the good tracking of the glucose profile.

Flexible glove sensor glucose prediction results

Figure 5.19 shows the results obtained from the data collected during the three separate OGTTs completed by volunteer #7 using the flexible antenna. Using the wrapper feature selection technique, only 9 features out of the 42 features are selected along with the rational quadratic as kernel for the GP which provides the lowest mean percentage error as shown in Figure 5.19 (A). The dataset obtained from volunteer #7 during three OGTT is composed of 63 observations. After normalization and feature selection, this data set is divided into two independent subsets: 2/3 training set and 1/3 testing set. The training set is used to build the GP using the 9 predefined features and the rational quadratic as a kernel. And the testing set is used to test the performance of the model. Since the number of observations is small, this process is repeated 10 times by randomly dividing the dataset into training and testing sets.

We achieved a MARD ranging between 0.01 and 18.26 with a mean percentage error of 3.83%. As shown in Figure 5.19(B), the estimated glucose levels provided by the proposed system match well the reference blood glucose levels, and follow successfully the upward and downward trends of the reference blood glucose levels. More importantly, the results show no delay between the estimated and the reference blood glucose values. More results are shown in Figure 5.20, presenting the estimated glucose levels obtained during 8 different OGTTs using the flexible antenna.

The glove sensing system is capable of achieving an overall MARD of 6.08%

60
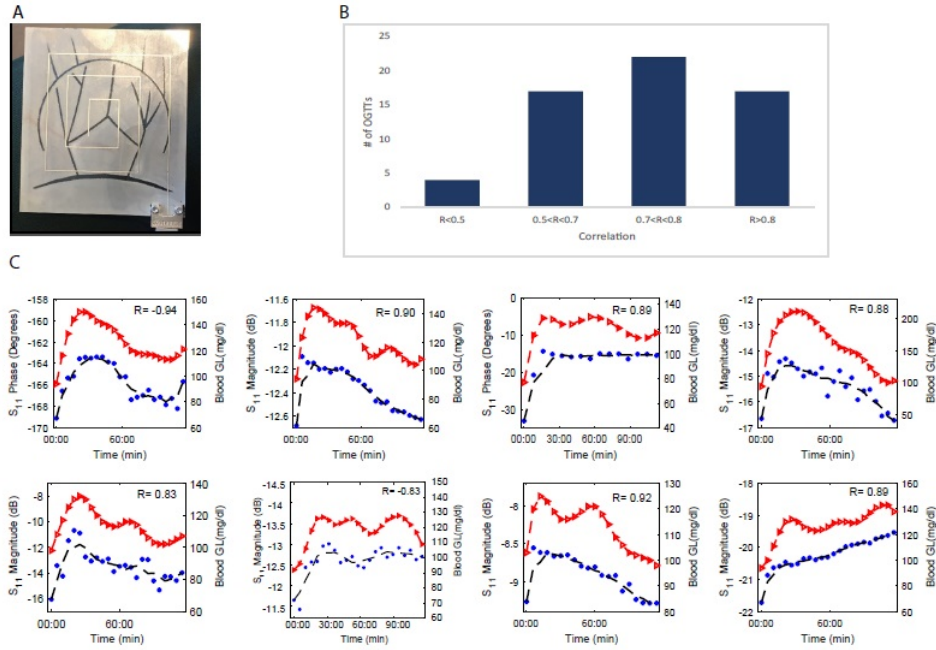
Figure 5.16: Human trials on healthy volunteers using the flexible antenna. (A), The fabricated flexible antenna prototype. (B), Best correlations obtained between the features (S11 magnitude and phase) and the reference blood glucose levels. We were able to have high correlated features for the majority of the 62 OGTTs experiments. (C), Antenna's response during representative 8 samples chosen from the 62 OGTTs experiments. The blue curve shows the S11 response versus time during an OGTT. This curve follows well the blood glucose profile curve shown in red, achieving high correlations and indicating good tracking of the glucose profile. We can notice also that there is no significant time lag between the antenna's response and the blood glucose peaks.

and 6.18% for the semi-flexible and flexible glove sensors respectively for the collected data from all the volunteers during the 63 total OGTTs. These values show exceptional accuracy; they are comparable to the error obtained by self- monitoring systems available in the market [64]. To prove the repeatability, the Clarke's error grid analysis including the data of the 21 volunteers is shown in Figure 5.18 (B) for the semi-flexible glove sensor and in Figure 5.20 (B) for the flexible glove sensor. We notice that all the estimations fall in the clinically acceptable zones (zone A and B) with 96.04% of the data in zone A and the remaining 3.96% in zone B for the semi-flexible prototype and 94.96% in Zone A and 5.04% in zone B for the flexible prototype. Moreover, 89.78% of estimated values, using the flexible antenna, are within 15% error, 94.96% are within 20% error, 98.86% are
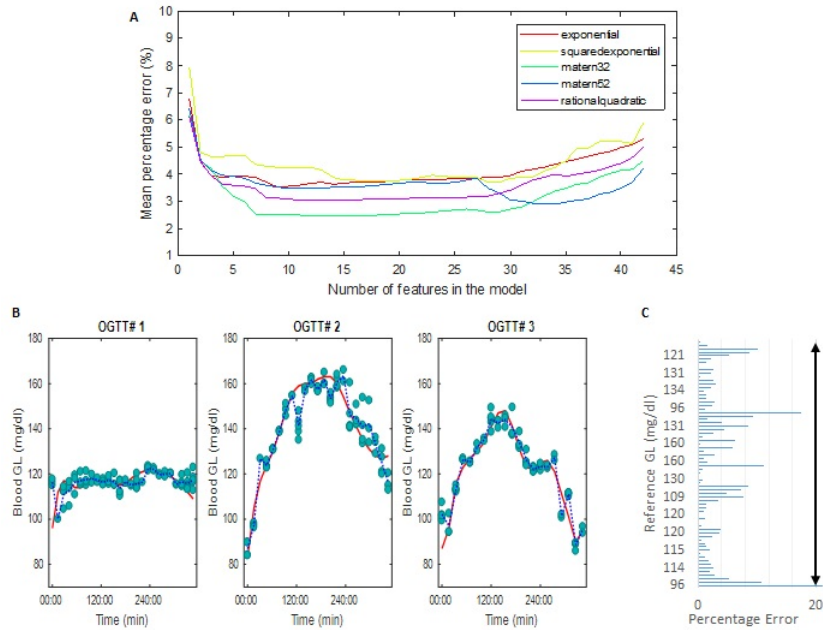
Figure 5.17: Feature selection and glucose estimation using the semi-flexible antenna tested on volunteer #2. The data collected during the 3 OGTTs completed by volunteer #2 are added together and used for both the feature selection and the model building. (A), The mean percentage error as a function of the number of features in the model using the wrapper feature selection technique. We can notice that the matern32 is providing the lowest mean percentage error. (B), The predicted glucose levels obtained by the proposed sensing system versus the reference blood glucose levels (in red), using GP. The data is randomly divided into two sets: 2/3 to build the model and 1/3 to test its performance. Because of the limited number of observation in the datasets, this process is repeated 10 times .The green filled circles represent the predicted glucose levels obtained during the 10 repetition of process and the blue dotted curve is the mean predicted value. Using the wrapper for the feature and the kernel selection, Matern32 as kernel function along with the first 12 features are utilized to build the model. (C), The bar chart shows the percentage error of each observation. The error ranged between 0.02 and 21.2 with a mean percentage error of 3.35%.

within 30% and 99.71% are within 40% error (These percentages are obtained for the total 1430 estimated points). The proposed glucose EM-based sensors are capable of achieving good matching between the estimated and actual (reference) glucose level, providing further confidence in the potential of the designed antennas to monitor glucose noninvasively and continuously.
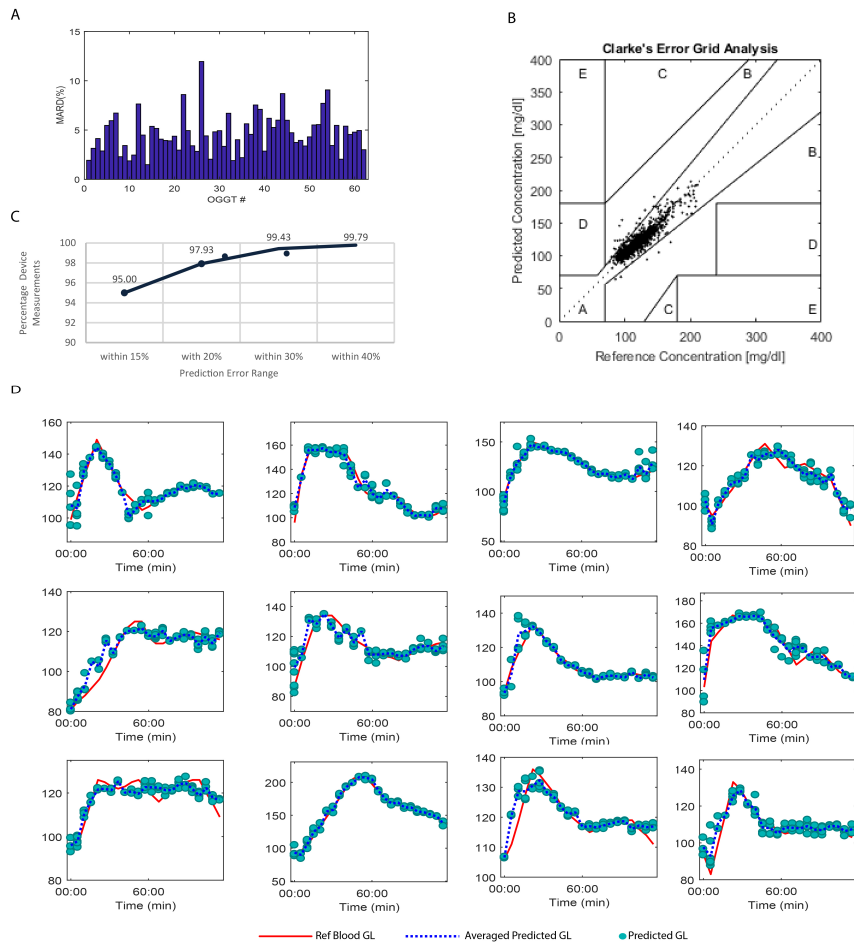
Figure 5.18: Estimated blood glucose levels during human trials on healthy volunteers using the semi-flexible antenna. (A), for each of the 63 experiments we achieved a MARD below that 12% with a MARD of 5.304% averaged over all the 63 experiments. (B), CEG for all the OGTT conducted by the 21 volunteers showing the averaged estimations of 1427 data point. All the estimated values are in the acceptable zones A and B with the majority in zone A (96.77%). (C), 93.48% of estimated values are within the 15% MARD error, 96.78% are within 20% MARD error, 99.09% are within 30% MARD error and 99.65% are within 40% MARD error. (D), blood glucose estimation using the GP model. Actual glucose levels (red) compared with the estimated glucose levels over time (green dots shows the estimations resulting from the 10 random repetitions in most cases closely overlapping and the blue curve shows the mean estimation) for 12 representative OGTTs chosen from a total of 63 OGTTs. The predicted blood glucose levels match well the reference blood glucose levels, and follow successfully the upward and downward trends of the reference blood glucose levels.
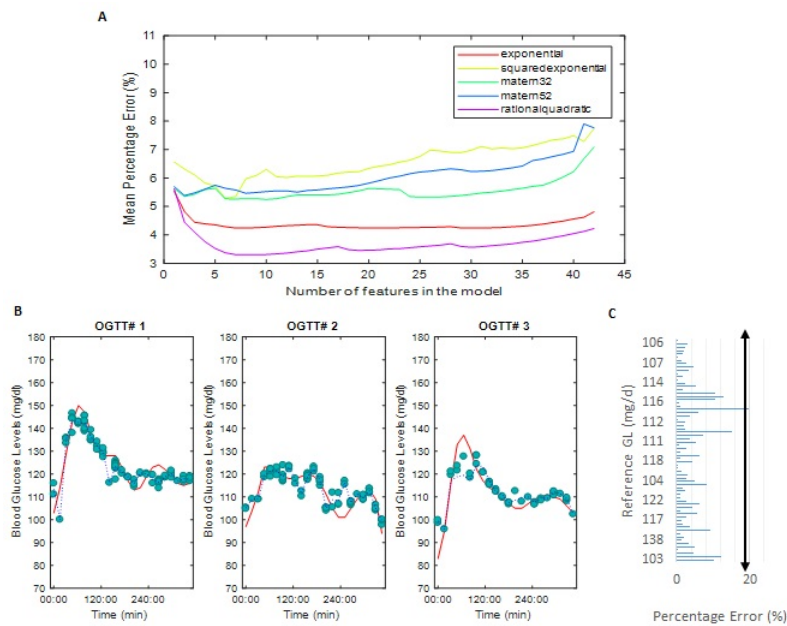
Figure 5.19: Feature selection and glucose estimation using the flexible glove sensor tested on volunteer #7. The data collected during the 3 OGTTs completed by volunteer #7 are added together and used for both the feature selection and the model building. (A),The mean percentage error as a function of the number of features in the model using the wrapper feature selection technique. We can notice that the rational quadratic is providing the lowest mean percentage error. (B),The predicted glucose levels obtained by the proposed sensing system versus the reference blood glucose levels (in red), using GP. The data is randomly divided into two sets: 2/3 to build the model and 1/3 to test its performance. Because of the limited number of observation in the datasets, this process is repeated 10 times .The green filled circles represent the predicted glucose levels obtained during the 10 repetition of process and the blue dotted curve is the mean predicted value. Using the wrapper for the feature and the kernel selection, rational quadratic as kernel function along with the first 9 features are utilized to build the model. (C),The bar chart shows the percentage error of each observation. The error ranged between 0.01% and 18.26% with a mean percentage error of 3.83%.

5.3.4 Gender based analysis

To assess if there is a sensitivity difference detected by the proposed sensor between male/female volunteers we relied on unpaired Student's t-tests/ Welch's t-test. A P value higher than 0.05 is considered statistically not significant and hence no significant difference is reported between the two groups. We found that both genders provided very similar sensitivity towards the glucose variations with no significant difference in terms of mean correlation and MARD (Male, n = 30;

64
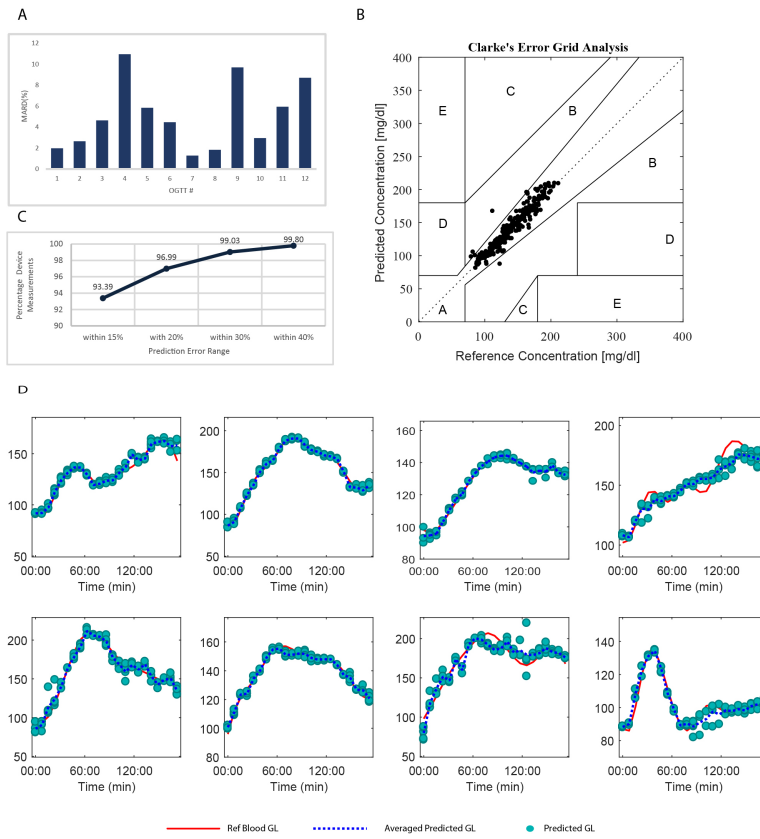
Figure 5.20: Estimated blood glucose levels during human trials on healthy volunteers using the flexible antenna. (A), for each of the 62 experiments we achieved a MARD below that 15% with a MARD of 4.7% averaged over all the 62 experiments. (B), CEG for all the OGTT conducted by the 21 volunteers showing the averaged estimations of 1399 data point. All the estimated values are in the acceptable zones A and B with the majority in zone A (97.9%). (C), 95% of estimated values are within the 15% MARD error, 97.93% are within 20% MARD error, 99.43% are within 30% MARD error and 99.79% are within 40% MARD error. (D), blood glucose estimation using the GP model. Actual glucose levels (red) compared with the estimated glucose levels over time for 12 representative OGTTs chosen from a total of 62 OGTTs. CEG for all the OGTT conducted by the 21 volunteers.

Female, n = 32). This was performed on the antenna data collected from the 21 volunteers (including 10 male and 11 female volunteers), using the glove sensors, where each one was subject to three OGTTs. Additionally, no significant gender-based shift in the correlated frequencies is observed (Male, n = 30; Female, n = 32) as shown in Figure 5.21.

65
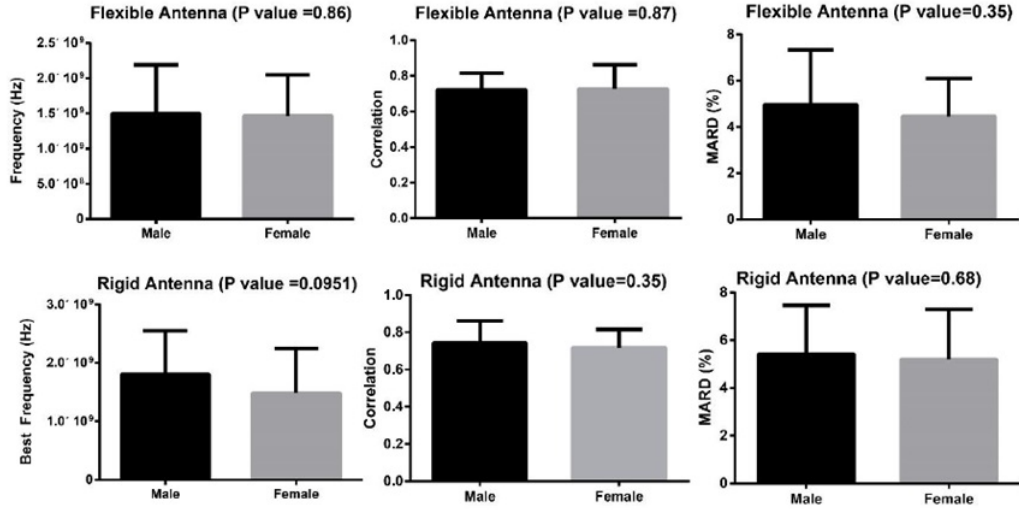
Figure 5.21: Gender-Based analysis for the flexiblle and semi-felxible glove sensor. The averaged means $\pm$ SD of frequency, correlation and MARD for both antennas are shown obtained from ~ 63 experiments (30 male and 33 female). *P value as calculated by Student t-test.

5.4 Discussion

In this chapter we evaluated the performance of the designed glove antennas in different experimental setups. The in-vitro experiments demonstrated the ability of the proposed sensors to detect very small glucose variations over the diabetic range. We were also able to verify the importance of concentrating EM waves into the vessels' network. The ex-vivo experiments, on the other hand, demonstrated the ability of the proposed system to provide good sensitivity towards the glucose variations when placed in proximity to a lossy medium such as the mammalian skin, fat and muscle layers. During this experiment the flexible antenna demonstrated better sensitivity, which is explained by its superior on-body matching response.

The proposed sensing system satisfies all the following requirements: its ability (1) to detect very small glucose glycemic variations (10 mg/dl) over the hypo- to hyper glycemic range, demonstrated during in-vivo experiments, and (2) to maintain a good sensitivity in the presence of a lossy medium, verified during ex-vivo experiments.

In this chapter, the sensors were tested separately. In chapter 7, we added multiple sensors to the system and we combined the antennas into a multi-location, multi-sensing system to calibrate out some perturbing factors.

Chapter 6

Experimental measurements and results for the sock sensor design

This chapter presents the performance of the proposed sock sensors in different experimental setups. We started with in-vitro experiments, where we proved the capability of the proposed designs to monitor small variations of glucose levels. After that we validated the performance of the proposed system when tested on healthy and diabetic human volunteers.

6.1   In-vitro measurements

6.1.1   Scattering parameters versus glucose levels

The sock sensor's S11 magnitude and phase at different glucose levels are shown in Figure 6.1 and Figure 6.2 respectively. Around 35 measurements are taken from each antenna design. Glucose concentration of the FBS solution is varied with small steps from 50 mg/dl to 500 mg/dl. Good correlation between the S11 parameters and the glucose levels is achieved. The S11 magnitudes of the different antenna designs at different glucose levels versus the frequency are shown in Figure 6.1 left. The S11 magnitude versus the reference glucose levels obtained by the commercial invasive glucometer is shown in the right plots of Figure 6.1. The straight cyan line is the S11 fitted curve showing the trend of the antenna's response when the glucose levels increase.

High correlation coefficient values were obtained for the three different designs indicating a strong linear relationship between the antenna's response and the glucose variation. We can notice that the three proposed designs were capable of achieving very good sensitivity towards the glucose variations. Both S11 magnitude and phase provided very good sensitivity towards the glucose variations capturing the hypo-to hyper glycemic variations with high sensitivity.
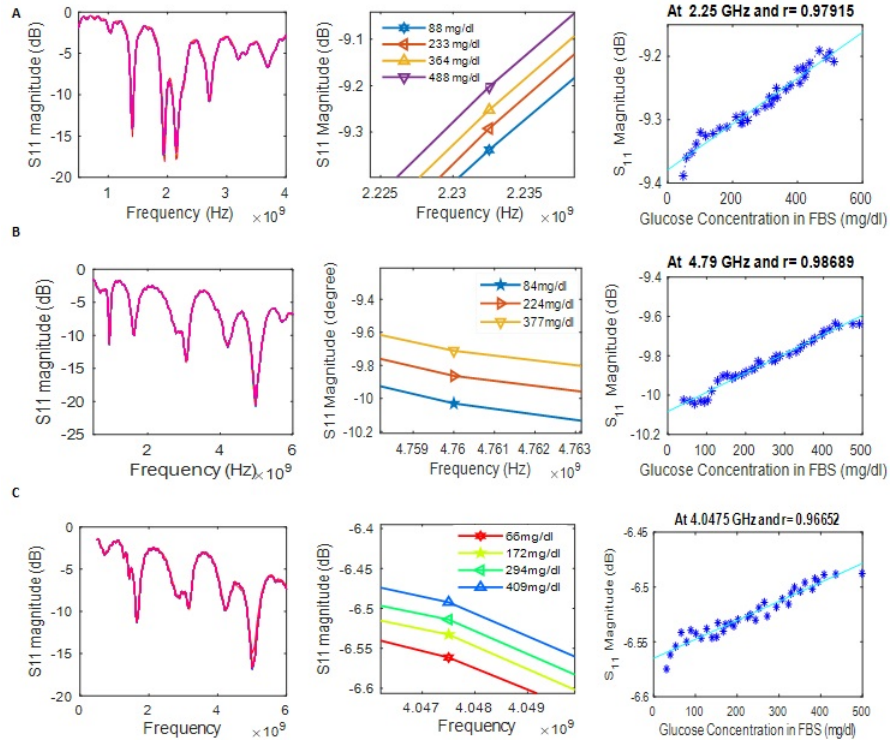
Figure 6.1: Sock sensor's magnitude response to glucose variation during in-vitro experiments. (A), Design #1. (B), Design#2. (C), Design #3.

6.1.2 Regression modeling prediction results

Figure 6.3 shows the prediction results for the three sock sensor designs during in-vitro experiments. Figure 6.3 (A) shows the mean percentage error in function of the number of features entered to the model for the different kernel functions using wrapper as a feature selection technique. It's clear that, for the three designs, the mean percentage error, or cross validation error, decreases when more features are added to the model until it reaches a minimum value and then it starts to increase again. For antenna design #1 and #3, the wrapper technique resulted in a mean percentage error which dropped from 9% to around 4% for the best number of features and kernel function. For the antenna design #2, the mean percentage error dropped from 5% to around 2%. Figure 6.3 (B) presents reference glucose levels Vs the estimated glucose levels using GP regression models for the three sock sensor designs. In the left plot, the results for design #1. Using the rational quadratic as kernel function along with 8 features to build the model, a MARD of 5.37% is achieved. As for design #2, Matern 32 is utilized as kernel function along with 13 features to build the model achieving a MARD of 7.38%. The squared exponential provided the lowest mean percentage error using 15 features for design #3 achieving a MARD of 8.25%.

68
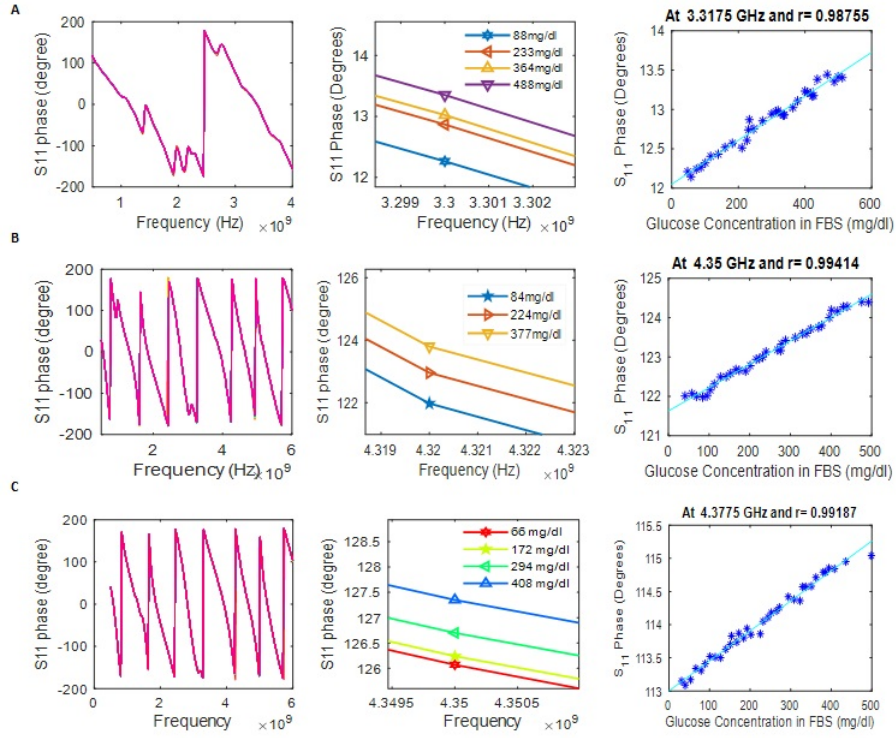
Figure 6.2: Sock sensor's phase response to glucose variation during in-vitro experiments.(A), Design #1. (B), Design#2. (C), Design #3.

6.1.3 Response to common interferants

To evaluate the effect of some common interferants, including metformin, oleic acid, panadol and fructose, on the proposed sensor's response, glucose and these interferants were added to the FBS solution in concentrations much higher than their physiological ranges. We added successively 50 mg/dl of MET, OA, PAN, FRU and GLU to the same FBS solution. The S11 parameters showed minimal to no shift when the interferants were added for the three designs as shown in Figure 6.4. In contrast, a significant shift of S11 parameters is produced when the same amount of glucose is added to the solution, resulting in a correlation with the glucose levels of $R > 0.9$ for the three proposed antennas.

The three proposed designs provided high sensitivity and high selectivity towards the glucose variations with very similar correlations between the S parameters and glucose levels. In the following experiments we used antenna design #3, corresponding to the quasi-array antenna composed of 4 elements with non-identical slots.
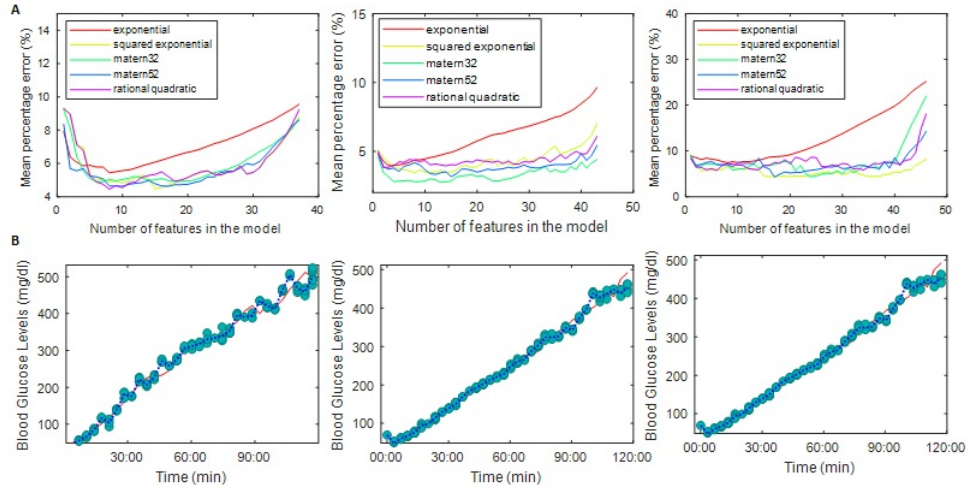
Figure 6.3: Feature selection and glucose levels estimation using sock sensor, tested during in-vitro experiment. (A), Features and kernel selections. The mean percentage error as a function of the number of features in the model using Left: Using the rational quadratic as kernel function along with 8 features sock sensor design #1 achieved a the lowest percentage error. Middle: for sock sensor design #2, Matern 32 kernel function achieved the lowest mean percentage error with 13 features to build the model. Right: The squared exponential kernel function provided the lowest mean percentage error using 15 features for design #3. (B), Glucose levels estimation and model performance. The estimated glucose levels obtained by the proposed sensing system versus the reference glucose levels in the FBS solution (in red), using GP. The green filled circles represent the predicted glucose levels obtained during the 10 repetition of process and the blue dotted curve is the mean predicted value. Left: sock sensor design #1 prediction results with a MARD of 5.37%. Middle: sock sensor design #2 achieved a MARD of 7.38. Right: The mean percentage error between the reference and the predicted glucose levels using antenna design #3 is 8.25%.

6.2 Clinical Trials

We evaluated the sock sensor design #3 on healthy and diabetic subjects to demonstrate its ability to monitor the blood glucose levels in real-time settings during OGTTs. A total of 28 volunteers were included in this experiment, 10 healthy and 18 diabetic, where each one underwent one OGTT.

Experimental setup

A total of 28 volunteers (10 healthy and 18 diabetic) were recruited in this study. The IRB approved the experiments and all volunteers signed a consent form. Subjects were considered eligible for the study if they were between 18 and 70
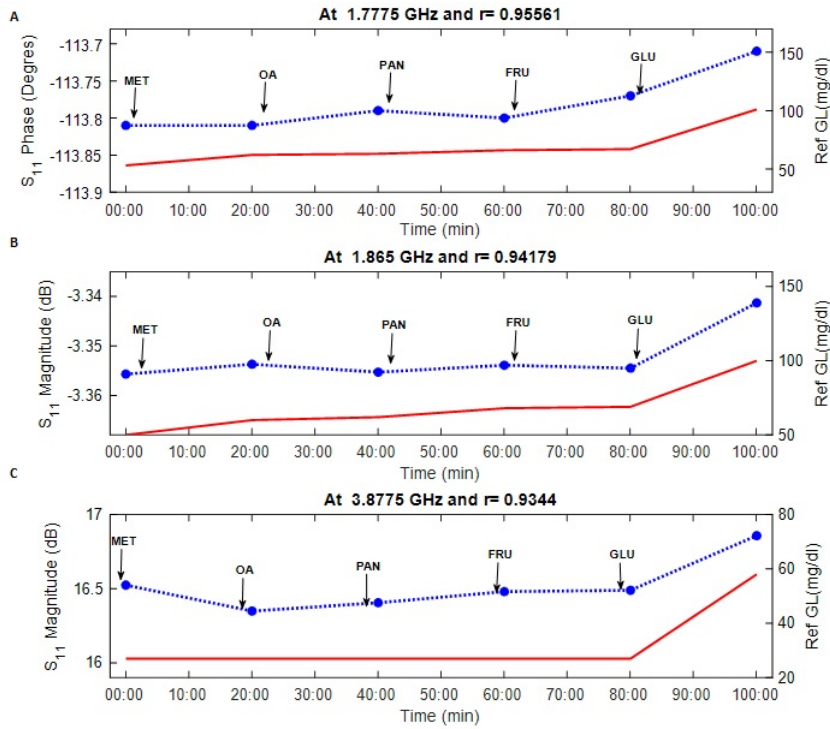
Figure 6.4: Selective response of the sock sensors to glucose (Glu).(A), antenna design #1 S11 response to different interferants. (B), antenna design #2 S11 response to common interferants and (C), antenna design # 3 S11 response to the different interferants.

years of age and able to provide informed consent. There were no restrictions on either race, sex or ethnicity. Substance abuse, lactation, pregnancy, and being part of an interventional trial were the exclusive criteria. Each volunteer participated in one OGTT experiment. The proposed sock sensor was placed on the corresponding sensing location and fixed for the entire OGTT 2-hour time span as shown in Figure 6.5 (A).

6.2.1   Scattering parameters Versus glucose levels

Figure 6.5 (B) left shows the S11 phase variation with time at 3.35 GHz during one OGTT for a healthy volunteer. We notice that the S11 phase (blue curve) follows the trend of blood glucose profile (red curve), achieving a very good correlation of 0.93. Figure 6.5 (B) Right shows the S11 magnitude variation with time at 2.74 GHz for a diabetic volunteer showing a high correlation of 0.98 between the actual glucose levels and the antenna's S-parameters. The correlation between the S-parameters and the glucose levels for the 28 OGTTs are shown in Figure 6.5 (C). We can see that out of the 28 OGGTs, 16 had a correlation higher than 0.8.

Figure 6.6 show sock sensor's response during representative 11 samples chosen from the 28 OGTTs experiments.
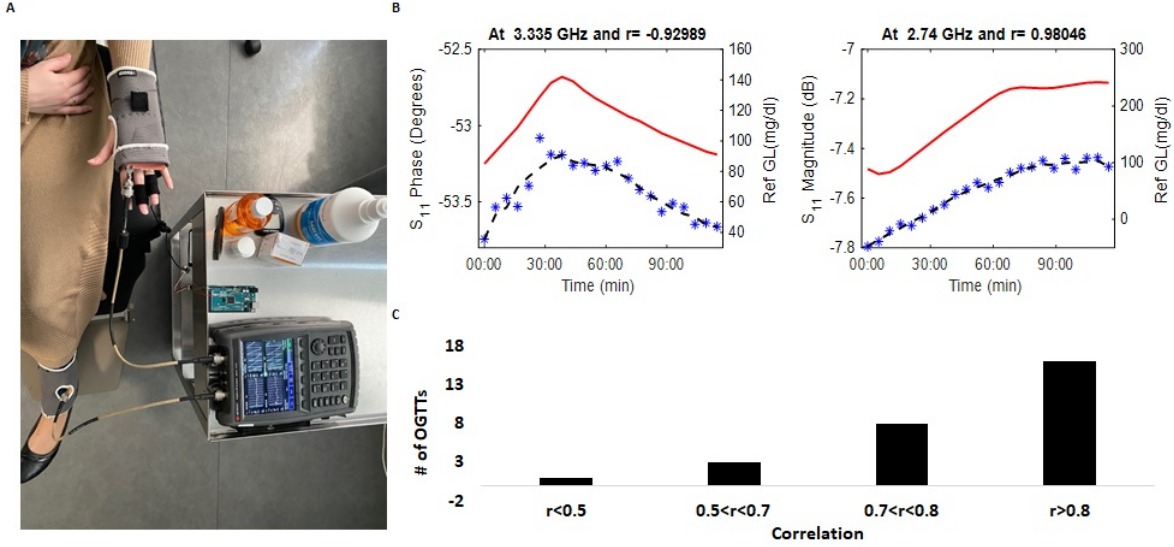
Figure 6.5: Human trials on healthy and diabetic volunteers using the sock sensor design #3. Real-time, continuous glucose monitoring on healthy and diabetic volunteers. (A), The experimental setup; the antenna is placed on the volunteer's leg. (B), Antenna's response during OGTT. Left: S11 phase variation with time at 3.35 GHz during one OGTT for a healthy volunteer. We notice that the S11 phase (blue curve) follows the trend of blood glucose profile (red curve). This curve follows well the blood glucose profile curve shown in red, achieving a high correlation of 0.93 between the two measurements. Right: S11 magnitude variation with time at 2.74 GHz for a diabetic volunteer showing a high correlation of 0.98 between the actual glucose levels and the antenna's S-parameters. (c), The correlation between the S-parameters and the glucose levels for the 28 OGTTs. We can see that out of the 28 OGGTs, 16 had a correlation higher than 0.8.

6.2.2 Regression modeling results

The flexible sock sensor design #3 is fixed on the volunteers' leg as shown in Figure 6.5. The non-invasively estimated blood glucose levels obtained by the GP model for a one OGTT of a healthy volunteer, shown in Figure 6.7 (A), match well the upward and downward trends of the reference blood glucose levels achieving a MARD of 0.926%. For this experiment, we relied on 16 features selected by the wrapper feature selection technique along with the rational quadratic as kernel for the GP, which provides the lowest mean percentage error as shown in Figure 6.7 (A) top. Figure 6.7 (B), shows the results for a diabetic volunteer,
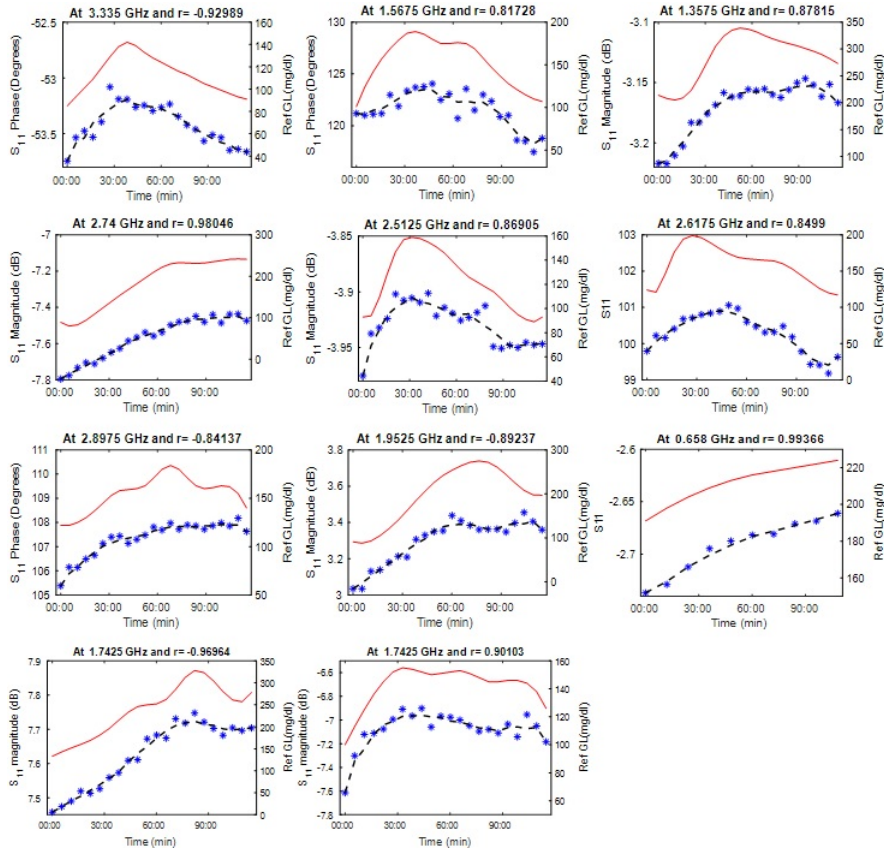
Figure 6.6: Sock sensor response during OGTTs on healthy and diabetic volunteers. Sock sensor's response during representative 11 samples chosen from the 28 OGTTs experiments.

where we achieved a MARD of only 0.62%. For this experiment, we relied on only 10 features selected by the wrapper feature selection technique along with the rational quadratic as kernel for the GP.

The leg sensing system achieves an overall MARD of 3.48% across all the volunteers, 3.57% for the diabetic and 3.31% for the control. To prove repeatability, the CEG analysis for all 28 OGTTs is shown in Figure 6.8 (B). The mean estimated glucose levels fall 100% into the clinically acceptable zones (97.85% in Zone A and 2.15% in B) for the sock sensor prototype. Moreover, 96.20% of the estimated values are within 15% error, 97.85% are within 20% error, 99.17% are within 30% and 99.50% are within 40% error. More results are shown in Figure 6.8 (D), showing the results for 8 healthy and diabetic volunteers obtained using the flexible sock sensor.
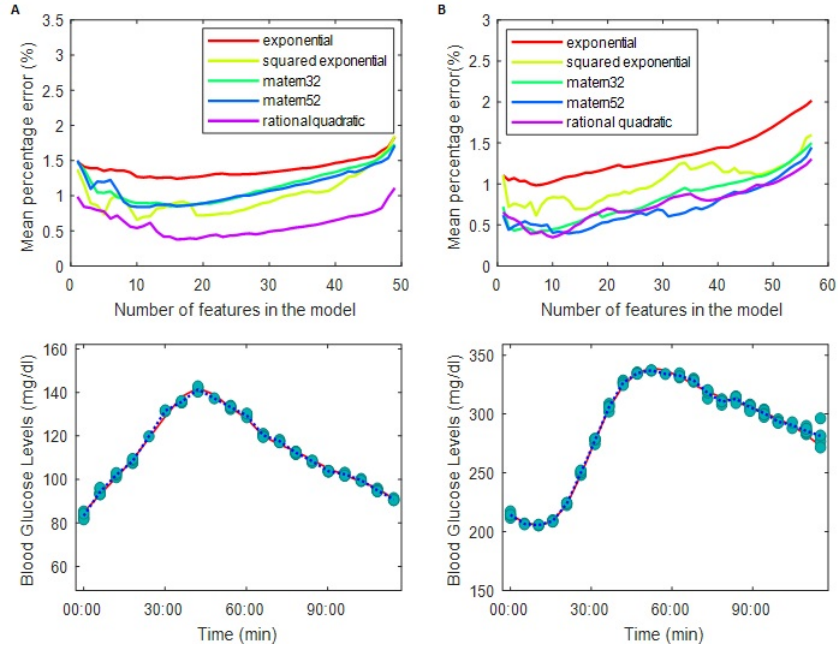
Figure 6.7: Feature selection and glucose estimation using the flexible sock sensor (design #3). (A), the sock sensor tested on healthy volunteer. (B), sock sensor tested on a diabetic volunteer.

6.3 Discussion

We are able to achieve very good matching between the estimated blood glucose levels by the proposed system in comparison to the reference blood glucose levels with a very low percentage error. In addition, our system is able to successfully follow the increase and decrease of these levels. More importantly, the obtained results show no delay between the estimated and the reference blood glucose values. This observation indicates that our proposed system is monitoring the glucose present in the blood, hence verifies one of our main design characteristics which is the choice of the frequency range. The antenna's waves at these frequencies infiltrate sufficiently into the underlying tissues, reaching the blood layers and hence providing direct information about the changes in the "blood" dielectric properties.

The proposed sensors, tested separately, achieved very good matching between the raw S11 data collected from the EM-sensors and the reference glucose levels, providing confidence in the potential of the proposed non-invasive when tested in controlled environments. The sensors provided also very high selectivity toward glucose compared with other interferants and very good glucose prediction accuracy. We also noticed that the response of the antennas varied from one volunteer to another while maintaining the multi-band, on-body matching characteristics. This is mainly attributed to the difference of the underlying tissue compositions
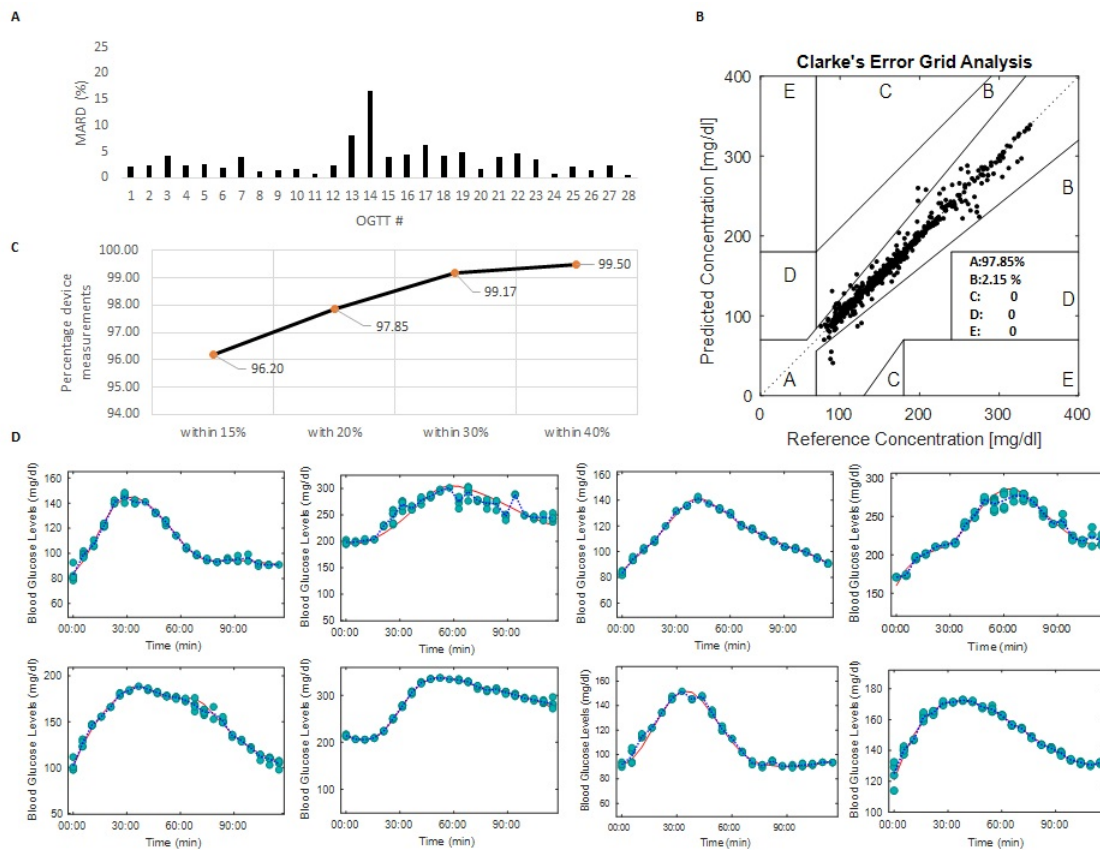
Figure 6.8: Estimated blood glucose levels during human trials on healthy and diabetic volunteers using the sock sensor. (A), for each of the 28 experiments we achieved a MARD below that 20% with a MARD of 3.48% averaged over all the 28 experiments. (B), CEG for all the OGTT conducted by the 28 volunteers showing the averaged estimations of 605 data point. All the estimated values are in the acceptable zones A and B with the majority in zone A (97.85%). (C), 96.20% of the estimated values are within 15% error, 97.85% are within 20% error, 99.17% are within 30% and 99.50% are within 40% MARD error. (D), blood glucose estimation using the GP model. Actual glucose levels (red) compared with the estimated glucose levels over time for 8 representative OGTTs chosen from a total of 28 OGTTs.

between one person and the other, and more precisely, to the difference in terms of: skin thickness, skin color, hydration level, sweat and hair density. In chapter 7, we added multiple sensors to the system and we combined the antennas into a multi-location system to calibrate out these perturbing factors.

Chapter 7

Calibration using environmental and physiological sensors

In this chapter we evaluated the proposed sensors in different experimental setups. First, we tested the performance of the proposed system when we collected data simultaneously from two different locations. After that we added multiple sensors to the system to take into consideration different environmental factors such as temperature, humidity, sweat and movement. Finally, we provide, in this chapter, a comparison between the different testing scenarios.

7.1   Introduction

Previous clinical trial's results showed good correlation between the dielectric signal and the actual blood glucose levels with very promising accuracy. However, in daily-life situations, the dielectric spectroscopy could be affected by a variety of environmental and physiological factors. These perturbing factors include ambient temperature and humidity, skin temperature, skin conductance which is mainly affected by the sweat, and motion which could affect the sensor-skin contact. As a result, any noninvasive glucose monitoring system based on EM technology must also take into consideration the different perturbing factors. Hence, we introduce a strategy for fully noninvasive glucose monitoring system that allows the proposed EM technology to be integrated in a multi-sensing wearable format. The system is composed of two flexible EM- Vessels-like sensors and multiple environmental and physiological sensors. The EM- based sensors are designed to monitor the glucose variations from different body locations simultaneously, integrated inside wearable apparels, and continuously monitor the glucose levels of deep vasculatures without the operational difficulties or instabilities encountered by other conventional approaches. Additional environmental and physiological sensors are also incorporated inside the apparels as shown in Figure 7.1. Each sensor provides non-invasive and continuous monitoring of the

different perturbing factors.
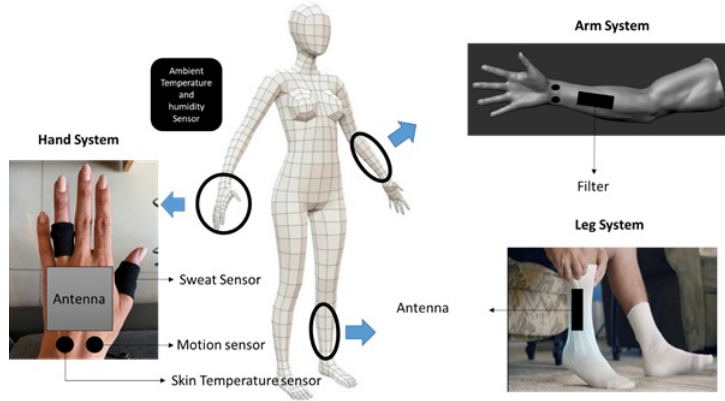
Figure 7.1: Illustration of the multi-location multi-sensing system. The system is composed of EM sensors for glucose measurements targeting the hand, leg and arm along with the environmental and physiological sensors for skin temperature, sweat, ambient temperature, ambient humidity and movement measurement sensors.

7.2 One system multiple locations

To overcome the technical difficulties introduced by some environmental factors and to improve the sensitivity of the device, first we joined the proposed sensors into a multi-location system. In one experiment, we joined a filter designed to target the arm vessels [78] along with the hand flexible antenna. In another experiment, we joined the flexible hand antenna with the leg antenna.

7.2.1 Glove antenna and armband filter joined system

The glove antenna and the filter are joined into a multi-location system targeting the hand and the arm. The system is tested on six healthy volunteers recruited for this experiment. Each volunteer underwent one OGTT resulting in six OGTTs in total. During each OGTT, around 23 measurements are recorded. The same procedure as before is adopted and each OGTT is processed separately. The respective responses, towards the variation of glucose levels, of both the antenna and filter are obtained from a portable VNA as shown in Figure 7.2. The VNA is connected to the sensors, while uniformly sweeping the frequencies over the 0.5-3 GHz range.

Figure 7.2 displays the antenna's and the filter's individual S parameters versus glucose levels for one volunteer. For this volunteer, the filter's third configuration provided the highest correlation between the S parameters and the glucose levels.

By combining the responses of both sensors and relying on the wrapper technique to select the most important features, we are able to reduce the MARD from 2.84% for the antenna alone to 0.91% for the combined system.
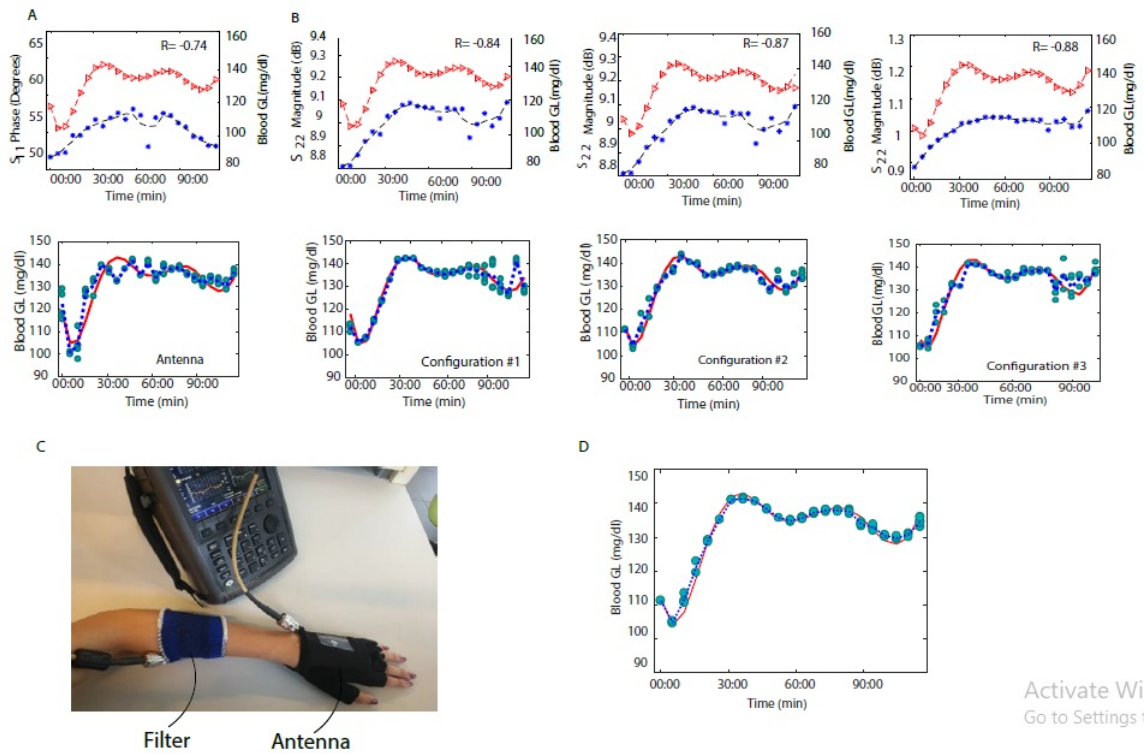
Figure 7.2: Multi-location system with the hand antenna and the arm filter response during one OGTT. The antenna and the filter are simultaneously tested on six healthy volunteers. We first evaluated the response of each sensor. (A) Top: Antenna's response for one volunteer. Bottom: Blood glucose estimation using the GP model. (B) Filter's response using three different tuning states. (C) Multisystem setup. (D) Multisystem blood glucose estimation.

We notice during the initial set of human trials that the response of the proposed sensors varied between patients (Figure 7.3). Hence, by monitoring the glucose levels using both the antenna and the tunable filter, we are able to tailor the proposed sensing system to better capture the specific individuals' characteristics. The wrapper feature selection technique helped us capture or identify the best combinations of features obtained from the different tunings of the filter and the antenna device. The arrows in Figure 7.3 are intended to indicate that each person may interact with each tuning differently; however, it emphasizes that the best set features obtained from the different sensors' settings indeed provide the best predictions.
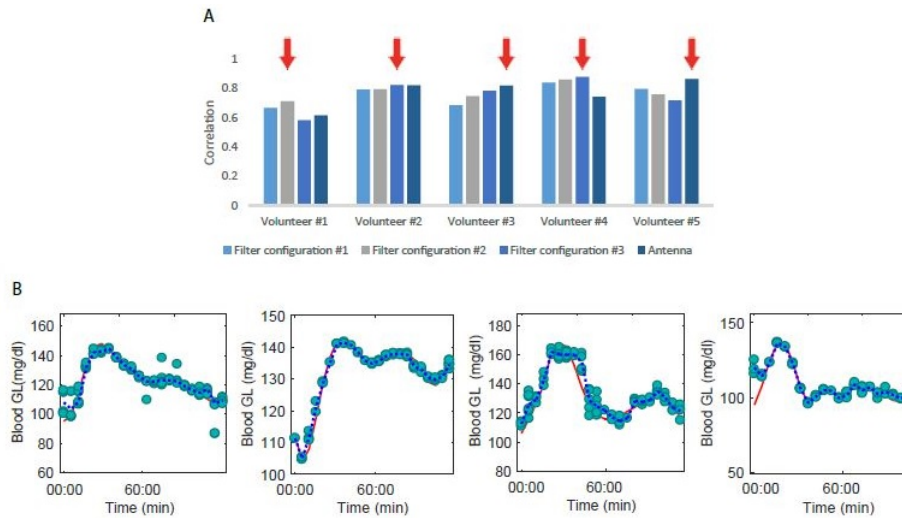
Figure 7.3: Multi-location system with the hand antenna and the arm filter. (A), Personalized monitoring. For each volunteer, the antenna and the filter responded differently, as shown in the bar plot, depending of the subject's physical characteristics. The red arrow indicate the sensor achieving the highest correlation between the senor's response and the actual glucose level. By combining the responses of both sensors, we relied on the wrapper technique to select the most significant features for each volunteer among the features obtained from the different configurations and sensing devices. (B), blood glucose estimation using the GP model. Actual glucose levels (red) compared with the estimated glucose levels over time (green dots shows the estimations resulting from the 10 random repetitions in most cases closely overlapping and the blue curve shows the mean estimation) for 4 representative OGTTs chosen from a total of 6 OGTTs. The results show very good agreement between the estimated and the reference glucose levels. CEG for all the OGTT conducted by the 6 volunteers.

7.2.2 Glove antenna and sock antenna joined system

The glove antenna and the sock antenna are joined into a multi-location system. The system is tested on 10 healthy volunteers and 18 diabetic patients recruited for this experiment. Each volunteer underwent one OGTT resulting in a total of 28 OGTTs. During each OGTT, around 23 measurements are recorded. The same procedure as before is adopted and each OGTT is processed separately. The respective responses, towards the variation of glucose levels, of both the Hand antenna and Leg antenna that are integrated respectively within the glove and the sock for one volunteer are shown in Figure 7.4. For this volunteer, the leg antenna provided lower prediction error of only 0.6% compared with the hand antenna, which achieved a MARD of 2.85%. By combining the responses of both sensors and relying on the wrapper technique to select the most important fea-

tures, we are able to reduce the MARD from 2.85% for the hand antenna alone to 0.4% for the combined system.
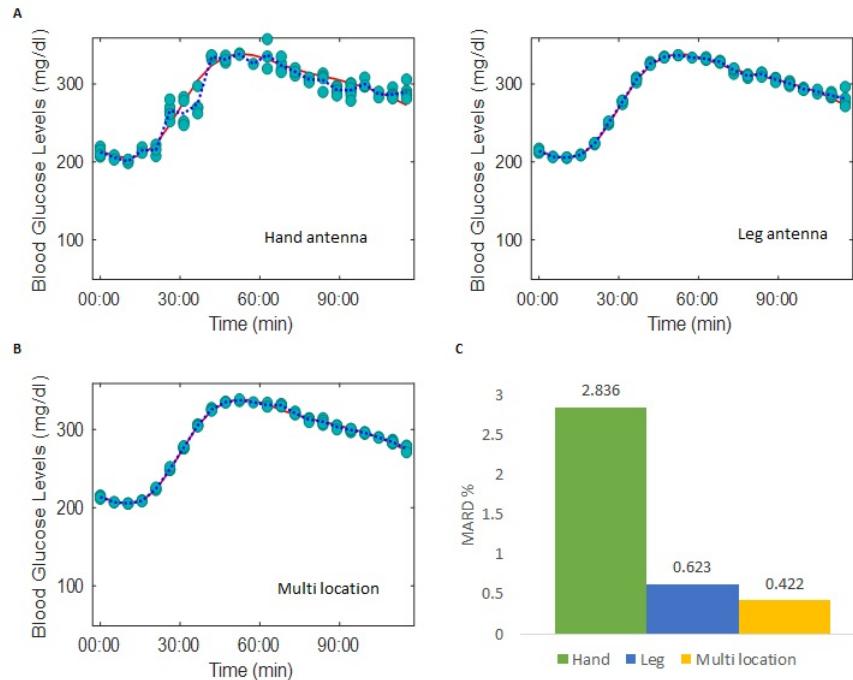
Figure 7.4: Multi-location system with the hand antenna and the leg antenna. The hand antenna and the leg antenna are simultaneously tested on 8 healthy and 8 diabetic volunteers. We first evaluated the response of each sensor alone. (A) Left: Hand Antenna's glucose prediction for one volunteer using the GP model. Right: Leg Antenna's glucose prediction for one volunteer using the GP model. (B) Left: Multi-location system blood glucose estimation. (C) Comparison between the standalone and combined system in terms of mean percentage error of the glucose levels prediction. The bar plot, shows that the multi- location system provided lower prediction error compared with the standalone system. By combining the responses of both sensors, we relied on the wrapper technique to select the most significant features for each volunteer among the features obtained from the two sensing devices.

Figure 7.5 shows a comparison between prediction errors for hand antenna used alone, leg antenna used alone and the combined system for all the experiments. As we can see, the combined multi-location system provided the lowest MARD (Figure 7.5 (A) and (B)). We believe that the multi-location system reduces the impact of interfering factors in real-life condition such as surface temperature, humidity, and movement by monitoring the glucose levels from two different locations. However we also noticed that each sensor could be used alone, providing predictions in the clinically acceptable zones, as shown in the CEG in Figure 7.5

(C).
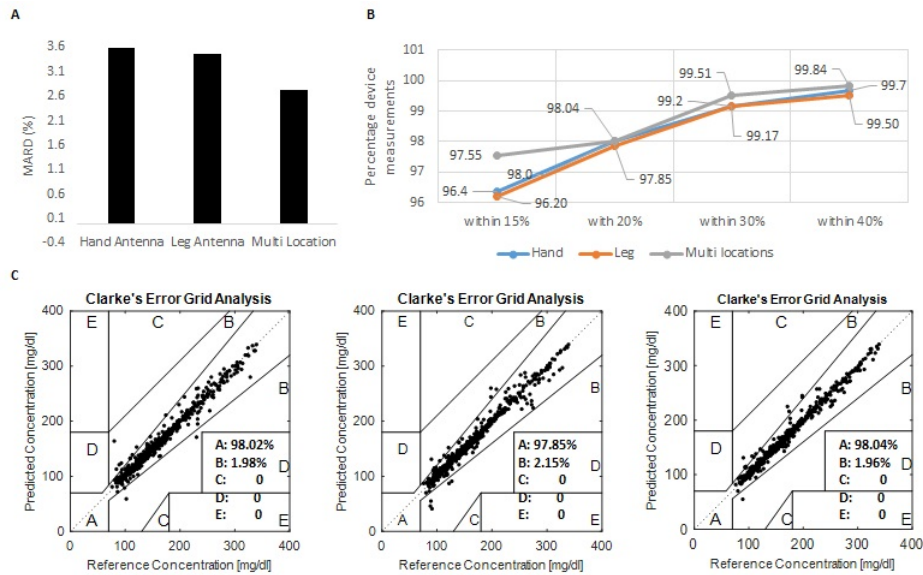
Figure 7.5: Comparison between the standalone and combined multi-location system. (A), for the 28 experiments we achieved a MARD below that 4% with a MARD of 3.58% averaged over all the 28 experiments for the hand antenna alone, 3.48% for the leg antenna alone and 2.73% for the combined system. (B), For the hand antenna alone: 96.4% of estimated values are within the 15% MARD error, 98% are within 20% MARD error, 99.2% are within 30% MARD error and 99.70% are within 40% MARD error. For the Leg antenna alone: 96.2% of estimated values are within the 15% MARD error, 97.85% are within 20% MARD error, 99.17% are within 30% MARD error and 99.5% are within 40% MARD error. For the combined multi-location system: 97.55% of estimated values are within the 15% MARD error, 98.04% are within 20% MARD error, 99.51% are within 30% MARD error and 99.84% are within 40% MARD error. The multi-location system shows superior performance compared with the standalone systems. (C), CEG for all the OGTT conducted by the 28 volunteers for the standalone systems and the combined system. Left: CEG analysis when using the hand antenna alone. Middle: CEG analysis when using the leg antenna alone. Right: CEG analysis when using the combined system. All the estimated values are in the acceptable zones A and B with the majority in zone A.

7.3 One System with multiple environmental/ physiological sensors

In the previous experiments we found that dielectric spectroscopy allows continuous, noninvasive glucose monitoring through skin and underlying tissues. The results in controlled clinical trials showed good correlation between the dielectric signal and the actual blood glucose levels with very promising accuracy. However, in daily-life situations, the dielectric spectroscopy could be affected by a variety of environmental and physiological factors. These perturbing factors include ambient temperature, humidity, skin temperature, skin conductance which is mainly affected by the sweat, and motion which could affect the sensor-skin contact.

To test and compensate for the possible influence of some environmental effects on the EM sensors readings, we created a sensing array comprising: Skin temperature sensor, sweat sensor, environmental temperature and humidity sensor and a motion sensor. All these sensors are embedded inside the designed glove and sock.

7.3.1 Skin Temperature Sensor

Skin temperature can provide clinical information about many aspects of human physiology including various skin injuries and diseases [79] which could affect the dielectric properties of the MUT. Additionally, skin temperature monitoring is needed to take into the account and reduce the temperature variation in the readings of the EM sensors through a built- in signal processor.

A Philips 21091A skin-surface temperature probe [80] was used for skin temperature monitoring and fixed inside both the glove and the sock as shown in (Figure 7.6). The accuracy of the probe is ± 0.1 ℃ for temperatures ranging between 25℃ and 45 ℃, and ±0.2 ℃ otherwise (0-60 ℃). The collected data are sent via Bluetooth to a phone application.

7.3.2 Skin conductance response (SCR) sensor

The SCR known also as galvanic skin response (GSR) measures the variation in the electrical conductivity of the skin which varies with its moisture level. These variations are mainly due to the skin sweat generated by the sweat glands and can be utilized to estimate the sweat rate. The GSR can be measured in terms of conductance, resistance and electro- physiological potential. The conductivity of the skin increases when the sweat rate increases [81]. The sensor measures the electrical conductivity between two electrodes and is considered a type of ohmmeter.

The GROVE GSR sensor [82] is integrated inside the glove monitoring the skin

conductivity using two Ag/AgCl electrodes fixed on the skin. A small voltage of 0.5 V is applied between the two electrodes. And by relying on ohm's law, the electrical conductivity of the skin is measured using the current flow between the two electrodes. The GSR sensor is wired to an Arduino to collect and save the data.

7.3.3 Environmental temperature and humidity sensor

Since the environmental temperature and humidity may affect directly the electrical properties of the tissues under test specifically the dielectrical constant and the loss tangent, compensation for these two factors is crucial in our application. In [83] the authors proved that the ambient temperature has a higher effect on the EM-sensor response than humidity.

To test and compensate for environmental temperature and humidity potential effects, a CC2650STK, Sensor Tag Development kit [84] is added to the proposed system to monitor the ambient humidity and temperature of the test environment. The collected data are sent via Bluetooth to a phone application.

7.3.4 Motion sensor

Motion could affect the EM-sensor to skin contact, hence to take into consideration these movements effect on the S-parameters readings, we added a FLORA Accelerometer sensor [85] to the proposed system. The sensor is wired to an Arduino to collect and save the 3-axis accelerometer data.

7.3.5 Multi-location and multi-sensing system results

To evaluate the performance of the proposed multi-location, multi-sensor system, clinical trial was carried out on 10 healthy and 18 diabetic subjects. The blood glucose levels of these volunteers were varied during OGTTs. Signals from the arm and leg antennas along with the integrated sensors were monitored during 2hours OGTT for each volunteer. One of the study goals is to check the effect of the temperature, humidity, skin temperature, galvanic skin response and movement on the EM-signal and to compensate for these perturbations.

The responses, towards the variation of glucose levels, during one OGTT using the multi-sensing, multi-location-system are detailed in Figure 7.6. Normalized data collected from the environmental/physiological sensors: skin temperature, humidity, ambient temperature, GSR and motion in terms of X, Y and Z as measured by sensors integrated in the glove are shown in Figure 7.6 (A). These signals along with the S parameters collected from the leg and hand antennas are used to predict the glucose levels. Using the wrapper feature-selection technique, we are able to identify the most important features for each volunteer by analyzing their individual data and we are able to compensate for the perturbations caused

by the different environmental and physiological factors. GP regression model is adopted as before and each OGTT is processed separately. The comparison between the standalone and combined system in terms of mean percentage error of the glucose levels prediction shows that the multi-sensing system provided lower prediction error compared with the standalone system.

For this volunteer, shown in Figure 7.6 ,the leg antenna provided lower prediction error of only 0.93% compared with the hand antenna which achieved a MARD of 2.15%. By combining the responses from both sensors along with the signals from the physiological/environmental sensors we are able to reduce the MARD from 2.15% for the hand antenna alone to 0.61% for the combined system improving the results by 3.5 folds.
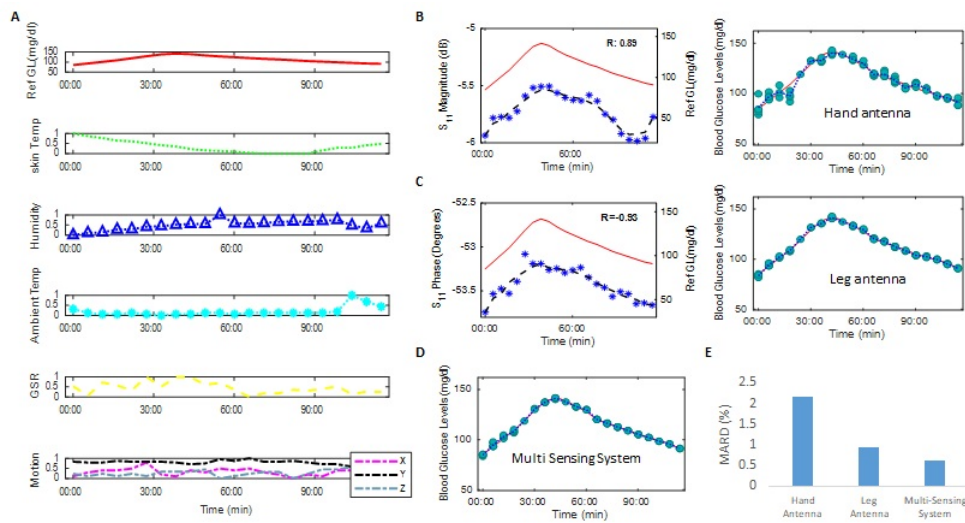
Figure 7.6: On-body real-time analysis during one OGTT experiment. (A), Normalized data collected from the environmental/physiological sensors: skin temperature, humidity, ambient temperature, GSR and motion in terms of X, Y and Z as measured by sensors integrated in the glove. (B), Left: real-time raw S11 data collected from the hand antenna. Right: Glucose prediction using the GP model when relying only on the hand antenna data. (C), Left: real-time raw S11 data collected from the leg antenna. Right: Glucose prediction using the GP model when relying only on the leg antenna data. (D), Left: Multi-sensing system blood glucose estimation. E, Comparison between the standalone and combined system in terms of mean percentage error of the glucose levels prediction. The bar plot, shows that the multi-sensing system provided lower prediction error compared with the standalone system. By combining the responses of sensors, we relied on the wrapper technique to select the most significant features for each volunteer among the features obtained from the two sensing devices.

Figure 7.7 shows a comparison between prediction errors for the hand antenna

used alone, the leg antenna used alone and the multi-sensing, multi-location system for all the 28 experiments. The CEGs for all the OGTT conducted by the 28 volunteers for the standalone systems and the multi-sensing, multi-location system are shown in Figure 7.7 (B). All the estimated values are in the acceptable zones A and B with the majority in zone A. The multi-sensing system resulted in 99.01% of the predictions in zone A and the remaining 0.99% predictions in zone B. It achieved: 98.18% of estimated values, within the 15% MARD error, 98.84% within 20% MARD error, 99.67% within 30% MARD error and 99.83% within 40% MARD error. The multi-sensing system shows superior performance compared with the standalone systems. And if we compared the MARD values obtained by these three setups, the combined multi-location multi-sensing system provided the lowest MARD of only 2.45%, for the 605 prediction points, as shown in Figure 7.7 (A).

7.4   Discussion

The multi-location, multi-sensing system reduces the impact of interfering factors in real-life condition such as surface temperature, humidity, and movement when monitoring the glucose levels from the EM sensors and compensating for the perturbing factors by adding the physiological and environmental sensors. However we also noticed that each sensor could be used alone, providing predictions in the clinically acceptable zones, as shown in the CEG in Figure 7.7.
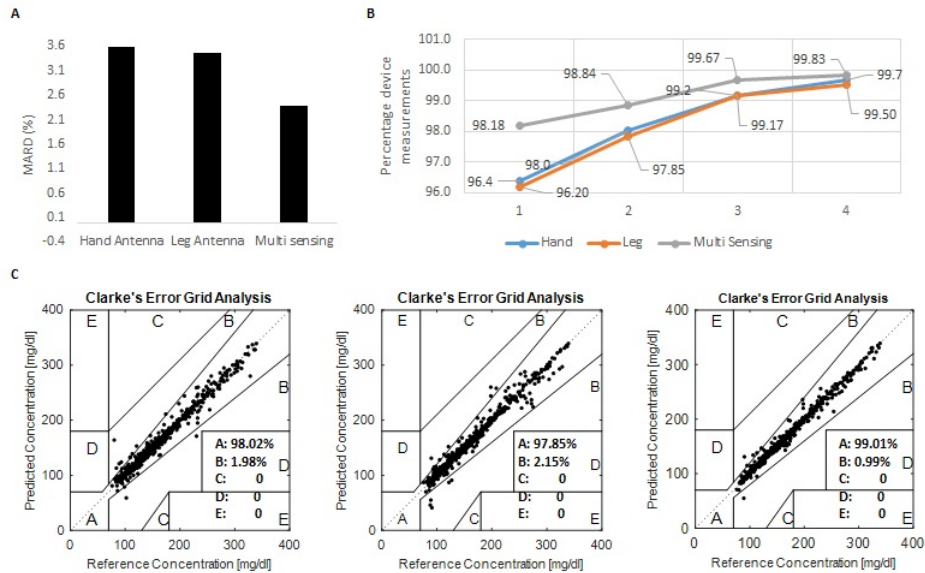
Figure 7.7: Comparison between the standalone and combined multi-location system. (A), for the 28 experiments we achieved a MARD below that 4% with a MARD of 3.58% averaged over all the 28 experiments for the hand antenna alone, 3.48% for the leg antenna alone and 2.45% for the mutli-sensing system. (B), For the hand antenna alone: 96.4% of estimated values are within the 15% MARD error, 98% are within 20% MARD error, 99.2% are within 30% MARD error and 99.70% are within 40% MARD error. For the Leg antenna alone: 96.2% of estimated values are within the 15% MARD error, 97.85% are within 20% MARD error, 99.17% are within 30% MARD error and 99.5% are within 40% MARD error. For the combined multi-sensing multi-location system: 98.18% of estimated values are within the 15% MARD error, 98.84% are within 20% MARD error, 99.67% are within 30% MARD error and 99.83% are within 40% MARD error. The mulit-location system shows superior performance compared with the standalone systems. (C), CEG for all the OGTT conducted by the 28 volunteers for the standalone systems and the combined system. Left: CEG analysing when using the hand antenna alone. Middle: CEG analysis when using the leg antenna alone. Right: CEG analysis when using the multi-location and multi-sensing system. All the estimated values are in the acceptable zones A and B with the majority in zone A.

Chapter 8

Conclusion and Future Directions

In this thesis, we provide proof of concept for a novel non-invasive, multi-location glucose monitoring system, based on a multi-sensing array integrated into wearable apparel. The concept is founded on EM sensors fabricated on ultrathin, flexible substrates designed specifically to concentrate the EM waves toward the targeted veins and arteries. EM-based sensing technologies are ideal for cheap, miniaturized, portable, and wearable biomarker monitoring solutions. As a first prototype, we targeted the hand and the leg as sensing locations. A wearable glove and sock will ensure comfort for the patients in different scenarios (work environment, physical activities, school). Many other locations could be considered. EM waves are transmitted into the body reaching the desired veins and arteries and allowing the extraction of information directly from the blood. To improve the sensitivity of the EM sensors several factors were considered: (1) they are designed to operate in the UHF and microwave bands allowing enough penetration depth of the EM waves to reach the blood vessels and hence providing good sensitivity towards glucose variation. (2) The slots are inspired by the blood vessel's network. The multiple slots result in a multi-band response allowing the system to sense the glucose variation at different frequencies with enhanced sensitivity due to the alignment between the antenna slots and the underlying vasculature anatomy. This allows focusing the EM waves on the targeted veins and arteries and results in improved sensitivity. (3) They are designed to operate when loaded with a lossy medium (on-body matching); this is intended to maintain the multi-band operation of the antenna when loaded with the human hand. These EM sensors are designed to target simultaneously multiple body locations. To calibrate out the different perturbing factors affecting the dielectric spectroscopy multiple environmental and physiological sensors were added to the system.

The system is validated on serum, animal tissues, and in a clinical setting. Serum-based and ex-vivo experiments demonstrate high precision across the diabetic glucose range (10mg/dl - 600mg/dl). Human trials exhibit clinical accuracy of 98% on fifty-five healthy and diabetic subjects who underwent around hundred OGTTs. Results are validated on the sensors (leg and hand sensors) used sep-

arately and collectively. The multi-sensing, multi-location approach greatly improved the accuracy of the blood glucose level estimation. The system captures the clinical glycemic variations without any time lag, reporting up to 98% correlation between the system's physical parameters and blood glucose levels. To our knowledge, this is one of the rare studies that assess the sensitivity of the proposed sensors on serum containing several ranges of glucose (10mg/dl to 600 mg/dl), on ex-vivo animal tissues exposed to a wide range of glucose (10 mg/dl to 600mg/dl) and in a clinical trial.

8.1 Future Directions

In this work, we developed a painless continuous wearable glycemic monitoring multi-sensor system that could be used by all age groups of diabetic and non-diabetic people. The fact that the proposed biosensors are streamlined, moving away from the typical patches/wristbands and more into embedded sensors fixed inside fashionable accessories and textiles that blend into patient's daily life is what makes our solution unique. The patients, of all age groups, could continuously monitor the glucose levels using his/her daily wearable accessories without the need to wear a specific patch. By adding multiple sensors to the proposed system and monitoring the blood glucose from different locations, we were able to further improve the system's sensitivity. In addition, the multi-sensing system provided personalized monitoring of the glucose levels, based on the patient's characteristics. The obtained results are highly encouraging showing comparable results with minimally-invasive, FDA-approved systems. Besides improving the quality of life of diabetic patients, especially children, such non-invasive continuous glucose-monitoring technology could pave the way for the development of a full closed-loop artificial pancreas system.

Several aspects of this research are still ongoing work in progress targeting to expedite its deployment for real-world applications. A brief overview of the work in progress is presented here along with an outlook towards potential future developments of this technology.

The next steps include:

- Peripheral circuit miniaturization: This encompasses reducing the overall size of the VNA, which can be used as a back-end circuitry for the system. This will make our system fully wearable, allowing us to test its performance on large-scale clinical trials.

- Energy sustainability: There is a need for providing efficient energy harvesting approach to sustainably power the proposed wearable system. High-energy consumption is a crucial challenge in wearable sensors. Energy could

be harvest from different sources including wearable, portable and sustainable sources such as solar light, bio-fluids, human motion, and wifi.

- Large scale clinical trials: We aim at testing the wearable system in large scale international multi-center multi-phase clinical trials, which will include diverse volunteers from all around the MENA region, UK and USA. Such clinical trials will allow us to take into account different age groups and different skin pigmentation and test the sensitivity of the proposed system towards different physiological conditions including obesity, cardiovascular diseases, and other diabetes complications.

- Data analytics: In this thesis, we relied on the Gaussian process regression technique to relate S11 coefficients to actual blood glucose concentrations based on the available data sets. With time, calibration is needed to account for physiological changes. Self-calibration is possible where additional sensors along with intelligent machine learning techniques are employed. Large-scale clinical trials will pave the way for a holistic data analytics framework that enables robust modeling with self-calibration techniques.

- CGM on the cloud: We aim at developing a software that fully automates data collection and processing from all the integrated sensors inside the proposed multi-sensing system. Similarly, an application could be developed for computers, tablets, smartphones, and watches to allow the patients to monitor their glucose levels on their portable devices. Furthermore, connecting the system to the cloud allows the patients to share their results with and follow up closely with physicians who in turn can provide them with personalized treatment regimens based on their individual glycemic profiles. This will help in the management of the progression of the disease.

Appendix A

Abbreviations

IF   Interstitial Fluid
CGM   Continuous Glucose Monitoring
EM   Electromagnetic
MUT   Medium Under Test
SMBG   Self Monitoring of Blood Glucose
HbA1c   Hemoglobin A1C
OGTT   Oral Glucose Tolerance Test
IVGTT   Intravenous Glucose Tolerance Test
UHF   ultrahigh frequency
FDA   Food and Drug Administration
DOP   Depth of Penetration
PET   Polyethylene terephthalate
AED   Electronics Desktop Simulator
CNC   Computerized Numerical Control
QWT   Quarter-Wave Transformer
SAR   Specific Absorption Rate
EU   European
FBS   Fetal Bovine Serum
VNA   Vector Network Analyzer
PBS   Phosphate-Buffered Saline
IRB   International Review Board
GP   Gaussian Process
PLS   Partial Least Square
LASSO   Least Absolute Shrinkage and Selection Operator
LWPLS   Locally Weighted Partial Least Square
PCC   Pearson Correlation Coefficient
FFS   Forward Feature Selection
MARD   Mean Absolute Relative Difference
SEP   Standard Error of Prediction
CEG   Clarke Error Grid

SCR   Skin Conductance Response
GSR   Galvanic Skin Response

Bibliography

[1] S. Wild, G. Roglic, A. Green, R. Sicree, and H. King, "Global prevalence of diabetes: estimates for the year 2000 and projections for 2030," *Diabetes care*, vol. 27, no. 5, pp. 1047–1053, 2004.

[2] M. R. Burge, S. Mitchell, A. Sawyer, and D. S. Schade, "Continuous glucose monitoring: the future of diabetes management," *Diabetes Spectrum*, vol. 21, no. 2, pp. 112–119, 2008.

[3] WHO, "Diabetes."

[4] M. Cardosi and Z. Liu, "Amperometric glucose sensors for whole blood measurement based on dehydrogenase enzymes," *Dehydrogenases; Canuto, RA, Ed.; InTechOpen: London, UK*, pp. 319–354, 2012.

[5] R. A. Gabbay, "New developments in home glucose monitoring: Minimizing the pain," in *Can J Diabetes*, Citeseer, 2003.

[6] D. B. Keenan, J. J. Mastrototaro, G. Voskanyan, and G. M. Steil, "Delays in minimally invasive continuous glucose monitoring devices: a review of current technology," *Journal of diabetes science and technology*, vol. 3, no. 5, pp. 1207–1214, 2009.

[7] P. Bollella, S. Sharma, A. E. G. Cass, and R. Antiochia, "Microneedle-based biosensor for minimally-invasive lactate detection," *Biosensors and Bioelectronics*, vol. 123, pp. 152–159, 2019.

[8] E. Renard, "Implantable glucose sensors for diabetes monitoring," *Minimally Invasive Therapy & Allied Technologies*, vol. 13, no. 2, pp. 78–86, 2004.

[9] D. Deiss, A. Szadkowska, D. Gordon, A. Mallipedhi, I. Schütz-Fuhrmann, E. Aguilera, C. Ringsell, C. De Block, and C. Irace, "Clinical practice recommendations on the routine use of eversense, the first long-term implantable continuous glucose monitoring system," *Diabetes technology & therapeutics*, vol. 21, no. 5, pp. 254–264, 2019.

[10] S. Sharma, Z. Huang, M. Rogers, M. Boutelle, and A. E. Cass, "Evaluation of a minimally invasive glucose biosensor for continuous tissue monitoring," *Analytical and bioanalytical chemistry*, vol. 408, no. 29, pp. 8427–8435, 2016.

[11] M. Joubert and Y. Reznik, "Personal continuous glucose monitoring (cgm) in diabetes management: review of the literature and implementation for practical use," *Diabetes research and clinical practice*, vol. 96, no. 3, pp. 294–305, 2012.

[12] D. B. Keenan, R. Cartaya, and J. J. Mastrototaro, "Accuracy of a new real-time continuous glucose monitoring algorithm," *Journal of diabetes science and technology*, vol. 4, no. 1, pp. 111–118, 2010.

[13] A. Sieg, R. H. Guy, and M. B. Delgado-Charro, "Noninvasive glucose monitoring by reverse iontophoresis in vivo: application of the internal standard concept," *Clinical chemistry*, vol. 50, no. 8, pp. 1383–1390, 2004.

[14] L. Lipani, B. G. Dupont, F. Doungmene, F. Marken, R. M. Tyrrell, R. H. Guy, and A. Ilie, "Non-invasive, transdermal, path-selective and specific glucose monitoring via a graphene-based platform," *Nature nanotechnology*, vol. 13, no. 6, pp. 504–511, 2018.

[15] F. Dewarrat, L. Falco, A. Caduff, M. Talary, Y. Feldman, and A. Puzenko, "Measurement and simulation of conductive dielectric two-layer materials with a multiple electrodes sensor," *IEEE Transactions on Dielectrics and Electrical Insulation*, vol. 15, no. 5, pp. 1406–1414, 2008.

[16] A. Caduff, M. S. Talary, M. Mueller, F. Dewarrat, J. Klisic, M. Donath, L. Heinemann, and W. A. Stahel, "Non-invasive glucose monitoring in patients with type 1 diabetes: A multisensor system combining sensors for dielectric and optical characterisation of skin," *Biosensors and Bioelectronics*, vol. 24, no. 9, pp. 2778–2784, 2009.

[17] R. Kasahara, S. Kino, S. Soyama, and Y. Matsuura, "Noninvasive glucose monitoring using mid-infrared absorption spectroscopy based on a few wavenumbers," *Biomedical optics express*, vol. 9, no. 1, pp. 289–302, 2018.

[18] S. Lee, V. Nayak, J. Dodds, M. Pishko, and N. B. Smith, "Glucose measurements with sensors and ultrasound," *Ultrasound in medicine & biology*, vol. 31, no. 7, pp. 971–977, 2005.

[19] J. Kost, S. Mitragotri, R. A. Gabbay, M. Pishko, and R. Langer, "Transdermal monitoring of glucose and other analytes using ultrasound," *Nature medicine*, vol. 6, no. 3, pp. 347–350, 2000.

[20] S. K. Vashist, "Non-invasive glucose monitoring technology in diabetes management: A review," *Analytica chimica acta*, vol. 750, pp. 16–27, 2012.

[21] H. Choi, "Recent developments in minimally and truly non-invasive blood glucose monitoring techniques," 2017.

[22] D. Bruen, C. Delaney, L. Florea, and D. Diamond, "Glucose sensing for diabetes monitoring: recent developments," *Sensors*, vol. 17, no. 8, p. 1866, 2017.

[23] J. Hanna, J. Costantine, R. Kanj, A. Eid, Y. Tawk, and A. Ramadan, "Electromagnetic based devices for non-invasive glucose monitoring," in *2018 IEEE Conference on Antenna Measurements & Applications (CAMA)*, pp. 1–4, IEEE, 2018.

[24] H. Choi, S. Luzio, J. Beutler, and A. Porch, "Microwave noninvasive blood glucose monitoring sensor: Human clinical trial results," in *2017 IEEE MTT-S International Microwave Symposium (IMS)*, pp. 876–879, IEEE, 2017.

[25] J. Costantine, R. Kanj, A. Eid, J. Hanna, A. H. Ramadan, and Y. Tawk, "Antenna design for biomarker monitoring and methods of use," Dec. 26 2019. US Patent App. 16/453,264.

[26] J. Costantine, R. Kanj, A. Eid, J. Hanna, A. H. Ramadan, and Y. Tawk, "An antenna array of a group of antenna elements for biomaker monitoring, nerve stimulations and methods of use." US Provisional Patent.

[27] J. Costantine, R. Kanj, and A. Eid, "Novel non-invasive biological, chemical markers and tracers monitoring device in blood including glucose monitoring using adaptive rf circuits and antenna design," Apr. 11 2019. US Patent App. 16/152,990.

[28] A. Pfützner, F. Demircik, J. Pfützner, K. Kessler, S. Strobl, J. Spatz, A. H. Pfützner, and A. Lier, "System accuracy assessment of a combined invasive and noninvasive glucometer," *Journal of diabetes science and technology*, vol. 14, no. 3, pp. 575–581, 2020.

[29] O. Amir, D. Weinstein, S. Zilberman, M. Less, D. Perl-Treves, H. Primack, A. Weinstein, E. Gabis, B. Fikhte, and A. Karasik, "Continuous noninvasive glucose monitoring technology based on "occlusion spectroscopy"," 2007.

[30] E. Hadar, R. Chen, Y. Toledano, K. Tenenbaum-Gavish, Y. Atzmon, and M. Hod, "Noninvasive, continuous, real-time glucose measurements compared to reference laboratory venous plasma glucose values," *The Journal of Maternal-Fetal & Neonatal Medicine*, vol. 32, no. 20, pp. 3393–3400, 2019.

[31] A. Pfützner, S. Strobl, D. Sachsenheimer, A. Lier, S. Ramljak, and F. Demircik, "evaluation of the non invasive glucose monitoring device glucotrack in patients with type 2 diabetes and subjects with prediabetes," *Journal of Diabetes and Treatment*, 2019.

[32] H. Choi, S. Luzio, J. Beutler, and A. Porch, "Microwave noninvasive blood glucose monitoring sensor: Human clinical trial results," in *2017 IEEE MTT-S International Microwave Symposium (IMS)*, pp. 876–879, IEEE, 2017.

[33] S. Saha, H. Cano-Garcia, I. Sotiriou, O. Lipscombe, I. Gouzouasis, M. Koutsoupidou, G. Palikaras, R. Mackenzie, T. Reeve, P. Kosmas, *et al.*, "A glucose sensing system based on transmission measurements at millimetre waves using micro strip patch antennas," *Scientific reports*, vol. 7, no. 1, pp. 1–11, 2017.

[34] N. Medical, "Better diagnostics for life," 2021.

[35] R. Aronson, R. Rastogi, C. Mdingi, X. Chen, and K. Tweden, "First assessment of the performance of an implantable cgm system through 180 days in a primarily adolescent population with type 1 diabetes," 2018.

[36] W. Villena Gonzales, A. T. Mobashsher, and A. Abbosh, "The progress of glucose monitoring—a review of invasive to minimally and non-invasive techniques, devices and sensors," *Sensors*, vol. 19, no. 4, p. 800, 2019.

[37] T. Yilmaz, R. Foster, and Y. Hao, "Radio-frequency and microwave techniques for non-invasive measurement of blood glucose levels," *Diagnostics*, vol. 9, no. 1, p. 6, 2019.

[38] T. Karacolak, E. C. Moreland, and E. Topsakal, "Cole–cole model for glucose-dependent dielectric properties of blood plasma for continuous glucose monitoring," *Microwave and Optical Technology Letters*, vol. 55, no. 5, pp. 1160–1164, 2013.

[39] G. Kovacs and J. Sorger, "Interactions of electromagnetic waves with biological tissue," *BIOE 200C Spring*, 2005.

[40] P. H. Siegel, Y. Lee, and V. Pikov, "Millimeter-wave non-invasive monitoring of glucose in anesthetized rats," in *2014 39th International Conference on Infrared, Millimeter, and Terahertz waves (IRMMW-THz)*, pp. 1–2, IEEE, 2014.

[41] P. H. Siegel, A. Tang, R. Kim, G. Virbila, F. Chang, and V. Pikov, "Noninvasive in vivo millimeter-wave measurements of glucose: First results in human subjects," in *2017 42nd International Conference on Infrared, Millimeter, and Terahertz Waves (IRMMW-THz)*, pp. 1–2, IEEE, 2017.

[42] X. Xiao and Q. Li, "A noninvasive measurement of blood glucose concentration by uwb microwave spectrum," *ieee antennas and wireless propagation letters*, vol. 16, pp. 1040–1043, 2016.

[43] S. Saha, H. Cano-Garcia, I. Sotiriou, O. Lipscombe, I. Gouzouasis, M. Koutsoupidou, G. Palikaras, R. Mackenzie, T. Reeve, P. Kosmas, *et al.*, "A glucose sensing system based on transmission measurements at millimetre waves using micro strip patch antennas," *Scientific reports*, vol. 7, no. 1, pp. 1–11, 2017.

[44] H. Cano-Garcia, I. Gouzouasis, I. Sotiriou, S. Saha, G. Palikaras, P. Kosmas, and E. Kallos, "Reflection and transmission measurements using 60 ghz patch antennas in the presence of animal tissue for non-invasive glucose sensing," in *2016 10th European Conference on Antennas and Propagation (EuCAP)*, pp. 1–3, IEEE, 2016.

[45] H. Cano-Garcia, S. Saha, I. Sotiriou, P. Kosmas, I. Gouzouasis, and E. Kallos, "Millimeter-wave sensing of diabetes-relevant glucose concentration changes in pigs," *Journal of Infrared, Millimeter, and Terahertz Waves*, vol. 39, no. 8, pp. 761–772, 2018.

[46] R. Baghbani, M. A. Rad, and A. Pourziad, "Microwave sensor for non-invasive glucose measurements design and implementation of a novel linear," *IET Wireless Sensor Systems*, vol. 5, no. 2, pp. 51–57, 2015.

[47] T. Yilmaz, R. Foster, and Y. Hao, "Broadband tissue mimicking phantoms and a patch resonator for evaluating noninvasive monitoring of blood glucose levels," *IEEE transactions on Antennas and Propagation*, vol. 62, no. 6, pp. 3064–3075, 2014.

[48] H. Choi, J. Naylon, S. Luzio, J. Beutler, J. Birchall, C. Martin, and A. Porch, "Design and in vitro interference test of microwave noninvasive blood glucose monitoring sensor," *IEEE transactions on microwave theory and techniques*, vol. 63, no. 10, pp. 3016–3025, 2015.

[49] V. Turgul and I. Kale, "A novel pressure sensing circuit for non-invasive rf/microwave blood glucose sensors," in *2016 16th Mediterranean Microwave Symposium (MMS)*, pp. 1–4, IEEE, 2016.

[50] V. Turgul and I. Kale, "Simulating the effects of skin thickness and fingerprints to highlight problems with non-invasive rf blood glucose sensing from fingertips," *IEEE sensors journal*, vol. 17, no. 22, pp. 7553–7560, 2017.

[51] C. G. Juan, E. Bronchalo, B. Potelon, C. Quendo, E. Ávila-Navarro, and J. M. Sabater-Navarro, "Concentration measurement of microliter-volume

water–glucose solutions using q factor of microwave sensors," *IEEE Transactions on Instrumentation and Measurement*, vol. 68, no. 7, pp. 2621–2634, 2018.

[52] X. Li, *Body matched antennas for microwave medical applications*, vol. 72. KIT Scientific Publishing, 2014.

[53] Ansys, "Ansys electronics desktop," 2021.

[54] humanbodyanatomy, "Hand vein anatomy veins of the hand anatomy human hand anatomy archives – human."

[55] H. Gellman, M. J. Botte, J. Shankwiler, and R. H. Gelberman, "Arterial patterns of the deep and superficial palmar arches," *Clinical Orthopaedics and Related Research®*, vol. 383, pp. 41–46, 2001.

[56] C. Waldby, *The visible human project: Informatic bodies and posthuman medicine.* Psychology Press, 2000.

[57] J. Yanamadala, G. M. Noetscher, V. K. Rathi, S. Maliye, H. A. Win, A. L. Tran, X. J. Jackson, A. T. Htet, M. Kozlov, A. Nazarian, *et al.*, "New vhp-female v. 2.0 full-body computational phantom and its performance metrics using fem simulator ansys hfss," in *2015 37th Annual International Conference of the IEEE Engineering in Medicine and Biology Society (EMBC)*, pp. 3237–3241, IEEE, 2015.

[58] C. A. Balanis, *Antenna theory: analysis and design.* John wiley & sons, 2016.

[59] C.-y. Wang and D.-c. Cai, "Hand tool handle design based on hand measurements," in *MATEC Web of Conferences*, vol. 119, p. 01044, EDP Sciences, 2017.

[60] T. Laverghetta, "Microwave materials and fabrication techniques. (retroactive coverage)," *Artech House, Inc.(USA), 1991,*, p. 284, 1991.

[61] FUJIFILM, "Dimatix materials printer dmp-2850," 2021.

[62] D. Celik, "Computation of the cell phone-induced sar distribution in a 3d multi-layered model of the human head/brain using ansys hfss," *Ozen Engineering*, pp. 1–16, 2013.

[63] MATLAB, "Matlab version 9.2," 2017.

[64] "Accu-chek active blood glucose meter." Accessed: 2021-02-22.

[65] Y. Leal, W. Garcia-Gabin, J. Bondia, E. Esteve, W. Ricart, J.-M. Fernández-Real, and J. Vehí, "Real-time glucose estimation algorithm for continuous glucose monitoring using autoregressive models," *Journal of diabetes science and technology*, vol. 4, no. 2, pp. 391–403, 2010.

[66] J. Bondia, C. Tarín, W. García-Gabin, E. Esteve, J. M. Fernández-Real, W. Ricart, and J. Vehí, "Using support vector machines to detect therapeutically incorrect measurements by the minimed cgms®," *Journal of diabetes science and technology*, vol. 2, no. 4, pp. 622–629, 2008.

[67] R. Tibshirani, "Regression shrinkage and selection via the lasso," *Journal of the Royal Statistical Society: Series B (Methodological)*, vol. 58, no. 1, pp. 267–288, 1996.

[68] J. A. Robins, "Partial least squares revisited," *Long range planning*, vol. 3, no. 47, p. 131, 2014.

[69] A. Alin and C. Agostinelli, "Robust iteratively reweighted simpls," *Journal of Chemometrics*, vol. 31, no. 3, p. e2881, 2017.

[70] C. E. Rasmussen, "Gaussian processes in machine learning," in *Summer school on machine learning*, pp. 63–71, Springer, 2003.

[71] M. Zanon, M. Riz, G. Sparacino, A. Facchinetti, R. E. Suri, M. S. Talary, and C. Cobelli, "Assessment of linear regression techniques for modeling multisensor data for non-invasive continuous glucose monitoring," in *2011 Annual International Conference of the IEEE Engineering in Medicine and Biology Society*, pp. 2538–2541, IEEE, 2011.

[72] M. Ebden, "Gaussian processes for regression: A quick introduction," *GP-tutorial. pdf*, 2008.

[73] S. Pleus, C. Schmid, M. Link, E. Zschornack, H.-M. Klötzer, C. Haug, and G. Freckmann, "Performance evaluation of a continuous glucose monitoring system under conditions similar to daily life," 2013.

[74] W. L. Clarke, "The original clarke error grid analysis (ega)," *Diabetes technology & therapeutics*, vol. 7, no. 5, pp. 776–779, 2005.

[75] K. V. Honn, J. A. Singley, and W. Chavin, "Fetal bovine serum: a multivariate standard," *Proceedings of the Society for Experimental Biology and Medicine*, vol. 149, no. 2, pp. 344–347, 1975.

[76] "Understanding a1c, diagnosis." Accessed: 2021-02-22.

[77] S. aldrich, "Sigma glucose," 2021.

[78] M. Bteich, J. Hanna, J. Costantine, R. Kanj, Y. Tawk, A. Ramadan, and A. Eid, "A non-invasive flexible glucose monitoring sensor using a broadband reject filter," *IEEE Journal of Electromagnetics, RF and Microwaves in Medicine and Biology*, 2020.

[79] R. C. Webb, A. P. Bonifas, A. Behnaz, Y. Zhang, K. J. Yu, H. Cheng, M. Shi, Z. Bian, Z. Liu, Y.-S. Kim, *et al.*, "Ultrathin conformal devices for precise and continuous thermal characterization of human skin," *Nature materials*, vol. 12, no. 10, pp. 938–944, 2013.

[80] Philips, "Skin surface temperature probe disposable, sterilized, continuous monitoring."

[81] G. Begtrup, J. A. Bertrand, J. Heikenfeld, A. Morgan, and N. Weinle, "Sweat conductivity, volumetric sweat rate, and galvanic skin response devices and applications," Sept. 10 2019. US Patent 10,405,794.

[82] S. Wiki, "Grove - gsr sensor."

[83] C. Jang, J.-K. Park, H.-J. Lee, G.-H. Yun, and J.-G. Yook, "Temperature-corrected fluidic glucose sensor based on microwave resonator," *Sensors*, vol. 18, no. 11, p. 3850, 2018.

[84] T. Instruments, "Cc2650stk simplelink™ bluetooth low energy/multi-standard sensortag."

[85] Adafruit, "Flora accelerometer/compass sensor - lsm303 - v1.0."